Dual-Band Gap Waveguide Structure

Mehek Moutushy Rahman Mou

A Thesis
In the Department
Of
Electrical and Computer Engineering

Presented in Partial Fulfillment of the Requirements
For the Degree of
Master of Applied Science (Electrical and Computer Engineering)

at Concordia University
Montreal, Quebec, Canada

March 2024

CONCORDIA UNIVERSITY

SCHOOL OF GRADUATE STUDIES

This is to certify that the thesis prepared

By: Mehek Moutushy Rahman Mou

Entitled: Dual-Band Gap Waveguide Structure.

and submitted in partial fulfillment of the requirements for the degree of

Master of Applied Science (Electrical and Computer Engineering)

Complies with the regulations of this University and meets the accepted standards with respect to originality and quality.

Signed by the final examining committee:

Dr. Abdel-Razik Sebak ______________________ Chair

Dr. Ben Hamza ______________________ External Examiner

Dr. Abdel-Razik Sebak ______________________ Internal Examiner

Dr. Ahmed Kishk ______________________ Thesis Supervisor

Approved by ______________________

Dr. Zahangir Kabir, Graduate Program Director,

Department of Electrical and Computer Engineering.

March 6, 2024 ______________________

Dr. Mourad Debbabi, Dean,

Gina Cody School of Engineering and Computer Science.

Abstract

Dual-Band Gap Waveguide Structure

Mehek Moutushy Rahman Mou

A new dual-band electromagnetic band gap (DBEBG) periodic printed structure is presented here. Designing the periodic unit cell within the periodic boundaries is sufficient to determine the EBG or DBEBG. The concept of the dual-band unit cell is based on stacking two different periodic textures with different parameters. The upper band texture considers the top of the lower band surface texture as a deformed back. Thus, a form of interaction between them makes designing each band individually challenging. Therefore, a comprehensive parametric study is required to design a DBEBG that controls the stop bands. A unit cell with a period of 1.8 mm is presented, achieving a 13-24 GHz and 34-44 GHz DBEBG with the proper parameters.

The effect of inserting the printed ridge breaking the periodicity creates propagating modes within the EBG bands, guiding the electromagnetic waves between the upper conductor and the ridge and suppressing them elsewhere, named PRGW provides dual-band, 13-24 and 34-44 GHz. A dual-band ridge with two 90-degree bends is demonstrated with simulated results of 13-22 and 32-42 GHz. Bends affect guide's scattering parameters, influencing signal reflection and transmission. Discontinuities are common in microwave systems, necessitating investigation during design them. The dual-band power divider is designed within the DBEBG structure, providing 16-24 and 32.5-42.5 GHz. Two

quadrature hybrid couplers within a DBEBG support a lower band 14-26 GHz, 60% fractional bandwidth at 20 GHz and an upper band 33-41 GHz, 21.6% fractional bandwidth at 37 GHz. They maintain a 90° ±10° phase difference between coupled and through ports, with isolation levels below 10 dB. The dual-band design holds potential for millimeter-wave applications and dual-band filter design.

Acknowledgments

I would like to express my deepest gratitude to my Supervisor, Prof. Ahmed Kishk, for his endless support, guidance, and motivation throughout the master's program and for allowing me to work in his research group. His technical knowledge and guidelines have greatly influenced and inspired my research work.

I sincerely thank Prof Abdel-Razik Sebak and Prof. Robert Paknys for their excellent lectures during my coursework. Their unique teaching styles, methods, and feedback helped me to understand numerous fundamentals efficiently. I would like to thank the committee members for reviewing my thesis and providing valuable suggestions and constructive feedback.

I am thankful to my colleagues and friends from our research group Syed Muhammad Sifat, Dayo Sokunbi, Amir Ashkan Darvish, Christine SH, Parisa SH, Elham Moradi, Zhiyong Dong, and Mostafa Shady for their tremendous assistance and support. It was a pleasure to collaborate with you all.

Finally, from the core of my heart, I must thank my parents, my husband, and especially my little daughter (Mehrish) for their unconditional love, patience, and encouragement. Furthermore, none of this would have been possible without the Almighty **Allah**.

Table of Contents

List of Figures

List of Tables

List of Acronyms

LTE	Long Term Evolution
4G	Fourth Generation
5G	Fifth Generation
SMS	short message services
TE	Transverse Electric
TM	Transverse Magnetic
TEM	Transverse Electromagnetic Wave
QTEM	Quasi-Transverse Electromagnetic Wave
RGW	Ridge Gap Waveguide
SIW	Substrate Integrated Waveguide
GGW	Groove Gap Waveguide
PMC	Perfect Magnetic Conductor
PEC	Perfect Electric Conductor
AMC	Artificial Magnetic Conductor
PRGW	Printed Ridge Gap Waveguide
EBG	Electromagnetic Band Gap
1D	One-Dimensional
2D	Two-Dimensional
3D	Three-Dimensional
CST MWS	Computer Simulation Technology Microwave Studio
EM	Electromagnetic
FIT	finite integration technique
PCB	Printed Circuit Board
LHTL	left-handed transmission line
MMIC	Monolithic Microwave Integrated Circuit
BW	Bandwidth
MSL	Microstrip Line
MMW	Millimeter- Wave

Chapter 1

Introduction

Communication technology is growing too fast due to social impact and the vast number of users in recent decades. The advancement in the communication sector has blessed us by introducing the internet, secured wireless networks, email, geographical locations, and coordinates anywhere in the universe more cheaply, quickly, and efficiently. Due to globalization and social interaction, people are facilitated by the rapid advance of wireless communication compared to the past. Modern communication allows us to connect anytime with different gadgets, such as smartphones, tablets, laptops, and so on, which require high data rates and fast connectivity. These devices make our lives comfortable, easy, and quick by providing us with online business and class, video conferences, live streaming of sports, and any performance; as a result, high-speed internet and low-cost data are prerequisites.

These rising advancements in wireless communications, which need high data rates, widespread coverage, and available spectrum, have prompted researchers and industry to shift to higher frequencies and millimeter wave ranges. With advancements in communication systems, high-frequency microwave devices are rapidly expanding and necessary for modern 5G communication. RF components are miniatured at higher frequencies. As a result, it is necessary to establish a new trend of building single compact modules in which active, passive, and antenna components are all combined into the same package. However, installing passive components and guiding structures becomes challenging at millimeter wave bands based on conventional guiding structures such as microstrip lines and waveguides. Cavity modes cause surface waves and increase high dielectric and conductive losses in microstrip lines at higher frequencies. Waveguides are challenging to combine with integrated circuits and require an accurate manufacturing technique to provide proper electrical contacts when produced in distinct blocks.

1.1 Evolution of Wireless and Cellular Communications

Communication can be classified into two types: a. Wired and b. Wireless. Wireless communication has been more acceptable, popular, and easier in the past century. Most mobile and wireless communications operate at low frequencies, between 800 MHz to 3 GHz. Such frequencies have good propagation characteristics with less attenuation, low cost, and large wavelength, providing both long and short-distance coverage. The exponential growth of the number of users per coverage area switches the operators' focus on capacity rather than coverage area. However, one main goal of advanced wireless technology is high capacity with simultaneous streaming in a limited coverage area. The operators' lack of available spectrum is another issue due to the extension of 4G technologies, such as LTE, depending on spectrum availability. Wireless data transfer is not only bound to communication purposes but also has an outstanding impact on medical, surveillance, and radio broadcasting. For higher data transmission, wide bandwidth is mandatory, which can be realized using higher frequency bands [1]-[2].

The Bell Lab developed a cellular system in the 1970s and first developed commercially applicable and usable standards. The widening demand for commercial applications during the 1980s and 90s helped to deploy modern wireless mobile services. Technological advancement increased remarkably with the high consumer demand, while mobile communications are expected to reach 5G within 2020 during this journey [3]. The current wireless network helps our lives be easy, comfortable, and enjoyable, providing various media and devices. People have experienced a revolution in wireless mobile communication, which was a dream before. For example, people do not get the facility of 4G/5G in the blink of an eye or one day, besides much research, and come across many steps to reach it. Cellular mobile communication was first introduced in the 1980s, only for voice communication, called first generation 1G communication. After that, in the early 90s, the second generation 2G was launched with some new features added with voice communication based on digital signals for supporting short message services (SMS), conference calls, and call holding. Later on, the third generation 3G communication was established for voice and video transmission in the early 2000s. A download speed of 100 Mbps was introduced in fourth-generation 4G, providing for high data transmission and radio broadcasting [2]-[4]. Fifth-generation (5G) communication will offer more added characteristics over 4G. Although the LTE (4G) systems show much higher-ranked performance, human needs are still asking for more service improvements. However, mobile communication systems have gone through all these revolutions, and the new 5G or new mobile generation is expected to enable uninterrupted access to information, communication, and entertainment with massive numbers of users [5].

Many users supporting multiple services need high data rate transmission, which requires an ultra-wideband. At high data transmission, high attenuation, and propagation losses occur; as a result, the communication and cellular industry has focused on the millimeter wave frequency spectrum (30-300) to mitigate the growth of users. Although fiber optics communication can support high-speed data transfer, it requires expensive hardware installation. On the other hand, microwave communication is suitable for short-distance communication, but many devices and sensors make it more complex. However, considering all these facts, industry, and researchers focus more on millimeter-wave bands, appraising the immense benefit of this band. We are going to discuss more about it in a later chapter.

1.2 Conventional and Modern Guiding Structure

In the RF microwave fields, guiding structures of microwave signals are one of the challenging topics at present. Some limitations exist in microwave communication, but with the help of advanced microwave engineering, researchers are trying to overcome the hindrance of existing structures or presenting new types of structures, which are always demanding in communication systems. Wave propagation from guided or unguided structures follows Maxwell's wave equation, and many experiments and scientists are involved in establishing a full scenario of propagation of the electric and magnetic field inside this structure, satisfying some boundary conditions. With the wave propagation inside this structure, some modes are presented, such as TE, TM, TEM, and hybrid modes. Many structures can be demonstrated for wave propagation, such as parallel plate waveguides, rectangular waveguides, and circular waveguides [6].

The microwave frequency range is 300 MHz to 30 GHz. Transmission lines are preferred to be used in the microwave frequency range because they carry the signal as TEM waves. The main superiority of TEM modes is less dispersion and can carry signals at any frequency. The losses in the transmission lines depend on carrier frequency; if the carrier frequency increases, the losses increase. This advised us to use other guiding structures, such as waveguides. However, these types of guiding structures do not support the TEM mode but have much lower losses, enabling this guiding structure to be used in high-frequency ranges [6]. Various guiding structures are introduced in microwave applications, which can replace conventional structures in many ways, such as low cost, easy fabrication, etc. The coplanar waveguides, grounded coplanar waveguides, and microstrip lines are good examples of substrate-printed guiding structures. In the past decades, many modern guiding structures, such as substrate-integrated waveguides (SIWs) and ridge gap waveguides (RGWs), were introduced to be used in high-frequency applications and are more popular to replace traditional guiding structures. SIWs and RWGs both have some merits and demerits. The RGW propagates TEM mode with no dielectric loss because the signal propagates inside an air gap where SIW has more dispersion, which carries TE mode. Considering the conductor loss, although the RGW has a wider current distribution on the upper ground, the SIW has conductor losses inside the vias surrounding the guide. However, the fabrication of SIW is much easier than RGW, while the mechanical durability of the RGW is higher than SIW for the same component.

1.3 Applications of Millimeter Wave Band

The 30-300 GHz frequency range is known as the millimeter wave's band with a wavelength between 10 mm to 1mm. At this frequency band, the propagating signal attenuates due to the atmospheric absorption that restricts long-distance communication. The oxygen absorption level is high at mm-waves, and the propagation losses are higher in millimeter waves than in lower frequency bands. However, some other critical factors, like technical, mechanical, and environmental, affect the overall performance of the antenna at mm-wave bands, which are mentioned below [7]-[8].

- Weather: Rain, storm, cloud.
- Atmospheric Attenuation: Oxygen absorption and water stream absorption.
- Diffraction: Bending or chamfering.
- Scattering effects: Reflections, refraction, diffusion.

The wavelength is directly related to frequency; when the frequencies increase, the wavelength becomes shorter, and the reflective surface seems rougher, resulting in more diffused reflection

[9]. The mm-wave band is implied as an attractive candidate for the upcoming 5G communication system because it supports a huge amount of unlicensed spectrum. The following benefits of mm-wave that compel draw the attention of the researcher to use this band are presented here,

- Frequency reuse
- Unlicensed operation with low interference.
- Suitable for short-distance communication.
- Small-sized high-gain antenna.
- Secured transmission.

Millimeter wave systems are becoming attractive for point-to-point wireless communication, especially in cellular services in high-density areas, high-quality video transmission with gigabit data rate. Typical applications for radar systems include safety devices, cruise control, sensing, automatic braking, collision warning, etc.

1.4 Guiding Structure in Millimeter Wave Band

The existing classical technology, for instance, microstrip lines and waveguides, is complicated to implement the passive components and interconnect through these transmission lines. However, developing new technology with high performance and multi-functionality is needed. Some guiding transmission lines are suitable for high-frequency applications, whereas some are for low-frequency applications. On the other hand, some are beneficial for millimeter wave frequency.

We can classify striplines, microstrip lines, and coplanar waveguides are well suited for low-frequency applications [10]. When constructed on a dielectric substrate, it suffers from high dielectric losses, insertion loss, surface waves, and high cavity modes, leading to unwanted radiation that limits the acceptability of microstrip lines in millimeter wave bands.

In radio and microwave communication systems, the types of transmission lines depend on frequency; when the frequency increases, the transmission losses increase due to sheet resistance or dispersion mode of signals. Guiding structures like air-filled waveguides are low-loss structures with high power handling capacity. For example, circular and rectangular waveguides are the most impressive examples of guiding structures in high-frequency applications. Because of the high Q-factor, the rectangular waveguide is the most popular but not worthy for mm-wave bands. A rectangular waveguide is constructed in hollow tubes with four sidewalls where wave travels through this tube. Constructing sidewalls at an mm-wave band is challenging because, with increased frequency, the dimensions get narrower. As a result, the matching becomes complex and less precise. Therefore, the proper electrical contact between the plates becomes more challenging [6].

Much research has been done to propose and analyze modern guiding structures appropriate for mm-wave applications. Finally, the researchers found modern guiding structures such as substrate integrated waveguide (SIW), ridge gap waveguide (RGW), and the packaged microstrip line. SIW is a planar waveguide, which is realized in printed technology. The field in SIW travels in the substrate between two rows via holes replacing the vertical metal walls of hollow waveguides. Hence, the SIW shows dispersion characteristics similar to standard waveguides but can be adapted to printed circuit boards [11]. However, the main disadvantages of SIW are high dielectric losses due to the material used and radiation losses due to the vias holes, which do not provide a perfect metal shield in the mm-wave band. Another promising candidate is gap waveguide technology suited for mm-wave applications [12]. In the gap waveguides, the field travels in the air gap between parallel metal plates. The key characteristic of this technology is the use of a textured surface on one of the parallel plates, called an artificial magnetic conductor (AMC), which creates a high surface impedance condition, forcing a cut-off of all parallel modes [13]. The gap waveguide can be constructed in various versions based on the type of path and desired propagation characteristic, such as ridge gap waveguide (RGW) and groove gap waveguide (GGW), where the field propagates along metal ridges and grooves [14].

The key merits of gap waveguides are low loss, low profile, no electric contact between plates, cheap, and easy fabrication process. The printed version of the ridge gap waveguide is named printed ridge gap waveguide (PRGW) and is well suited for mm-wave applications. The bottom layer is plated using mushrooms and vias or metal pins (could be circular or square shapes), which control the electromagnetic band of the overall structure. The next section will discuss basic ideas about the new guiding structure in more detail.

1.5 Motivation and Objective of the Thesis

A gap waveguide (GWG) is an inserted ridge (parallel plate waveguide) or a groove waveguide inserted in an electromagnetic bandgap (EBG) periodic structure. The propagating waves of the guide operate within EBG to prevent energy from leaking from the guide sides, forcing the energy along the guiding structure without a need to close (shorten) the sides, avoiding the need for electrical contacts between the guiding structure parts. Therefore, the GWG becomes an attractive candidate to mitigate the problems behind traditional technology at higher frequencies, particularly millimeter frequencies. The GWG provides an interesting wide bandwidth of more or less a 2:1 bandwidth. This is sufficient for most applications, particularly in the upper millimeter wave ranges. However, for applications that require operations below the millimeter wave range and within the millimeter wave band, GWG with a single band is insufficient. Thus, there is a need for new guiding structures able to cover such dual or multi-band with faraway ranges. The design challenge for the next generation of wireless communication in mm-wave is envisioning an overall system with low area transceivers, cheaper and advanced packaging techniques, compressed size, and cost-effectiveness simultaneously. The gap waveguide technology was introduced not long ago as a favorable candidate for mm-wave applications that overcome the drawbacks faced by conventional technologies. This technology was first presented in 2009 by Kildal [13], using the basic concept of two parallel plate waveguides. RGW, in its ideal form, is a parallel plate waveguide of two metals with a specified width (loosely referred to as two parallel perfect electric conductors (PEC) and denoted as PEC/PEC) surrounded by extending one of the PECs and replacing the other by perfect magnetic conductor (PMC) separated by a gap less than a quarter of a wavelength ($\lambda/4$) suppressing any propagation between them. Thus, RGW acts as a parallel plate waveguide with no side leakage, providing a 2:1 bandwidth and an ultra-wide 3:1 bandwidth [15], [16], [31]. If a ridge is inserted in the bottom surface, the wave propagation will be within the ridge only. The magnetic conductor is realized by a periodic texture that acts as a high-impedance surface that we call an artificial magnetic conductor (AMC). However, the texture of the AMC surface could include guiding structures such as ridge, groove, or strip to complete a waveguide formation. Such structure supports quasi-TEM modes or TE modes controlled by the width of the PEC/PEC. Moreover, many articles were published to propose a printed version of RGW for better performance, centralization, and lower cost. Printed circuit technology can realize such a guiding structure, which is our current choice.

The main objective and contribution of the thesis are divided into three sections,

- The work's fundamental objective is to design a dual-band unit cell with two layered cells. The unit cell comprises two stacked dielectric substrates topped by an aired substrate below the top metallic plate. The unit cell consists of a large mushroom patch on the bottom grounded substrate etched on its top and connected to the lower metal plane by a conducting via. The intermediate substrate has four smaller mushroom patches of total size smaller or equal to the bottom patch, and each is connected to the lower patch by conducting vias. The total size of the one-unit cell is 1.8mm. The unit cell is designed to achieve two stop band gaps; one is for the lower band for 13-24 GHz and another for the upper band 34-44 GHz. Inserting a so-called printed ridge perturbing the periodicity creates propagating modes within the EBG bands, guiding the electromagnetic waves between the upper conductor and the ridge and suppressing them elsewhere. Two propagation modes can be achieved through this row of unit cells, mode 5 and mode 17, that allow propagation through the structure. The parametric study of 4 mushroom unit cells has been shown. The parameters affecting the unit cell's band gap include the air gap, substrate thickness in both upper and lower layers, patch width, and via radius. A unit cell of 4 mushroom patches looking downward has been introduced, and we intended to get dual bands, but unfortunately, dual bands do not acquire with this approach, so we stopped at that point. This approach acquires the dual-band when the air gap between two substrates is zero, which acts as a dielectric-filled SIW. The other proposal is a 9-mushroom patch unit cell that provides dual bands, one for 10-20 GHz and another for 35-45 GHz. This double-layer 9-mushroom patches unit cell allocates dual bands similar to 4 mushroom patches unit cells. As a result, we choose 4 mushroom patch unit cells for further experiments to avoid design complexity and computational time and expenses. This unit cell is suitable for dual bands so that anyone can use it based on their required frequency.

- The second objective is to design a ridge gap waveguide with the proposed unit cell. In the proposed gap waveguide, Q-TEM waves propagate through the air gap along with the ridge, providing bandwidth coverage of 13-24 GHz and 34-44 GHz. The design matches excellently except for the band 25-33 GHz, which has some ripple and out of band. The dimension of the ridge width is 1.2 mm, providing 31.5 Ω impedance, where 50 Ω can be acquired using an adapter or changing the ridge width. Later, 4 different design proposals of ridge gap waveguides were shown with the change in ridge position and conditions through dual band unit cells. All ridge gap waveguides provide dual bands, but slide changes the frequency range for both bands. Furthermore, two 90-degree bend lines are designed to support two bands, one for 13-22 GHz and another for 32-42 GHz, with outstanding matching but a little insertion loss due to the bends of lines.
- The final goal of this thesis is to construct a feeding network 1:2 (one input and two outputs) like a power divider of dual-band, having less insertion loss and an excellent matching level. A 1x2 dual-band power divider is achieved that generates two passbands, one for 16-24 GHz and another for 32.5-42.5 GHz, with a threshold below -10 dB and insertional loss below -5 dB. Two couplers are designed with the unit cell to achieve a similar band covering as a unit cell; one is for the lower band that generated 14-26 GHz with an excellent isolation level below -10 dB and fractional bandwidth of 60% at the center frequency of 20 GHz. Another coupler for the upper band was assigned 33-41 GHz with an outstanding isolation level below 10dB and a fractional bandwidth of 21.6% at the center frequency of 37 GHz. These designed couplers have the potential for Ku, K, and Ka-band applications.

The dual-band unit cell follows the PRGW technology. This thesis presents the development of

PRGW for various dual-band millimeter applications. Well, it is suited for dual-band filter design. Diplexer could be designed with this dual band unit cell for other communication purposes.

1.6 Thesis Outline

The thesis is divided as follows: **Chapter 2** covers a literature review of the gap waveguide technology, which is followed by a detailed discussion of hard and soft surfaces, periodic structures that will introduce the basic concept of gap waveguides, different types of gap waveguides will be briefly presented. **Chapter 3** introduces a proposed new unit cell named a dual-band unit cell. Conventional unit cells, such as single-layer mushrooms and square pin unit cells, and the band gap of all cells, such as 4 mushroom patches, look downward. 9 mushroom patch unit cells will also provide detailed analysis and parametric studies. **Chapter 4** shows the proposed dual-band printed ridge gap waveguide, four different dual-band ridge gap waveguides, the ridge with two 90-degree bend lines, and a dual-band 1x2 power divider. Two couples with a proposed unit cell will also be present here, one for the lower band and another for the upper band. Finally, **Chapter 5** summarizes the thesis outcomes and future work with valuable suggestions and applications of the proposed work.

Chapter 2

Literature Review of the Gap Waveguide Technology

The basic concept of a gap waveguide is ideally the two parallel plates waveguide of two parallel Perfect Electric Conductors (PEC) separated by a distance of h. The upper PEC is extended over the PMC plate to prevent leakage from the side walls. However, to suppress the waves between the PCE and PMC, the distance h must be less than a quarter of a wavelength ($\lambda/4$). Thus, the waves will only propagate between PEC-PEC with a mode similar to the parallel plate TEM mode and no propagation between PEC-PMC plates, as shown in Fig. 2.1a. Consequently, the gap waveguide (GWG) is generated, as shown in Fig. 2.1b. The PEC plate can be easily realized using metal conductors. To physically realize the PMC that does not exist in nature, an AMC (Artificial Magnetic Conductor) must be created as a high surface impedance [17] using a periodic structure. There are several ways to realize the GWG.

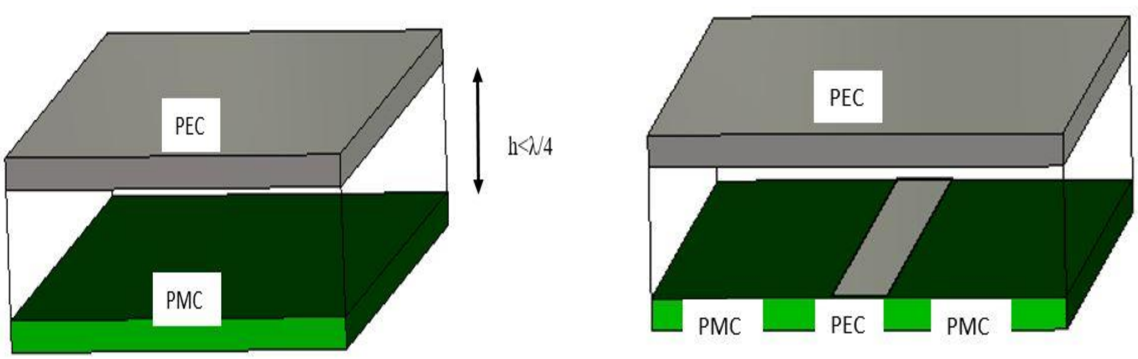

(a) (b)

Figure 2.1: Gap waveguide principle, (a) Ideal PEC-PMC parallel plates and (b) PEC-PEC parallel plates, surrounded by PEC-PMC.

In addition, a real gap waveguide can be realized with a metal strip, ridge, or groove embedded on both sides by a textured surface, providing a high impedance that allows only a quasi-TEM mode to propagate along the metal ridge or strip. Figures 2.1 (a) and (b) show the basic operating principle of gap waveguides.

2.1 Soft and Hard Surface

Metamaterials are artificial surfaces expressing electromagnetic properties not found in nature. The gap waveguide is based on the fundamental concept of metamaterials as hard and soft surfaces [18]. One useful property called magnetic conductor does not exist in nature. Many researchers have worked hard in the past few years to create metamaterial surfaces that could artificially generate magnetic conductivity, a so-called Artificial Magnetic Conductor (AMC), or, ideally, a Perfect Magnetic Conductor (PMC). Soft and hard surfaces are artificially metamaterials that support magnetic conductivity [19]. Generally, a soft surface prevents the wave from propagating, while a hard surface supports the wave to propagate. Transverse corrugations realize an ordinary soft surface. When the length d of corrugation is a quarter wavelength, the short circuit is transformed into an open circuit at the aperture of corrugation, and the surface impedance will be infinite along the direction of propagation. Soft surfaces are used to stop the propagation along it. These features are deployed in corrugated horn antennas with a transverse groove depth of $\lambda/4$ to reduce the side lobe level and decrease side lobes in the E-plane of microstrip and aperture antennas, cross-polarization, and coupling [20]-[21]. In contrast, a typical hard surface can be achieved by filling longitudinal grooves with a dielectric material to make its depth in Equation (2.1). The depth of the corrugation can be depicted using the Equation below,

$$d = \lambda/_4 \sqrt{\varepsilon_r - 1} \qquad \text{...} \quad (2.1)$$

where λ is the free space wavelength, ε_r is the dielectric constant of the material. The hard surface strengthens the wave propagation along the corrugation. When waveguide side walls are hard surfaces, quasi-TEM modes can propagate, and the transverse field distribution is uniform. This concept is used in horns to improve aperture efficiency in the miniaturized array elements in a cluster of horns illuminating a reflector for multi-beam applications [22]-[23].

Ideally, soft and hard surfaces can also be realized using PEC-PMC strips. For a hard surface, the waves propagate along the strips. On the contrary, soft surfaces stop any wave for any polarization and transverse to the direction of the strip. Figure 2.2 graphically illustrates the soft-hard surface realized with PEC-PMC strips relative to the electromagnetic wave propagation direction. The blue arrow indicates the direction in which the signal propagation is prohibited, whereas the yellow arrow reveals the permitted direction. The operation principle is similar to the PEC-PMC strips with a metal plate at the same distance above them, in which the waves propagate only along the longitudinal direction. In contrast, waves are attenuated or stopped in the transverse direction because of the anisotropic characteristic of the PEC-PMC strips [24].

In summary, the invention of soft and hard surfaces introduced the fundamental concept of the gap waveguide. Many applications have been innovated based on this concept in the antennas and electromagnetics research field.

2.2 Electromagnetic Band Gap

PMC does not exist, but it can be realized artificially. Thus, it is called an artificial magnetic conductor (AMC) using periodic structures in a two-dimensional space. Utilizing periodic structures, the Electromagnetic Band Gap (EBG) structure might be an excellent recognition. Electromagnetic Band Gap surfaces are high-impedance surfaces that prohibit propagating waves in all directions with a frequency range because of their isotropic characteristics [25]. The two most common EBG structures are a textured surface made of periodic metal pins named bed of

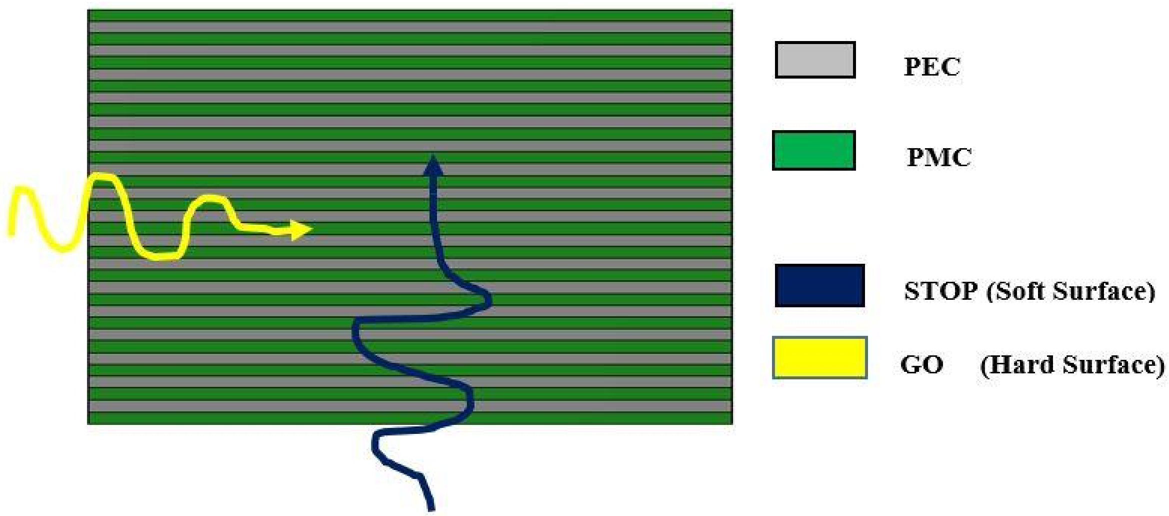

Figure 2.2: PEC-PMC strips along with soft and hard surfaces concerning the wave propagation directions.

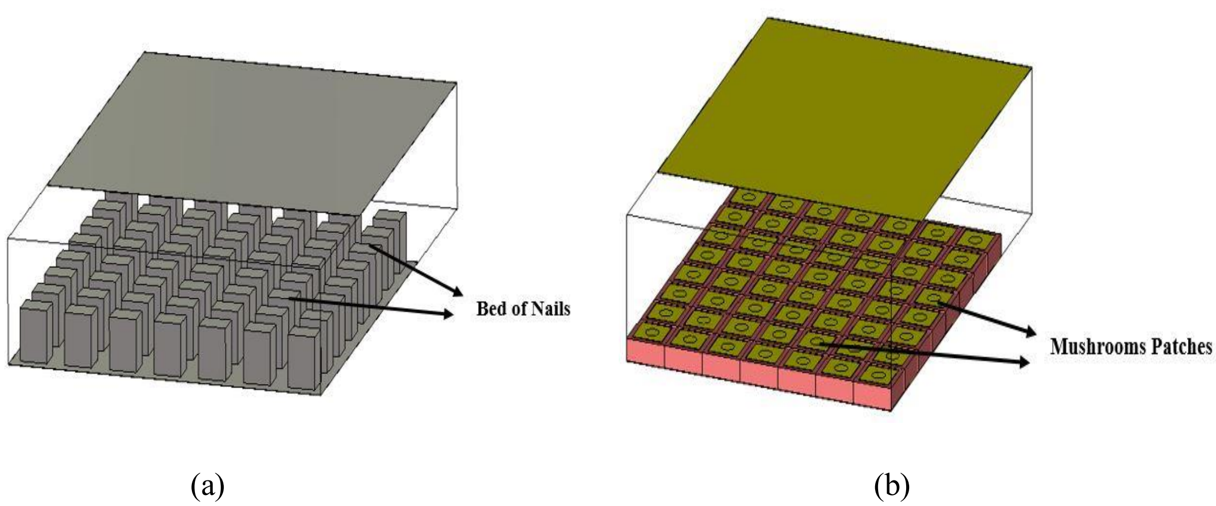

Figure 2.3: EBG realization, (a) Bed of nails in the bottom plate, (b) Mushroom patches on a dielectric substrate.

nails [26] and mushrooms EBG textures [25], depicted in Figure 2.3 (a), (b) where the top ground is kept up for a better view of the periodic surface.

Milling techniques are usually used to realize the bed of nails, and it is metal suitable for high-frequency applications. The pins act as a high-impedance surface within a stop band defined by a lower and upper cut-off frequency. The height of the pins will be in a range of $\lambda /4$ at the lower frequency of the operating bandwidth for transforming the bottom short circuit (PEC) to an open circuit (PMC) at the top of the pins. The pins' cross-section can take different shapes (square, circular, pyramidal, hexagonal, and so on) and are connected to the ground plane by posts through the pins themselves. In order to form a relationship with the dispersion, the stop band of a periodic bed of nails is predicted numerically [27].

Another type of EBG is recognized by replacing the pins with mushrooms on a dielectric substrate using printed circuit board technology. An array of periodic metal patches of various shapes, circular or square, is placed on the top of the surface above a substrate and connected to the ground plane by metal vias. The height of the substrate is usually less than a tenth of a wavelength ($h < \lambda /10$), where the vias are essential to suppress surface waves within the substrate of the structure. Then, the mushroom surface acts as a resonant parallel LC circuit with a surface impedance equal to the impedance of the parallel LC circuit, which creates a very high impedance at the resonant frequency [28]. As a result, the structure becomes very compact and acceptable for low-frequency applications.

2.3 Basic Concept and Operation Principle of Gap Waveguide

In 2009, for the first time, Kildal introduced the idea of gap waveguide technology [13]. A gap waveguide's operation principle is similar to a PEC-PMC parallel plate waveguide. Considering two parallel plates PEC-PMC, no propagation occurs as long as the distance between the plates is less than a quarter wavelength, $\lambda /4$, and all parallel plate modes will be suppressed [29]. By inserting the so-called PEC line inside the PMC surface, the wave propagates along the PEC-PEC line only; there is no propagation in the PEC-PMC region, and it acts as a stopband. Figure 2.4 demonstrates the core concept of gap waveguide. According to the previous explanation, the structure with a bed of nails or mushrooms can create a high impedance surface or EBG, also known as AMC surface, that stops wave propagation within the surface, and the ridge will allow the wave propagation to a certain direction. Hence, the idea of realizing a gap waveguide can be recognized with a metal ridge or grounded strips, which allows wave propagation with the first mode as a quasi-TEM mode to propagate along the metal strip. However, the perception of ridge gap waveguide came from the fundamental gap waveguide concept by Kildal as well. The following section will detail the ridge gap waveguide with an example.

In addition, a parallel plate cut-off region is also created in the air gap between PEC and PMC, which works as a high pass filter or low pass filter. This parallel plate waveguide that supports TEM mode is a zero cut-off mode, but no leakage happens in the case of sidewalls. Figure 2.5 illustrates the zero cut-off region with sidewalls of parallel plate waveguide.

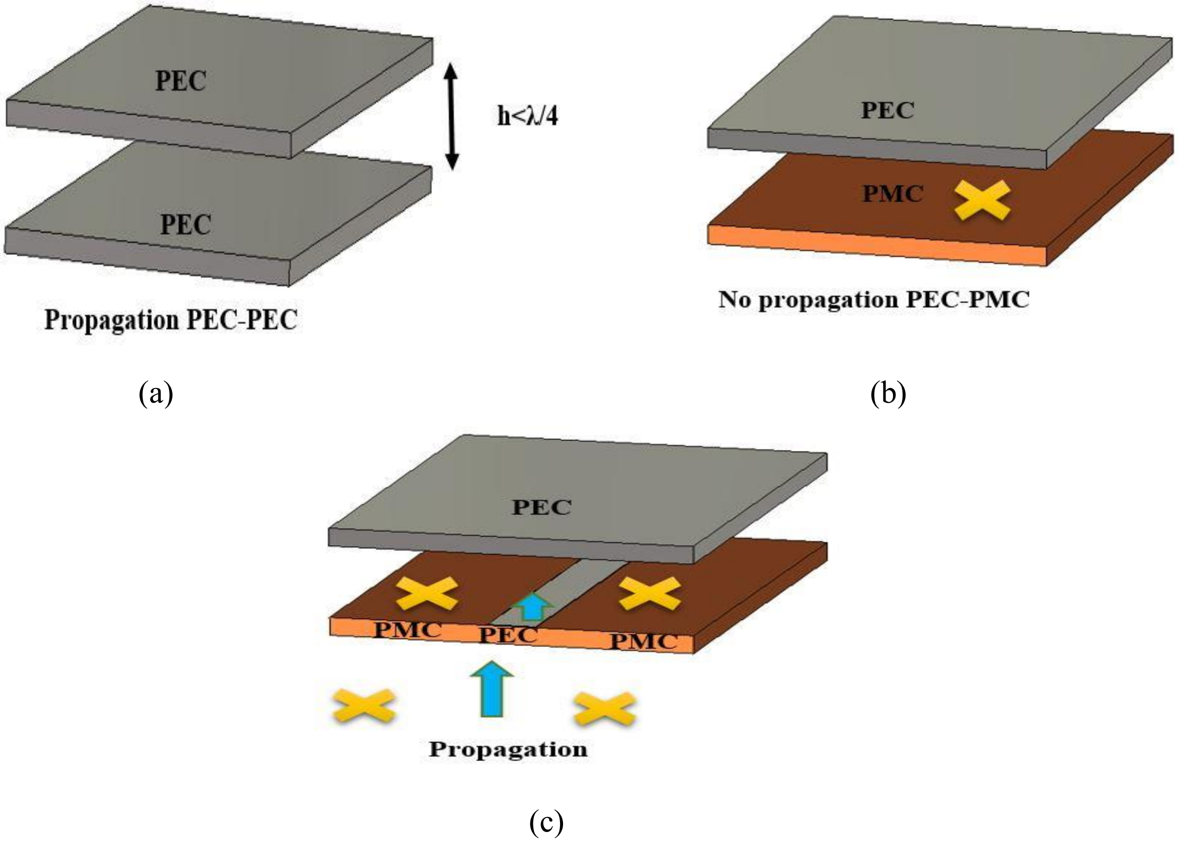

Figure 2.4: (a) PEC-PEC parallel plate (wave propagation), (b) PEC-PMC parallel plate (no wave propagation, and (c) Ridge embedded within the PMC bottom surface and upper surface PEC (wave propagate along with ridge PEC-PEC)

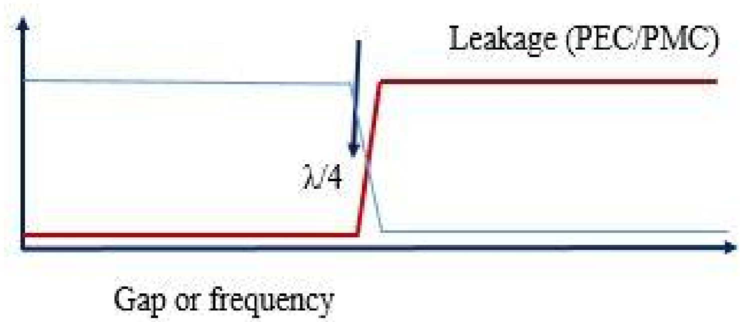

Figure 2.5 Zero cut-off region with no leakage from the side of the parallel plate waveguide.

2.4 Ridge Gap Waveguide

One of the popular guiding structures of a gap waveguide is the ridge gap waveguide. The idea of a ridge gap waveguide was derived by Professor Kildal in 2009 [13] and was patented in 2010-2011 as well [30]. The realization of a ridge gap waveguide is two parallel plates, one plate with periodic texture to eliminate the wave propagation in all directions except the desired path, and the upper plate is a smooth metal lid. The bed of nails or mushroom patches creates high surface impedance that stops wave propagation by installing a ridge within the periodic structure to perturb the periodicity and allow wave propagation to require directions. Still, other types of AMCs can be used around the ridge if necessary. When the ridge is presented, a quasi-TEM mode is established and propagates along the ridge within the stop band, and all other higher-order modes are forced to be cut off by the periodic bed of nails. This structure has no dielectric losses because it uses metal pins only. The ridge line does not need to be straight; it could be a bend line or split into several branches; no matter how it is, the field will follow the paths of the ridge. The bottom plate consists of a periodic structure that controls the band gap of the waveguide; it might be a bed of nails or mushroom patches. The separation between the ridge and the top metal should be less than λ /4 for propagation. There are no sidewalls as rectangular waveguides in a ridge gap waveguide; consequently, no leakage from the walls happens in a ridge gap waveguide.

The ridge gap is considered one of the most promising guiding structures due to low loss and high power handling capacity in millimeter-wave applications. It is also suitable for higher-frequency RF circuits and passive devices. For example, power dividers, bend transmission lines, and couplers could be designed in ridge gap waveguides [31]-[32]. Figure 2.6 portrays the ridge gap waveguide with the top ground plane moved up to show the geometry in detail for better understanding.

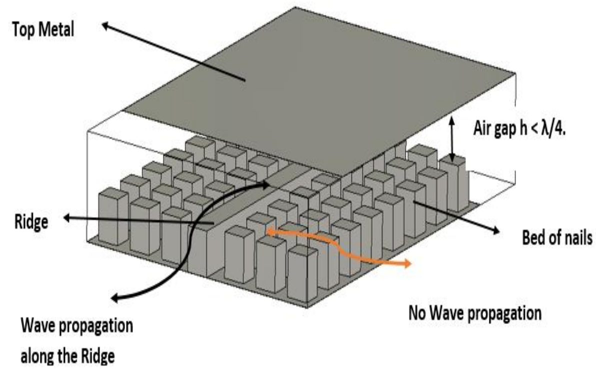

(a)

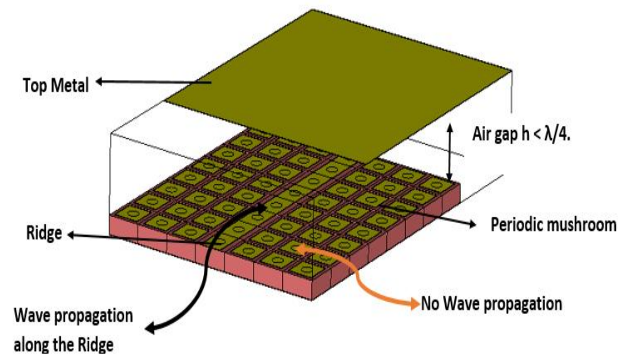

(b)

Figure 2.6: Ridge gap waveguide, (a) Ridge surrounded by metal pins or bed of nails, (b) Ridge confined by periodic mushroom patches.

2.5 Unit Cell Analysis

The basic building block of the ridge gap waveguide is the unit cell. In order to get different operating frequency ranges, a variety of shapes of unit cells can be designed. These could be circular, square, rectangular, and pyramidal, for pins and mushroom-type unit cells have circular or square patches. The first trial of the ridge gap waveguides is the nails with rectangular and circular shapes published as a basic shape with cross-section [30]. To increase the operating band, another shape, such as the pyramid-shaped unit cell, is considered; this technology, with the microstrip line technology, is called the packaging process [31]. As described in the previous section, the stop band of the unit cell provides the bandwidth where the structure suppresses the leakage outside the ridge. However, the stop band of the unit cell corresponds to the possible operating bandwidth of the entire ridge gap waveguide structure. EBG (electromagnetic bandgap) or AMC (Artificial magnetic conductor) can easily be recognized with the help of a bed of nails or mushroom cells in 2D or 3D. The unit cell controls the band gap of the ridge gap waveguide

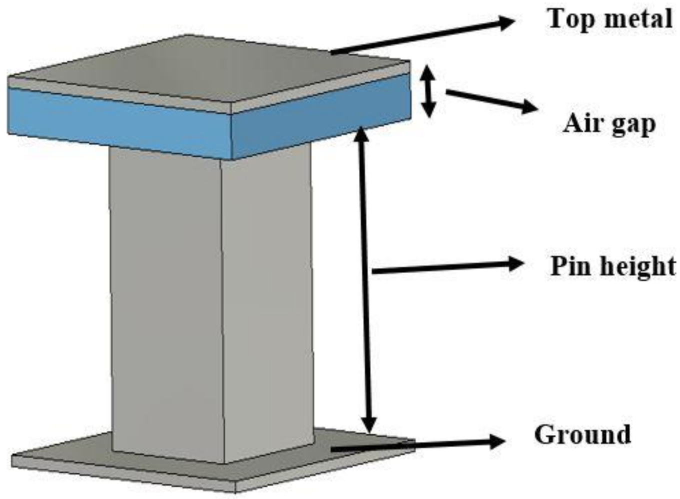

(a)

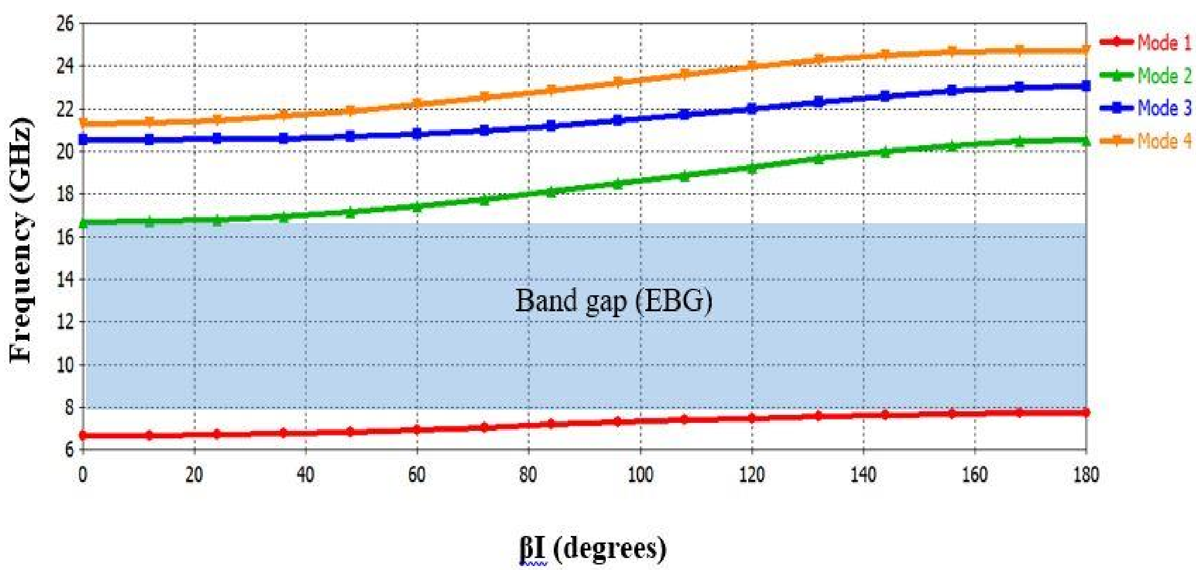

(b)

Figure 2.7: Unit cell of ridge gap waveguide (a) Geometry of unit cell structure, (b) Dispersion diagram of unit cell covering the band gap (8-16.5) GHz.

using the AMC surface. The bandgap of the unit cell is acquired from the Eigenmode solver of CST Microwave Studio software. Four important unit cell parameters play an outstanding role in changing the stop band.

First is the air gap between the two conducting plates where waves propagate. After that, the pin height or via height for mushroom cells. The next one is the radius of the pins or via. Finally, pin-to-pin distance or via-to-via distance represents the periodic structure's period. Changing these four parameters makes it possible to choose the bandgap according to the designer's requirements. Including these above four parameters, the shape of the unit cell has a vast effect on enhancing the bandwidth of the operating frequency of interest [33]. Figure 2.7 (a) illustrates the structure of the unit cell, and (b) represents the dispersion diagram of the corresponding unit cell where the stop band gap is (8-16.5) GHz. Thus, the band gap and frequency could be changed after changing the unit cell parameters.

2.6 Other Types of Waveguide

Except for ridge gap waveguides, there are some other types of gap waveguides available, the basic operating principle of which is similar to that of the gap waveguide. Still, the design and propagation paths are a little different. The most popular waveguide is the inverted microstrip ridge gap waveguide. Another common waveguide is the groove gap waveguide. The last, not on the list, is the microstrip ridge gap waveguide. The following section briefly discusses these three gap waveguides with pictorial examples.

2.6.1 Inverted Microstrip Gap Waveguide

The construction of an inverted microstrip gap waveguide is the substrate supported by the artificial magnetic conductor, which means the microstrip is loaded on top of the substrate above the bed of nails. As a result, the AMC forces the field to propagate in the air gap between the microstrip lines and the upper top metal [34]. The major benefit of the inverted gap waveguide is that it can be easily adapted to printed circuits. Due to propagation in the air, it has low dielectric losses. In order to match with 50 Ω line impedance in the air, a wider line can be used so less conduction losses happen in the inverted microstrip gap waveguide. The major problem associated

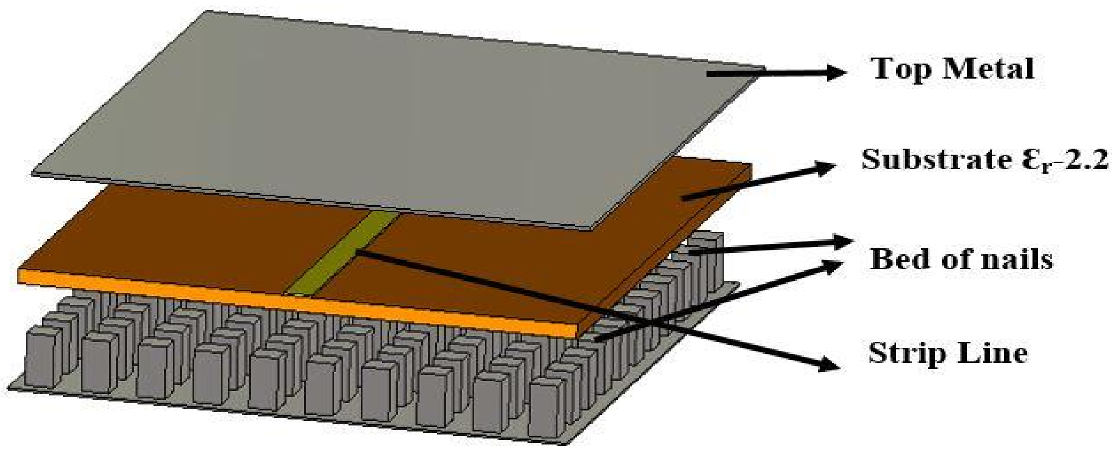

(a)

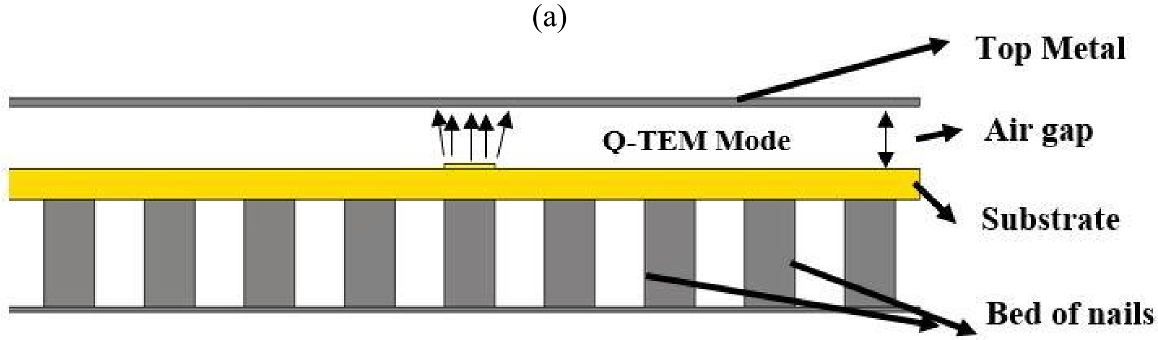

(b)

Figure 2.8: (a) The geometry of the inverted microstrip gap waveguide and (b) Cross-section view of the inverted microstrip gap waveguide where Q-TEM mode propagates.

with that at a certain operating frequency range of the microstrip line is that the inverted microstrip gap waveguide with pins becomes bulky. Figure 2.8 shows the geometry of the inverted microstrip gap waveguide made of AMC surface with metal pins and substrate and the cross-section view of this structure. The substrate used in this design is Roger RT5880, with a relative permittivity of 2.2, and the line width of the strip line is 4 mm. A quasi-TEM mode could be observed from the field distribution of the structure.

2.6.2 Groove Gap Waveguide

The groove gap waveguide is one of the most popular waveguides for mm-wave applications and

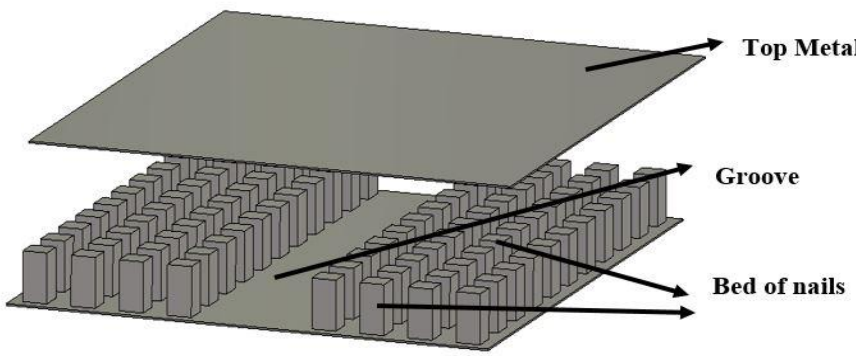

(a)

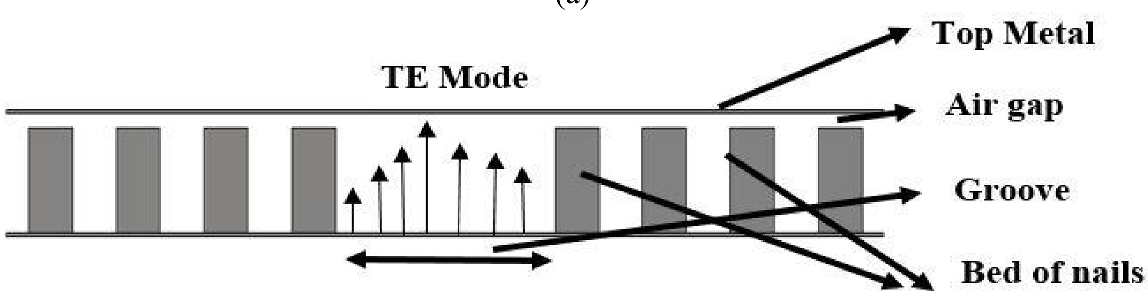

(b)

Figure 2.9: (a) The complete structure of the groove gap waveguide and (b) Cross-section view of the groove gap waveguide where TE_{10} mode is the dominant mode.

is suitable for high Q-factor filter designs [35]. In a groove gap waveguide, there is no ridge in the bottom plate, whereas the ridge is replaced by a groove embedded with pins on both sides of the structure. The working principle of a groove gap waveguide is similar to a rectangular waveguide because the groove gap waveguide supports TE/TM modes [36] with the merits of having no electric contact between two metal plates. The dominant mode of the groove gap waveguide is the same as the rectangular waveguide of TE_{10}. Due to the removal of the ridge in the groove gap waveguide, there is a large volume for current density; as a result, the losses are lower in the groove waveguide than in the ridge gap waveguide. The performance of the groove gap waveguide is more outstanding than that of other gap-type waveguides. Groove gap waveguide supports dual polarization, making it more beneficial for horn antenna applications. Low attenuation is one of the key advantages of groove gap waveguides. Figure 2.9 depicts the complete structure of the groove gap waveguide, where metal pins and the cross-section view of the groove gap waveguide surround the groove.

2.6.3 Microstrip Ridge Gap Waveguide

The working principle of microstrip ridge gap waveguide is similar to suspended microstrip lines, whereas the mushroom patches behave as AMC high surface impedance and wave propagate through microstrip ridgeline. The microstrip line is loaded on top substrate-connected metal vias, and mushroom surfaces are implanted on either side of the microstrip line. The propagation mode in ridge gap, inverted microstrip ridge, and microstrip ridge gap waveguide are equivalent to Q-TEM mode. The EM waves propagate through the microstrip line between the air gap and the upper top metal. The shape of mushroom patches might differ based on the designer's preference, such as square, rectangular, circular, etc. It is a printed version of a ridge gap waveguide with less conduction losses. This mushroom version of the microstrip ridge gap waveguide is more compact and suitable for low-frequency applications and other packaging techniques [27]-[28]. The fabrication time and technique are easier and faster than other gap waveguides. Figure 2.10 shows the layout of the microstrip ridge gap waveguide where the mushroom surface works as EBG and the cross-section view of the microstrip ridge gap waveguide.

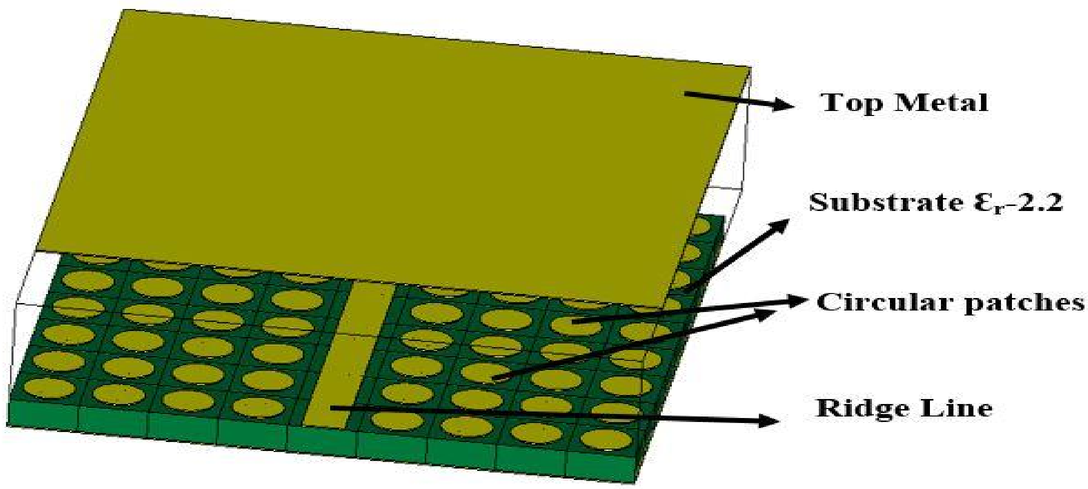

(a)

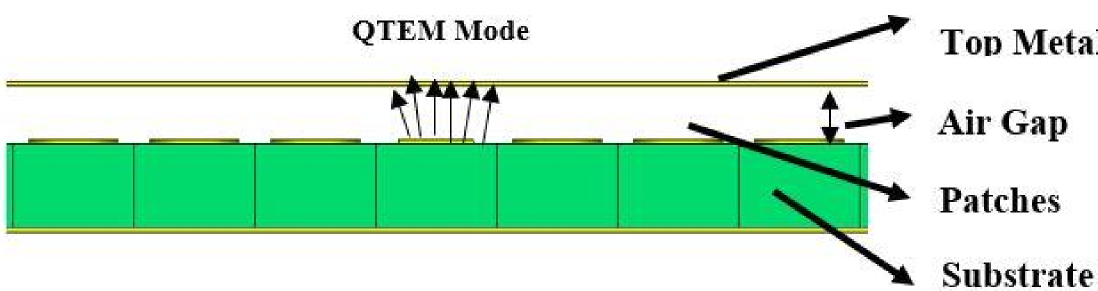

(b)

Figure 2.10 (a) The layout of the microstrip ridge gap waveguide and (b) Cross-section of the microstrip ridge gap waveguide.

In brief, the basic theory of gap waveguide technology, as well as the fundamental concept of EBG, is discussed in this chapter. Various types of gap waveguides, such as ridge gap waveguide, groove gap waveguide, inverted microstrip gap waveguide, and microstrip ridge gap waveguide, are described with geometry and cross-section view showing each waveguide's propagation mode. The propagation mode of all gap waveguides is Q-TEM mode, excluding the groove gap waveguide with TE mode to propagate. Unit cell analysis is also presented with a dispersion diagram in this chapter. Gap waveguide has low fabrication costs and less complexity. It is more compact and can be used in small devices, which is one of the main advantages of gap waveguide. The ridge gap waveguide is the most popular among all the gap waveguides. These waveguides are appropriate for low- and high-frequency applications, even at millimeter frequency and above. However, Gap waveguides, especially ridge gap waveguides, are now more popular for short and long-distance communication.

Chapter 3

Proposed Dual Band Unit Cell

Over the past few years, scientists and researchers have been doing intensive research on Electromagnetic Band Gap (EBG) structures, especially for their ability to suppress surface waves within a frequency band. Two particular properties of EBG that grab the researcher's attention are

1) To prevent the propagation of an electromagnetic wave within a frequency bandgap and

2) To exhibit frequency windows inside the band gap when the structure periodicity is broken due to the appearance of some defects of any structure.

These properties are extremely beneficial to realize high-gain antenna applications using EBG structures. However, EBG surfaces have a high surface impedance that blocks propagating waves in all directions within a frequency range because of their isotropic characteristics. EBG structures can be understood with two common periodic surfaces used in gap waveguides: periodic metal pins and mushroom-type texture structures [37]-[38]. Depending on the characterizations of the frequency band that will be propagated or prohibited, EBG structures can function as a bandpass filter or a bandstop filter [25], [39]-[40]. The basic building block of a gap waveguide is the EBG unit cell. The EBG unit cell can be of many shapes based on the required operating frequency ranges. The most common shapes are squire, circular, rectangular, and so on [30]. To expand the bandwidth of the structure, other shapes were incorporated, such as unit cells in the pyramid shape [31]. EBG is used in gap waveguide and antenna design to prevent leakage outside the ridge edges. The EBG can also be called stopband, within which the waveguide's operating bandwidth. Thus, the EBG controls the waveguide's operating bandwidth [26], [41]. Commercial software called

CST microwave studio is utilized for constructing and analyzing unit cells, and an Eigenmode solver is employed from CST to get the dispersion diagram. At the beginning of this chapter, a conventional single-layer unit cell is created and simulated for pins and mushrooms, along with a dispersion diagram of a row of cells with a center ridge. The proposed dual-band unit cell with a dispersion diagram and operating modes is described in the later portion of the chapter with the parametric studies that affect the stop-band gap of a cell. In addition, a mushroom cell looking downward and a dual-band 9 mushroom patches unit cell are also proposed with a dispersion diagram and row of a finite number of cells.

3.1 Conventional Single-Layer Unit Cell Analysis

The typical unit cell comprises a single layer of various shapes, such as metal pins and mushroom patches. To build the pin structure, two PEC conducting plates are attached to the ends of the pins, and an air gap is created above the pins between the PEC plates. These pins or mushrooms create AMC surfaces that are high impedance and stop the electromagnetic waves from propagating. Another periodic structure of the traditional unit cell is a mushroom texture surface with various shapes of patches, for example, circular, square, or pyramidal. The Eigenmode solver of the CST software is used to construct and simulate unit cells. The unit cell regulates the bandgap and operational bandwidth of the waveguide using the AMC surface.

3.1.1 Single-Layer Metal Pin Unit Cell

The first gap waveguide attempts used the unit cell's basic shapes, which were rectangular-shaped metal pins [30],[37]. After that, circular-shaped pins became popular for different frequency ranges. To analyze a standard EBG unit cell, a square metal pin unit cell is constructed with a cell size of 2mm. The height of the pin is 2.5 mm. It is connected with the ground metal plate (PEC), an air layer is placed above the pin whose dimension is 0.254 mm, and the thickness of the top and bottom metal plates is 0.015 mm. The width of the pin is 1.4mm. The periodic pins structure is built entirely of metal, and the periodic pins are produced using milling techniques. The pins

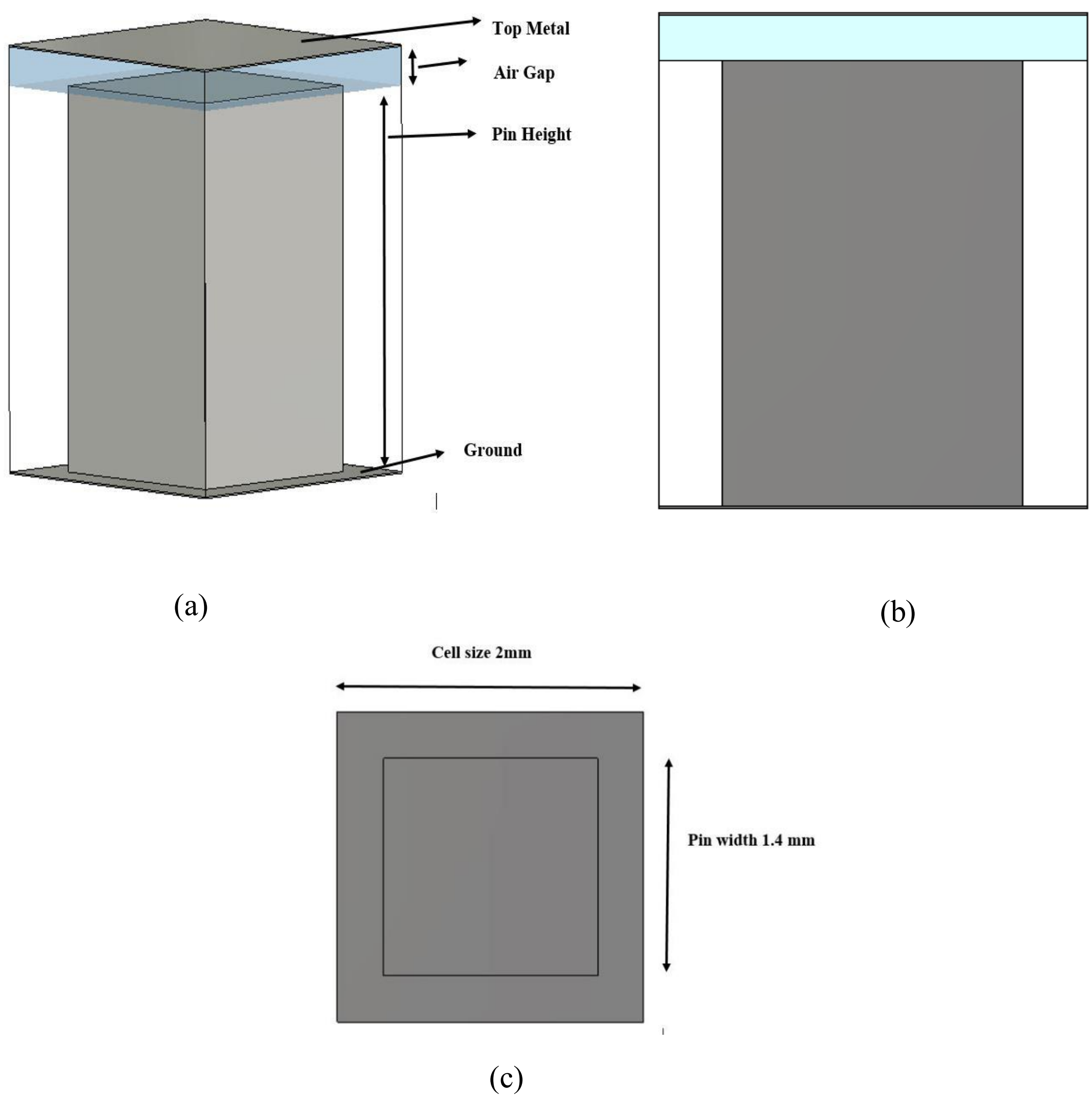

Figure 3.1: The geometry of pin unit cell (a) Unit cell with dimensions, (b) Cross-section view of the cell, and (c) Top view of pin cell.

function as a high-impedance surface within a stopband determined by a lower and an upper cut-off frequency. Figure 3.1 shows the geometry of the pin unit cell. However, based on the operating bandwidth's center frequency, the pins' height will be in a range of λ /4. Figure 3.2 provides the dispersion diagram for a periodic infinite pin unit cell. From the dispersion diagram, it can be observed that the first fundamental TEM parallel-plate mode or QTEM mode begins at zero frequency, and afterward, it veers off the light line and enters a cut-off below 25 GHz, emerging

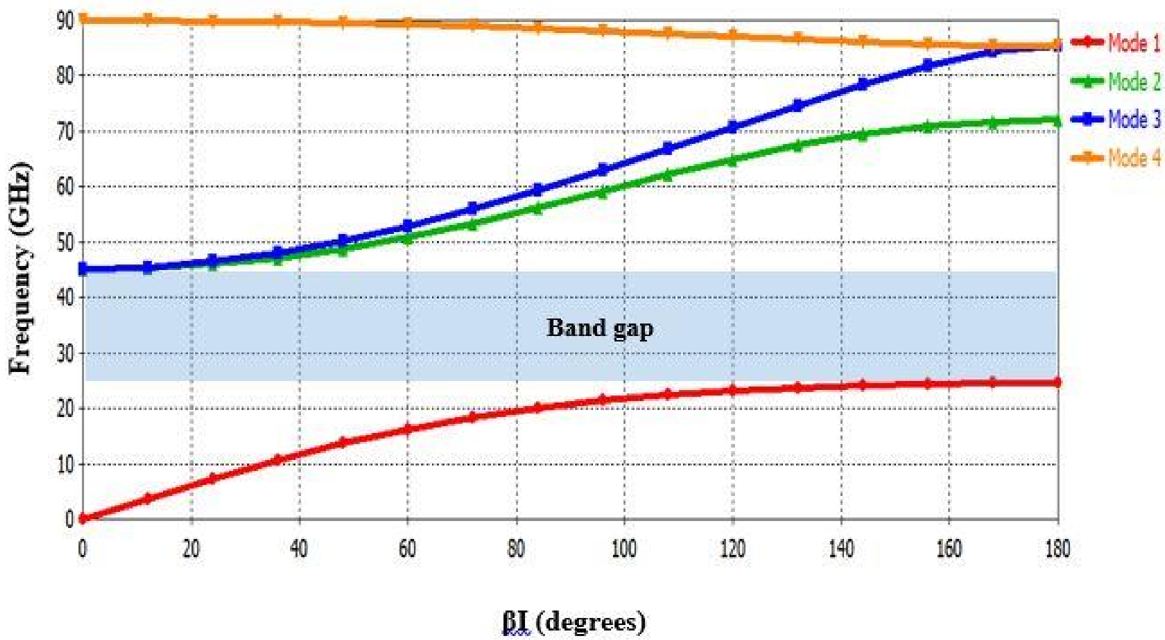

Figure 3.2: Dispersion diagram of a metal pin unit cell where the band gap is about (25-45) GHz.

again above 45 GHz. As a result, the band gap of the unit cell of the pin becomes (25-45) GHz. The air gap has a great influence on determining the stop band of the unit cell. If the air gap width between the pins and top metal is large, the stop band narrows or vice versa. Other parameters of the unit cell, such as pin height, pin width, and pin-to-pin distance, impact the band gap of the unit cell. Figure 3.2 clearly shows the band gap of the metal pin unit cell. Here, four modes are illustrated and represented by the dispersion diagram's bold blue color. The band gap can be noticed between modes 1 and 2. The x-axis provides the angle, and the y-axis provides the frequency of the dispersion diagram. However, the operating bandwidth of any gap waveguide based on this unit cell is 25-45 GHz.

3.1.2 Row of Unit Cell

The row of unit cells is the finite number of cells, and the middle pin is replaced by the ridge that allows electromagnetic waves for propagation. Periodic boundary conditions are applied to get an acceptable result. The dimension of each cell is the same as the unit cell. Figure 3.3 shows the construction of a row of cells and 3 periodic unit cells on both sides of the ridge with dimensions (a), (b) the cross-section view of cells, and (c) the top view of the row of cells. The row of cells is separated from the upper top metal by an infinite air gap sized 0.245mm along the z direction. The height of the row of pins is the same as the height of the pin. The ridge width is 1.4 mm, and the length is 2mm. A quasi-TEM mode is created and propagated within the stopband when the ridge is present. When a ridge is established, the bed of nails forces all other higher-order modes to be cut off.

The ridge does not have to be straight because the field will follow it even if the path is curved, bends, or splits into multiple branches. Figure 3.4 exhibits the dispersion diagram of the row of pin unit cells. Here, 9 modes are presented. It is evident from Fig. 3.4 that the stopband ranges from 25-45 GHz; within this range, mode no 7 is the only propagating mode. The propagating quasi-TEM mode is presented by a solid black line within the stop band. The light line, represented by the dashed black line, is used to portray the pure TEM mode in the substrate. Electromagnetic waves can propagate with this band along with a ridge through the air gap.

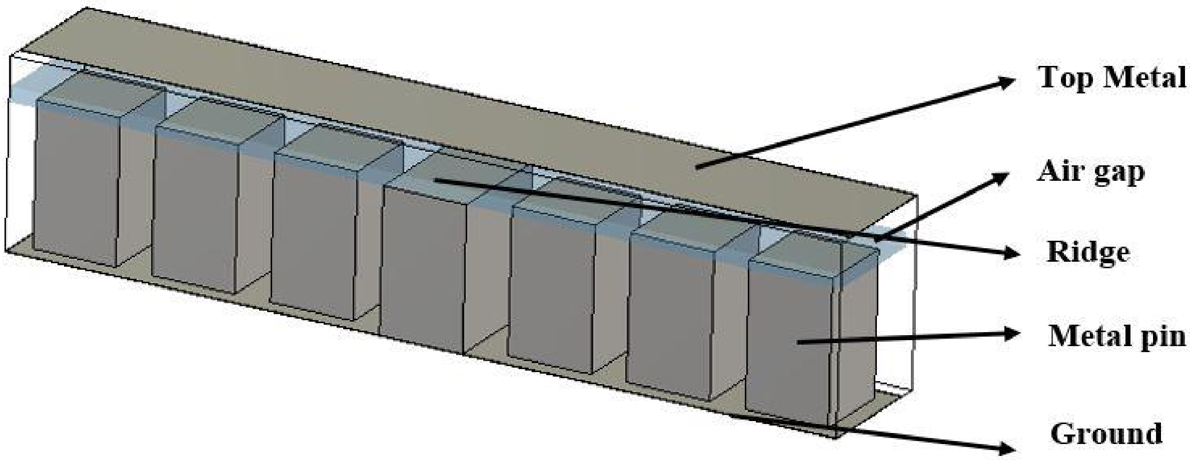

(a)

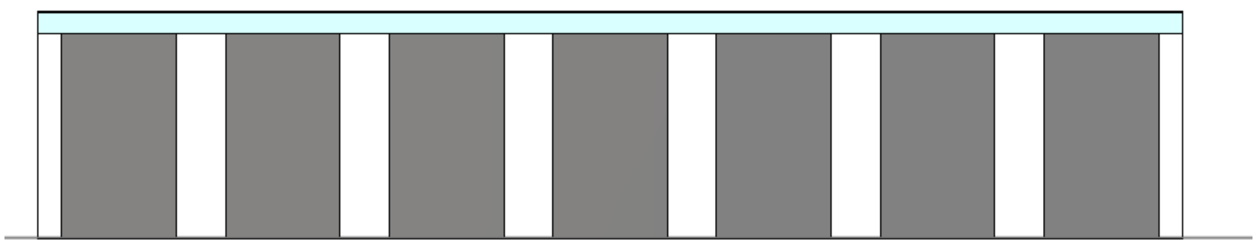

(b)

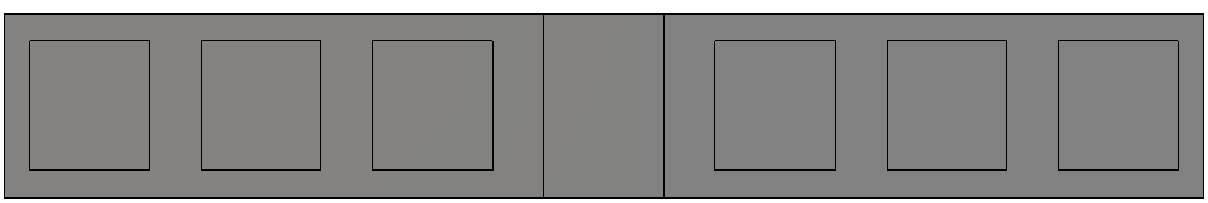

(c)

Figure 3.3: The layout of the row of pins with a ridge in the central (a) Row of pins with dimensions, (b) Cross-section view, and (c) Top view of row pins cell.

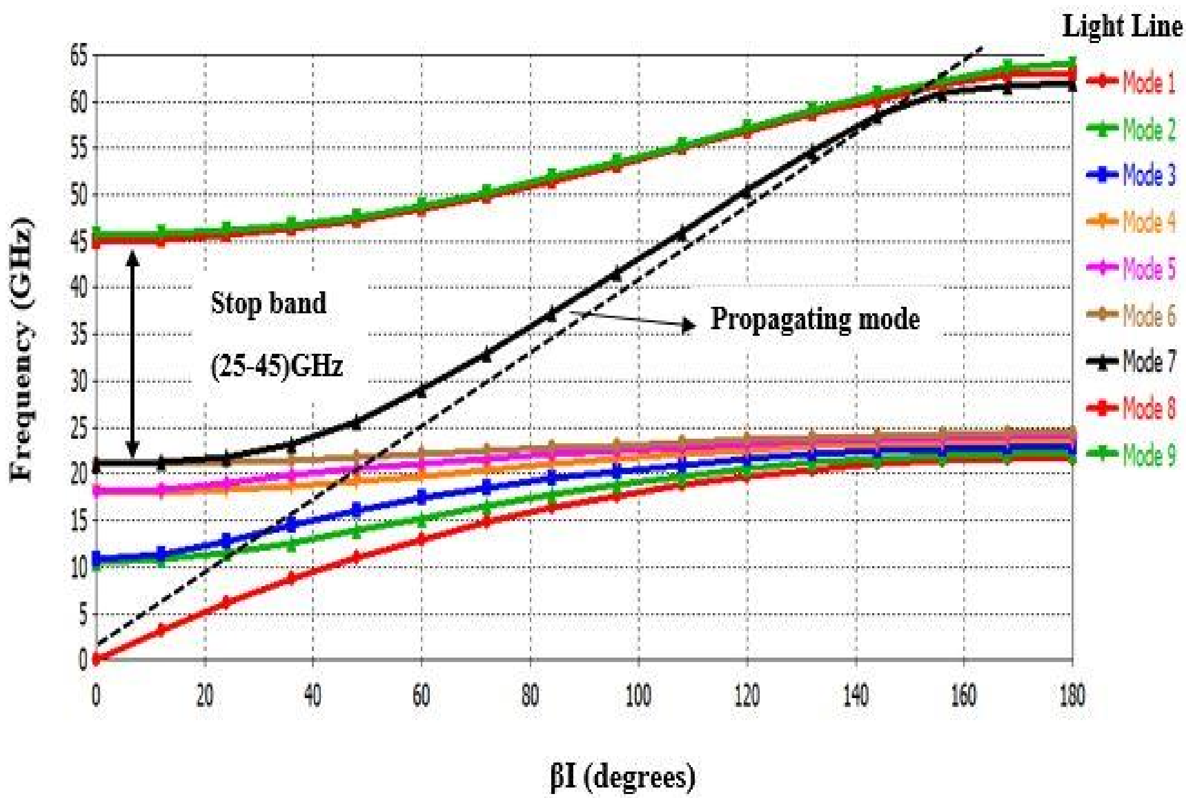

Figure 3.4: Dispersion diagram of the row of metal pin unit cells where mode 7 is the propagating mode.

3.1.3 Single Layer Mushroom Patch Unit Cell

The other types of common texture surfaces in EBG are mushroom types. The mushroom-type unit cell and patches can be circular, square, rectangular, pyramidal, etc. [38]. The mushroom-type surface is recognized with the printed circuit board technology [42]. A metal patch is placed on top of the substrate connected to the ground via holes to build the mushroom unit cell. The vias are required to suppress surface waves within the substrate when usually the height of the substrate is less than a tenth of a wavelength ($h < \lambda /10$). The air gap is between the patch and the top metal lid for wave traveling.

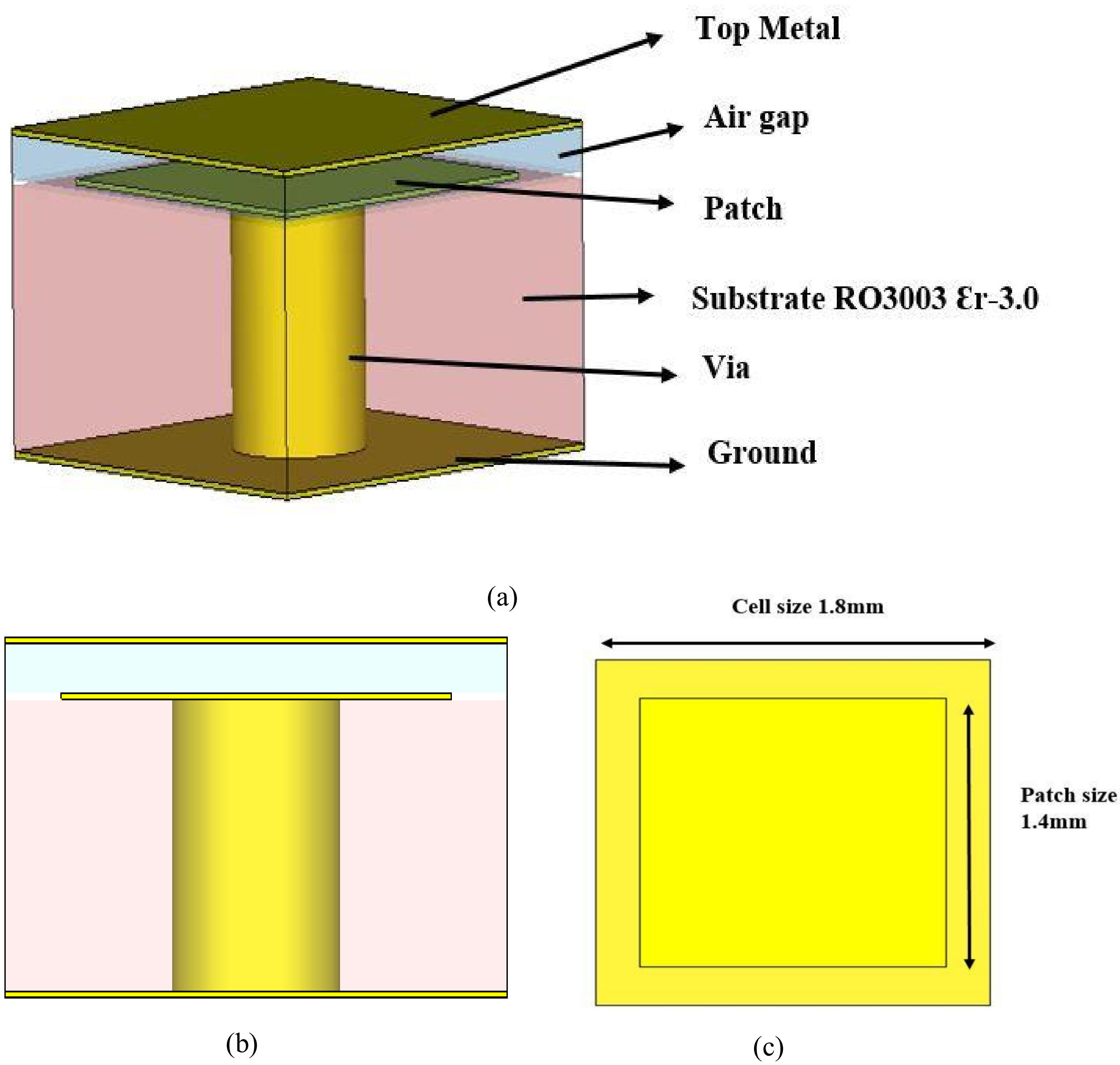

Figure 3.5: Configuration of mushroom patch unit cell (a) Mushroom patch with dimensions, (b) Cross-section view, and (c) Top view of the mushroom patch cell.

The mushroom surface acts as a resonant parallel LC circuit with a surface impedance equivalent to the impedance of the parallel LC circuit that becomes very high at resonance frequency [40]. The structure of the mushroom texture is very compact and appropriate for low-frequency applications. Figure 3.5 represents the configuration of the mushroom patch unit cell: (a) the mushroom cell with dimensions, (b) the cross-section, and (c) the top view of the cell. The cell size is 1.8 mm, and the patch size is 1.4mm. The via diameter is 0.3mm, which is copper metal. The substrate has RO3003 with permittivity of $\mathcal{E}r$ 3.0 having a thickness of 0.75 mm. The air gap from the patch to the upper plate is 0.254mm. The dispersion diagram provided by an EBG infinite periodic unit cell of the mushroom-type patch inside a parallel plate construction is depicted in Figure 3.6. The band gap is about 22-48 GHz, indicated by the green bold color. The stop band is displayed between modes 1 and 2, which are vertically polarized waves. Four modes are presented in the dispersion diagram from the Eigenmode solver of CST software.

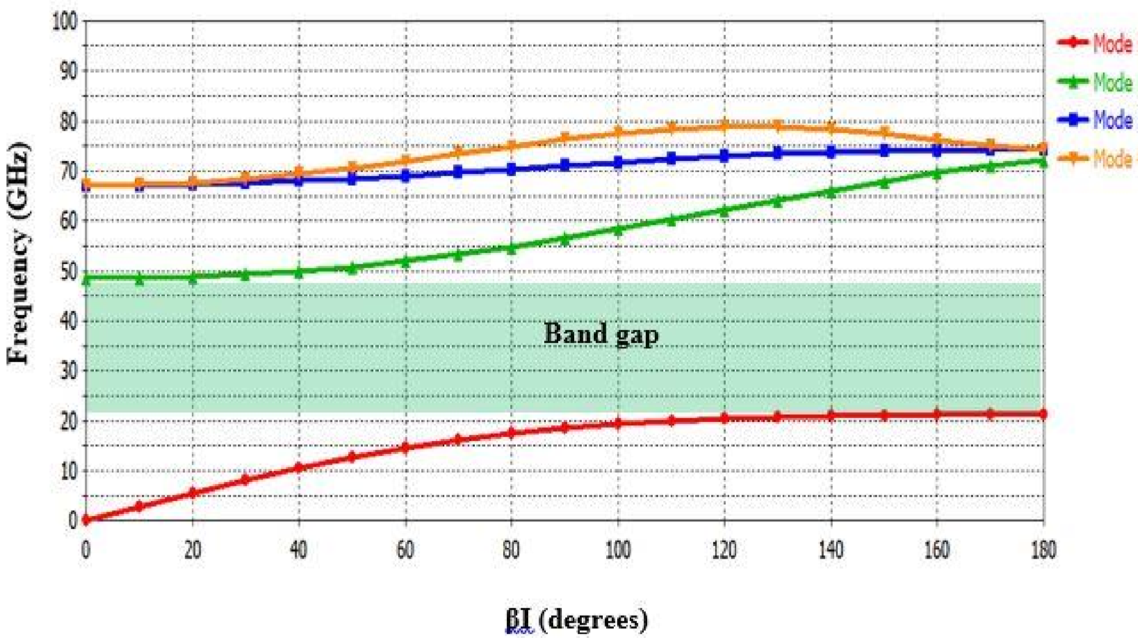

Figure 3.6: Dispersion diagram of mushroom patch unit cell where the band gap is about (22-48) GHz.

3.1.4 Row of Mushroom Patch Unit Cell

The row of unit cells is the recurrence of the same cells in 1D or 2D a finite number of times. To form a mushroom row of cells, the middle patch is replaced by a ridge patch and periodic boundary conditions are applied to get a satisfactory result. The width and length of the ridge patch are 1.4 and 1.8mm, respectively. The dimension of the row of cells is the same as that of the mushroom patch. In a row of cells, 3 cells are situated on both sides of the ridge patch. Waves propagate through the ridge patches, shown in the propagating mode in the dispersion diagram. Figure 3.7 portrays the row of cells of mushroom patches with dimensions (a), (b) the cross-section view, and

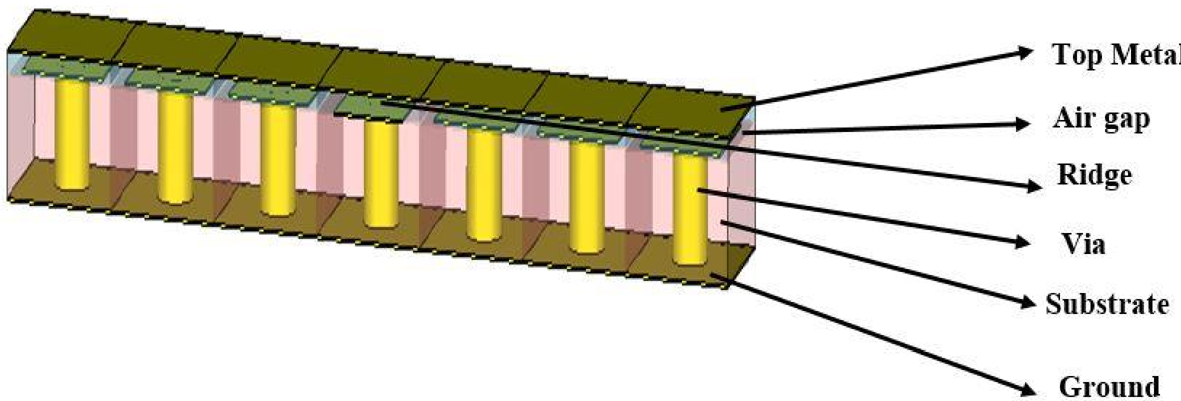

(a)

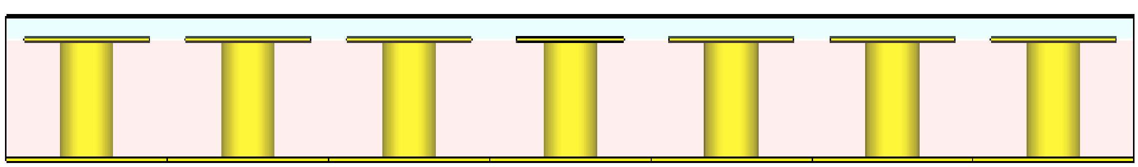

(b)

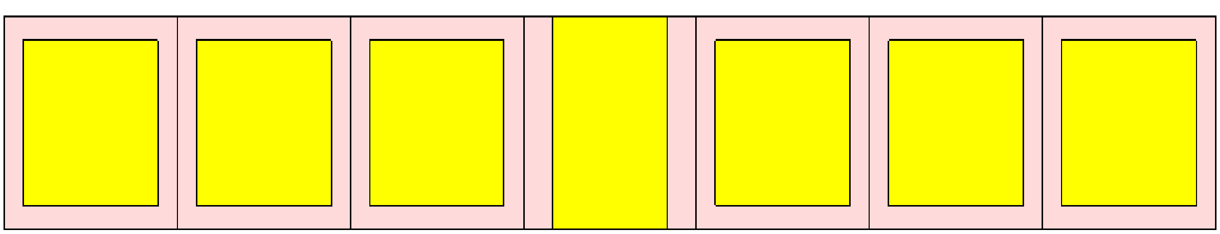

(c)

Figure 3.7: Geometry of a row of mushroom patch unit cells with a ridge in the central (a) Row of mushrooms with dimensions, (b) Cross-section view, and (c) Top view of a row of mushroom cells.

(c) the top view of a row of mushroom patch cells. A Q-TEM or TE mode is initiated when a ridge is presented in the cell's row and propagates within the band gap. Figure 3.8 illustrates the dispersion diagram of the row of cells where 10 modes are established. As can be seen, only mode no 7 is propagating with the band gap, which is (22-48) GHz. A solid black line within the band represents the propagating quasi-TEM mode. The light line, presented by the dashed black line, is used to depict the pure TEM mode in the substrate.

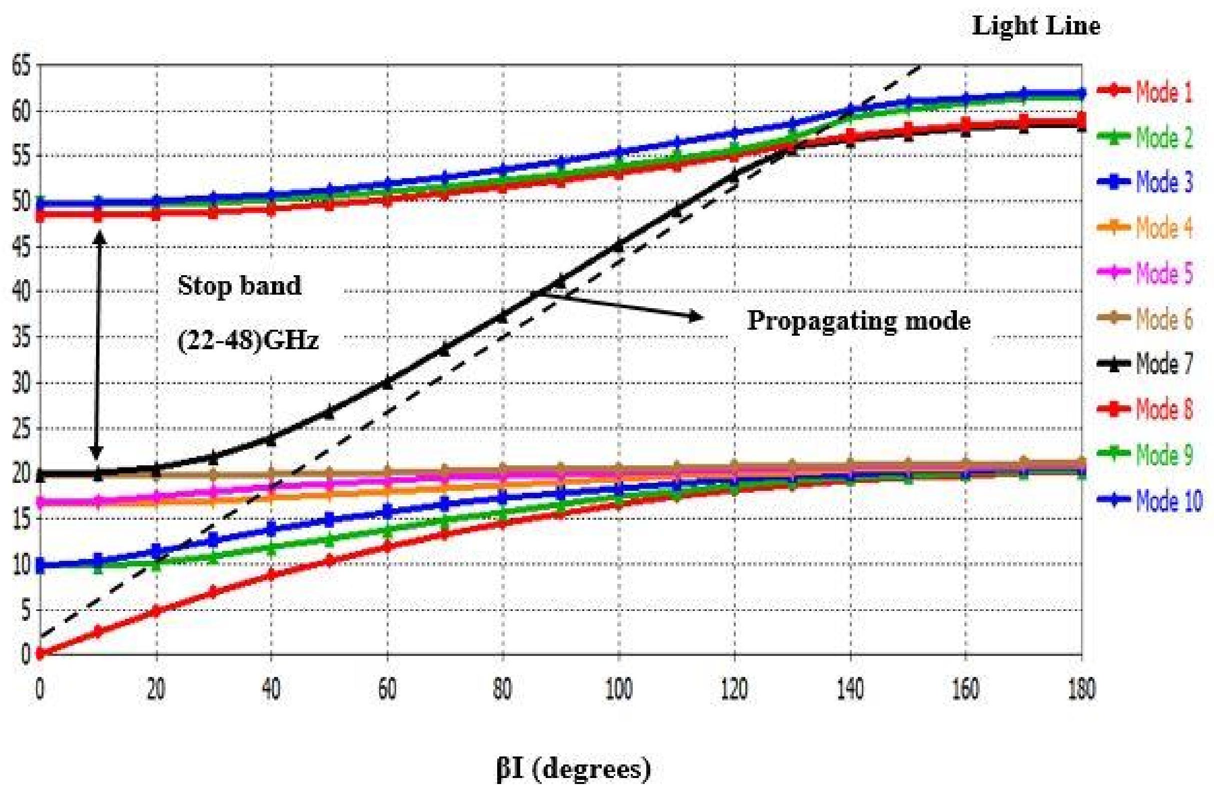

Figure 3.8: Dispersion diagram of a row of mushroom patch unit cells where mode no 7 is a propagating mode.

3.2 The Proposed Dual-Band Unit Cell

The proposed unit cell is designed to achieve dual-band. Each unit cell layer is stacked like a

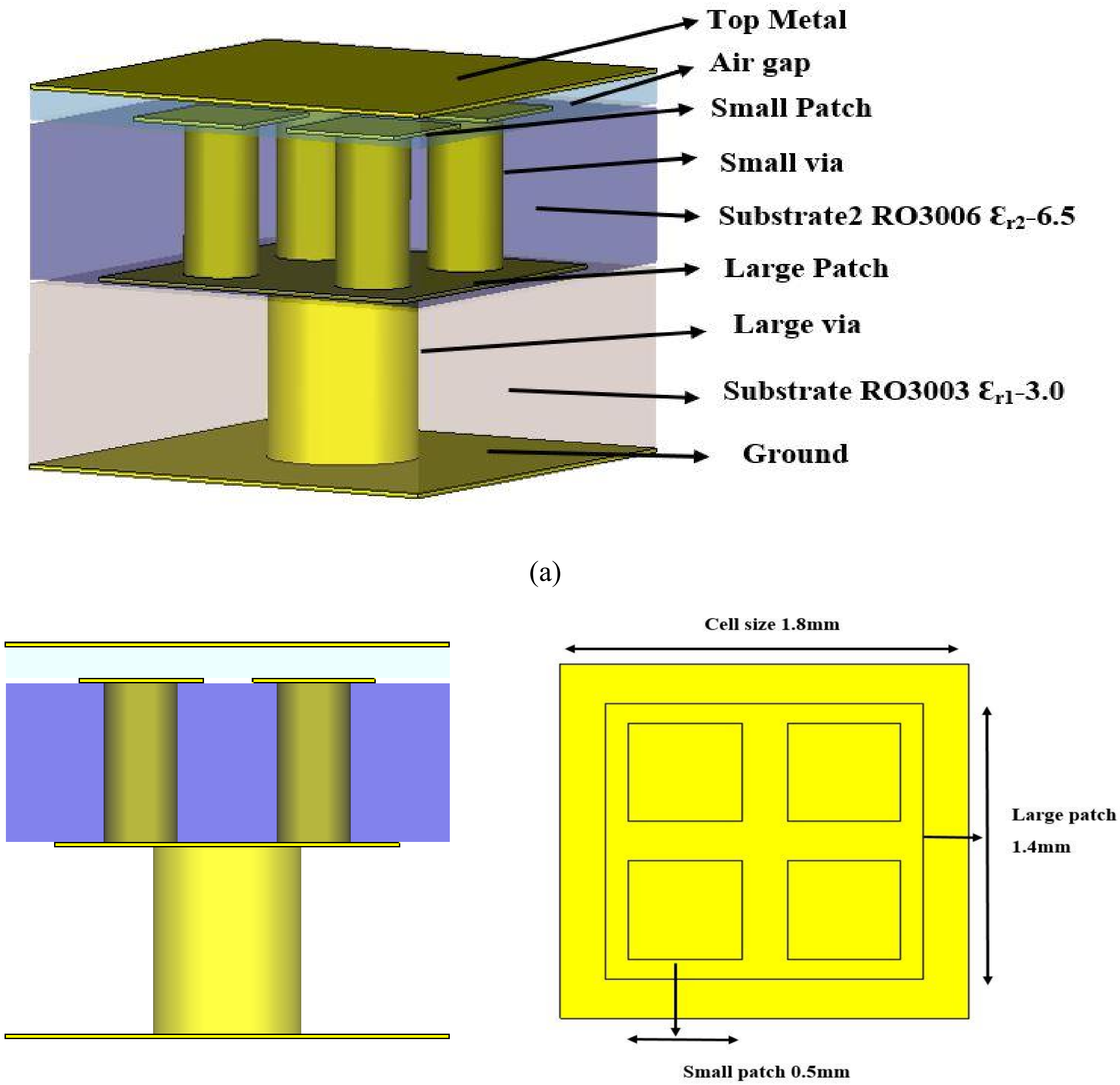

(b) (c)

Figure 3.9: Layout of dual-band mushroom patches unit cell (a) Mushroom patch with dimensions, (b) Cross section vision, and (c) Top vision of proposed mushroom patches.

sandwich on top of each other. The unit cell geometry consists of double substrates with a single mushroom patch in the lower substrate connected to the ground plane by conducting via. Four smaller mushroom patches are assigned in the second substrate; each is connected to the large patch by conducting vias. Figure 3.9 depicts the full structure of the proposed dual-band unit cell. The unit cell is 1.8mm, with square patches on both layers. The lower substrate RO3003 with permittivity $\mathcal{E}r1$ of 3.0 and upper substrate RO3006 with permittivity $\mathcal{E}r2$ of 6.5, with a thickness of 0.75 mm and 0.64 mm, is used for the mushroom patch unit cell. To construct the large patch, the width, via radius, top and bottom metal thickness is kept at 1.4 mm, 0.3mm, 0.0175 mm, as well as for the small patch width, small via radius are also kept at 0.5 mm, 0.15 mm. The air gap between the top metal lid and upper layer patches is about 0.127 mm. The stopband, which specifies the operating bandwidth of the structure, can be used to measure the performance of the unit cell. The EBG surface behaves like a high-impedance surface inside this bandwidth.

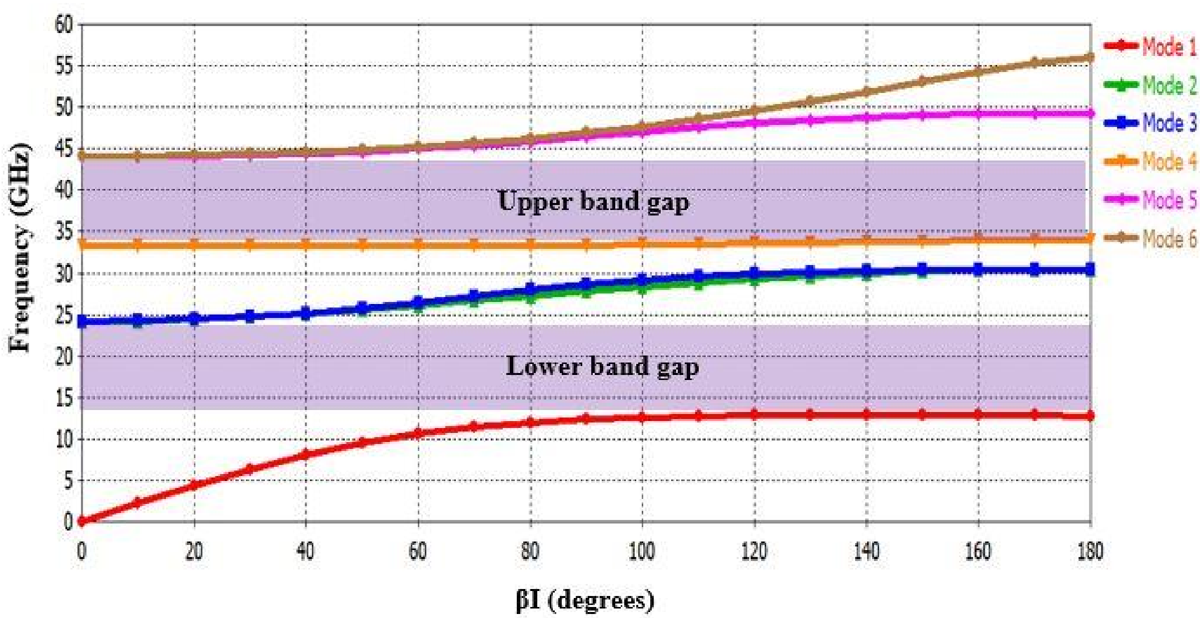

Figure 3.10: Dispersion diagram of a dual-band mushroom patch unit cell where the band gaps are (13-24) GHz and (34-44) GHz bands, respectively.

In terms of propagation, this bandgap only supports TEM or QTEM surface waves, not other waves, for example, TE or TM waves. The proposed unit cell provides two wideband gaps that allow only QTEM waves. The periodic boundary conditions are enough to analyze it.

To find the unit cell's electromagnetic band gap (EBG), a dispersion diagram is often acquired using the Eigenmode solver of commercial software CST Microwave Studio. Figure 3.10 illustrates a dispersion diagram of the proposed dual-band unit cell. The dispersion diagram shows how Mode 1 propagates parallel to the light line at lower frequencies, but as frequency rises, this mode becomes slower and does not interact with free space. A similar manner can be noticed for modes 2 and 3, which gradually become slower with higher frequency. As a result, the first stop band gap is achieved between frequency bands (13-24) GHz where no waves can propagate. The same behavior can be observed between modes 4 and 5, which gives a second band gap from frequency (34-44) GHz with no wave propagation between this band gap, named the forbidden band gap. The EBG band gaps are presented in bold purple color in the dispersion diagram. The numerical study performed in [43] presents that the design parameters can regulate the unit cell's bandgap, which is the air gap height and the substrates' thickness via diameter and patch width. The upper band gap is sensitive to all parameters used to design the unit cell. However, the dispersion diagram of the proposed unit cell allocates a dual-band gap, one for (13-24) GHz and another for (34-44) GHz. There is another band gap between mode 3 and mode 4, which can be ignored due to the narrow band gap.

3.2.1 Row of Dual-Band Unit Cell

A finite long transverse of row-unit cells with 1D periodic boundary condition is illustrated in Figure 3.11. Here, 5 unit cells are in one row, and the central patch is replaced by a ridge, allowing wave propagation within the EBG. All the dimensions of the transverse cells are the same except for the ridge patch, which is 1.2 mm in width and 1.8 mm in length, respectively. The ridge patch

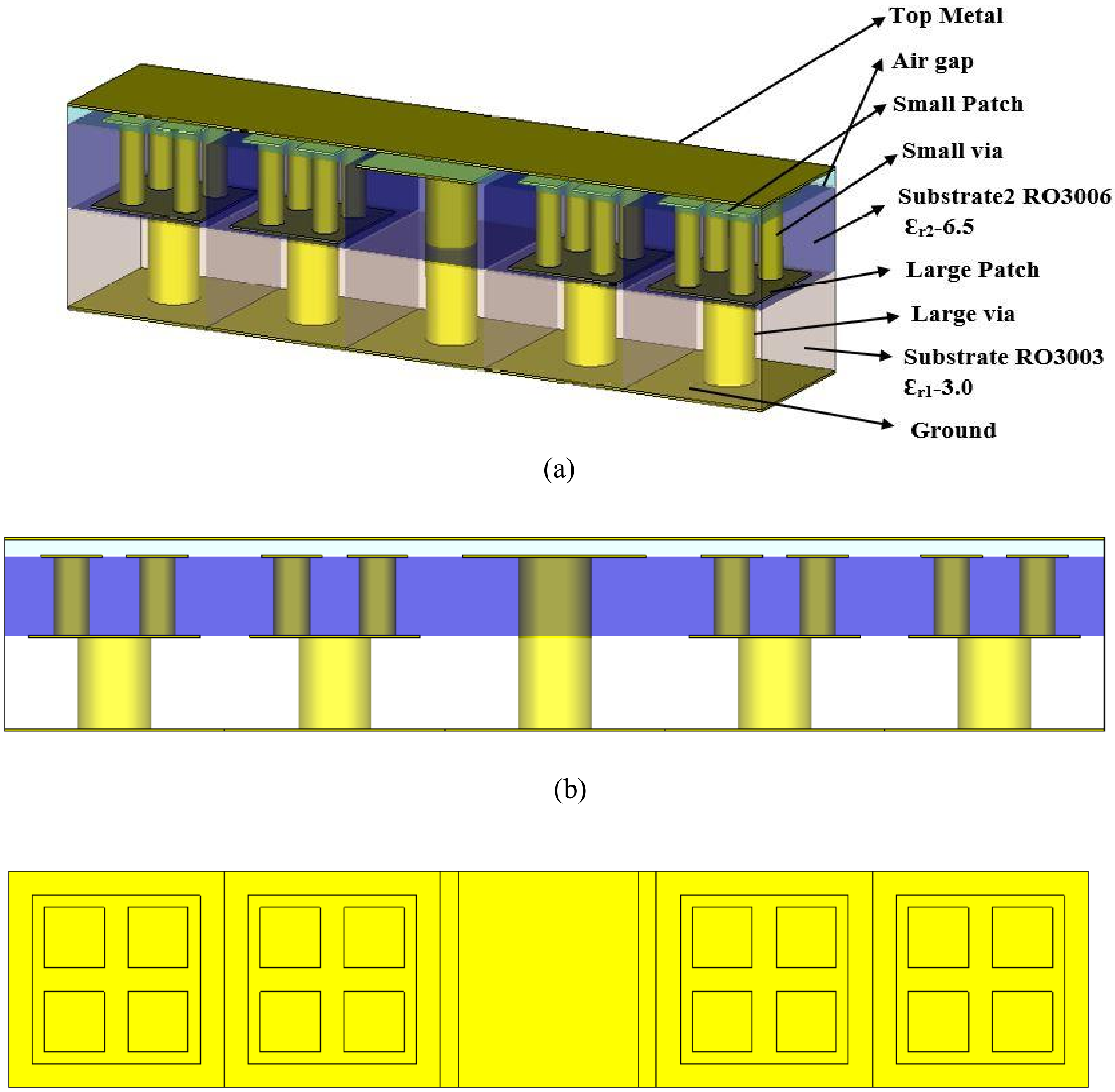

(a)

(b)

(c)

Figure 3.11: Structure of a row of cells of dual-band mushroom patches (a) Row of finite cells with dimensions, (b) Cross section view, and (c) Top view.

is separated from the top metal lid by the air gap of 0.127 mm, infinite along the z direction. A quasi-TEM mode is generated within the ridge patch when the ridge is attached and propagates within the stopband. All other higher-order modes are forced to be cut off by the EBG unit cells.

A dispersion diagram provides the stop band from EBG unit cells that can be acquired from the Eigenmode solver of CST software. Figure 3.12 represents the dispersion diagram of a row of dual-band unit cells. The dispersion diagram shows the propagation modes related to the inserted ridge within the EBG. As can be seen, mode 1 propagates parallel to the light line at a lower frequency, but as the frequency elevates, the mode becomes slower, does not collaborate with the

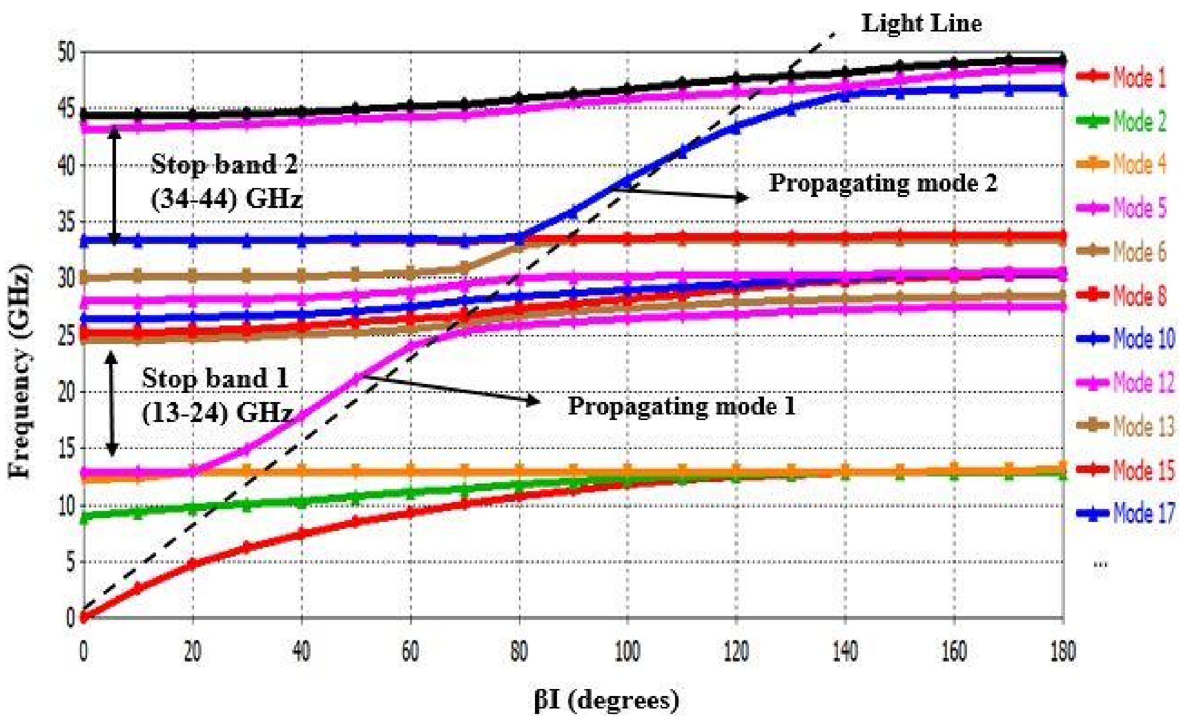

Figure 3.12: Dispersion diagram of a row of dual-band mushroom patches where mode no 5 and mode no 17, are propagating modes.

free space, and allocates the band gap in higher frequencies. Two propagating modes can be noticed in the dispersion diagram, represented by mode 5 (pink line) within 13-24 GHz and mode 17 (blue line) within 34-44 GHz, which are the quasi-TEM modes. The first propagating mode can be observed between modes 4 and 6, and the second propagating mode can be observed between modes 16 and 18. Another propagating mode could be notice mode no 13 (brown line), which is narrow and out of band and could be ignored. Comparing the Unit cell modes and the row cell modes, row cell modes are more due to the finite length of the cell that causes standing waves in the transverse direction of the ridge. The light line, sketched by the dashed black line, is used to display the pure TEM mode in both substrates of the unit cell.

3.2.2. Field Distribution of Each Mode of Dual Band Unit Cell

The dual-band unit cell has three layers; two of them are dielectric substrates stacked on each other, and on the top layer, there is an air gap where waves can propagate. Figure 3.13 presents the E-field distribution of each mode of the dual-band unit cell. As can be observed, most of the waves are trapped within the dielectric substrate, and few parts are propagating within the air. As a result, a Q-TEM mode will be produced by the difference in phase velocities between the two media. The periodic boundary condition is applied for the unit cell. The E-field of each mode also provides the polarization of field directions, which is vertically polarized along the Z direction. From the figure, the E-field distribution of 5 modes of the unit cell renders dual EBG bands. The vertically polarized E-fields can be noticed along the air gap on the top layer below the upper conducting surface of the cell. Only vertical E fields travel through the air gap of the cell. Figure 3.13 (a), (b), (c), (d), and (e) presents mode 1, mode 2, mode 3, mode 4, and mode 5, respectively and all are denoted by dB scale. Some fringing fields can be detected underneath the patches of the dielectric media of the cell. Some higher-order modes can exist due to the dual structure of the unit cell, but that is out of the desired band.

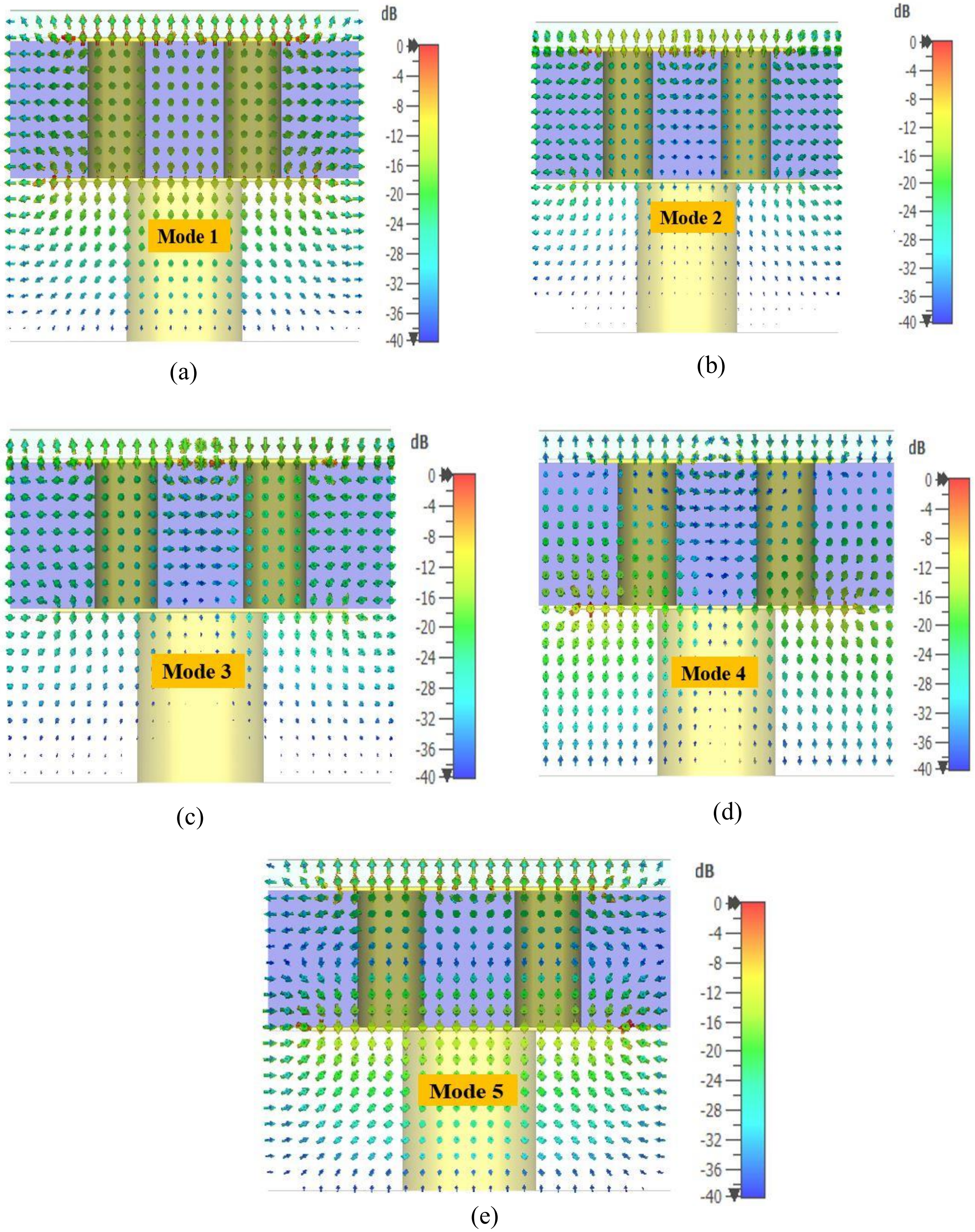

Figure 3.13. E-field distribution of (a) Mode 1, (b) Mode 2, (c) Mode 3, (d) Mode 4, and (c) Mode 5.

The proposed unit cell is designed to cover 13-24 GHz and 34-44 GHz bands, respectively, which is the operational bandwidth of a dual-band printed ridge gap waveguide. Dual-band millimeter wave application might be one prominent application with the dual-band unit cell.

3.3 Parametric Study of Dual Band Unit Cell

The proposed dual-band unit cell consists of a two-layer substrate, and on top of the layer, an air gap is placed to maintain a constant gap height. The upper layer of the unit cell has four mushroom patches connected to the bottom layer with conducting vias. The lower layer has one large mushroom patch that attaches to the ground conducting via. The upper and lower substrates are RO 3006 and RO 3003, with the relative permittivity (ε_{r2}) of 6.5 and (ε_{r1}) 3.0, respectively. The total size of the unit cell is 1.8 mm. The height of the upper layer, patch size, and via radius are 0.75 mm, 0.50 mm, and 0.15 mm, respectively. The height of the lower layer, patch size, and via radius are 0.64 mm, 1.4 mm, and 0.30 mm, respectively. An air gap size of 0.127 mm is set up on the top layer, and a metal thickness of 0.0175 mm is accommodated as a ground for the top and bottom of the whole structure. This is the optimized parameter of the proposed design. The unit cell regulates the band gap of the waveguide using the AMC surface. The Eigen-mode solver in CST Microwave Studio is used to determine the bandgap of the unit cell. Four essential elements have a substantial impact on the stopband. They are the air gap between two parallel metal plates, the height of the substrate, the via radius, and the patch width. The following paragraphs provide the parametric analysis of the unit cell that has a crucial effect on the band gap of the unit cell.

3.3.1 Effect of Air Gap

The first element of the unit cell is the air gap, which influences band gap and frequency change. Varying the air gap changes the capacitance of the vertical polarization that switches the frequency. Figure 3.14 shows the geometry of the unit cell, and Figures 3.15 (a), (b), and (c) present the EBG of varying the air gap and other parameters remain constant. Through the parametric analysis, we can easily understand which dimension is needed for our band of interest, and another can be utilized for other required choices. The EBG for lower and upper band gaps are 12-23 GHz and 30-43 GHz when air is 0.05 mm. The EBG for lower and upper band gaps are 13-24 GHz and 34-44 GHz when the air gap is 0.127 mm. The EBG for lower and upper band gaps are 12-23 GHz and 30-42 GHz when the air gap is 0.254 mm. The optimized best result for an air gap is 0.127 mm for the proposed dual-band unit cell. Table 3.1 provides the detailed air gap output and its respective dual-band EBG output.

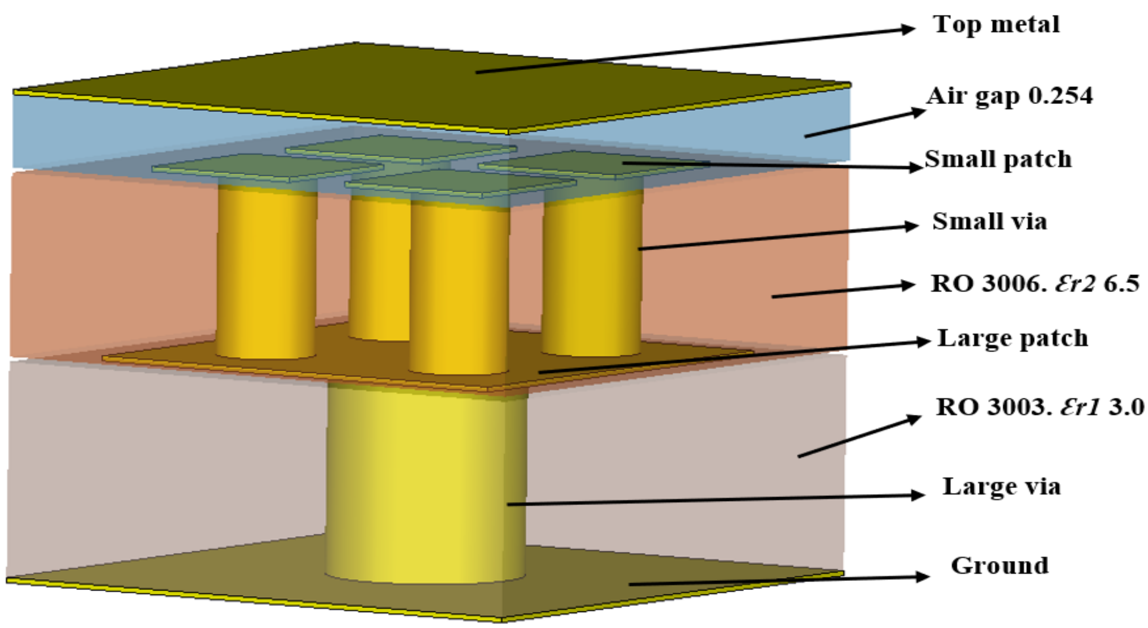

Figure 3.14 Geometry of unit cell (air gap variation)

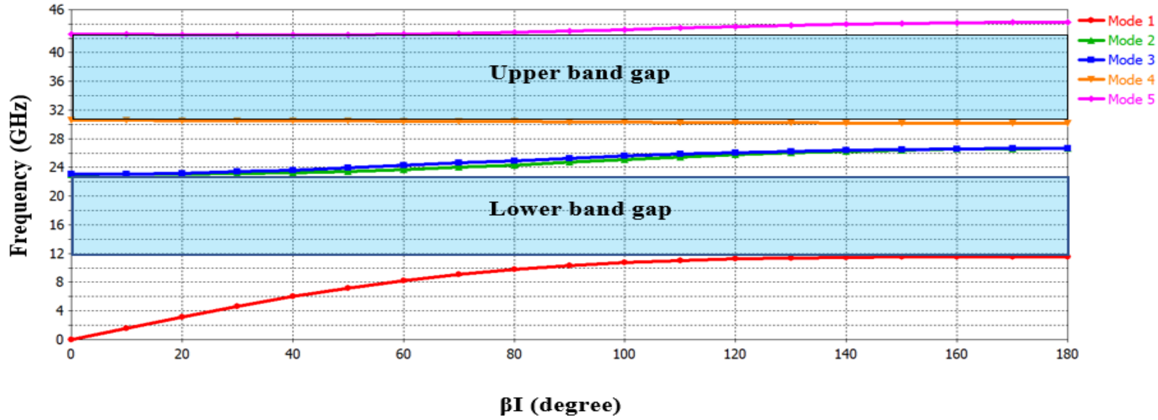

(a) Air gap is 0.05 mm

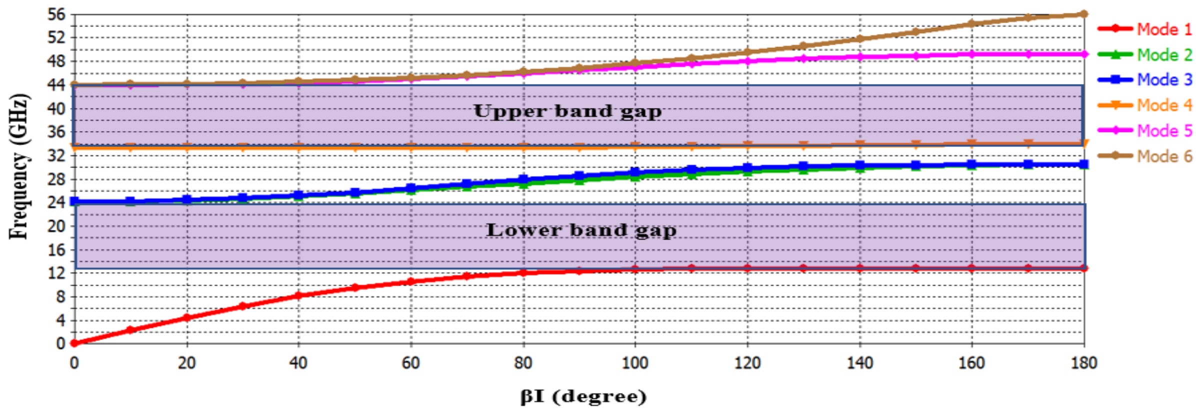

(b) Air gap is 0.127 mm

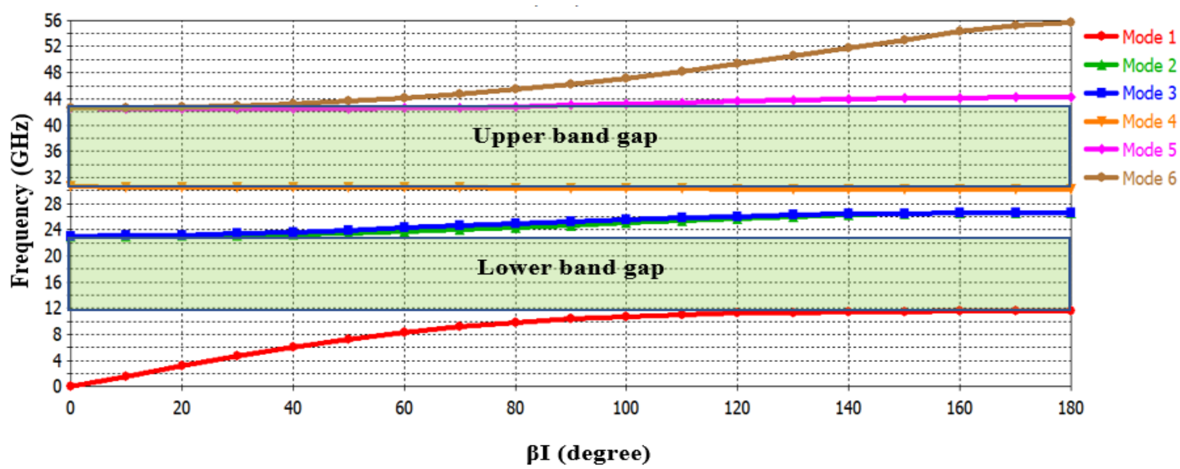

(c) Air gap is 0.254 mm

Figure 3.15 Dispersion diagrams of the unit cell when the air gap is (a) 0.05 mm, (b) 0.127 mm, and (c) 0.254 mm.

Table 3.1 Effect of air gap on EBG

air gap thickness (mm)	Lower EBG (GHz)	Upper EBG (GHz)
0.05	12-23	30-43
0.127	13-24	33-44
0.254	12-23	30-42

3.3.2 Effect of Substrate Thickness

The substrate thickness of the unit cell greatly influences the EBG band gap. The higher the thickness, the lower the band gap. In the proposed work, RO 3006 and RO 3003 are utilized with the relative permittivity of $\varepsilon r2$ 6.5 and $\varepsilon r1$ 3.0, respectively. The thickness of the substrate is taken from Roger's supplied datasheet.

3.3.2.1 Upper Substrate Thickness RO 3006 ($\varepsilon r2$ *6.5)*

The proposed dual-band unit cell has two layers of substrate. The upper layer substrate thickness is taken at 0.64 mm as the optimized dimension. By changing the thickness of the substrate, the EBG is changed, and frequency becomes shifted; even only one EBG band is achieved when the thickness is as small as 0.25 mm. A dual-band gap is acquired when the thickness is large, so proper thickness is necessary to get the desired band gap, keeping the other parameters constant in the analysis. Figure 3.16 depicts the configuration of a dual-band unit cell when the upper substrate thickness varies, and Figures 3.17 (a) and (b) show the EBG of changing the upper substrate thickness. The best outcome can be achieved from the optimized thickness of 0.64 for the upper substrate thickness. Table 3.2 presents the detailed output of upper substrate thickness and the acquired dual-band EBG output.

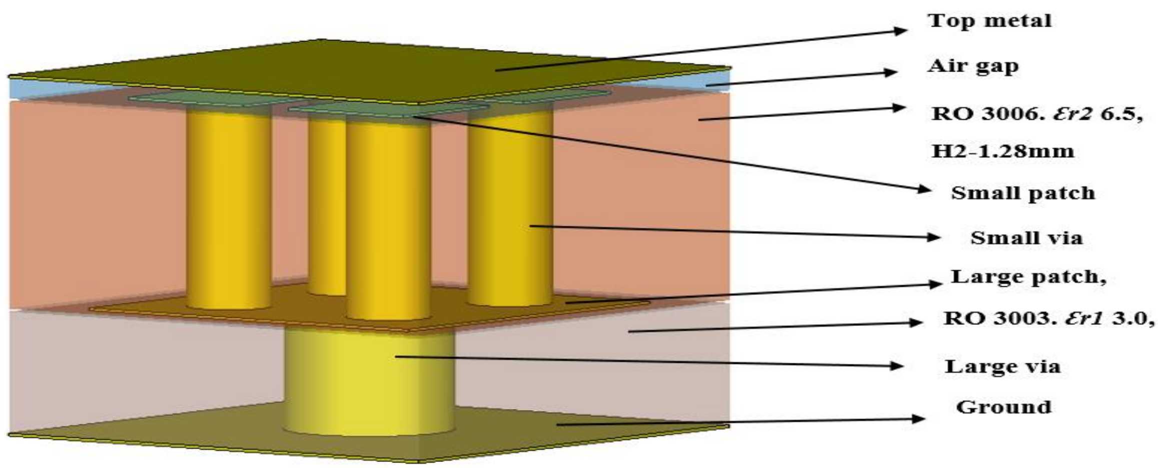

Figure 3.16 Geometry of the unit cell (upper substrate variation)

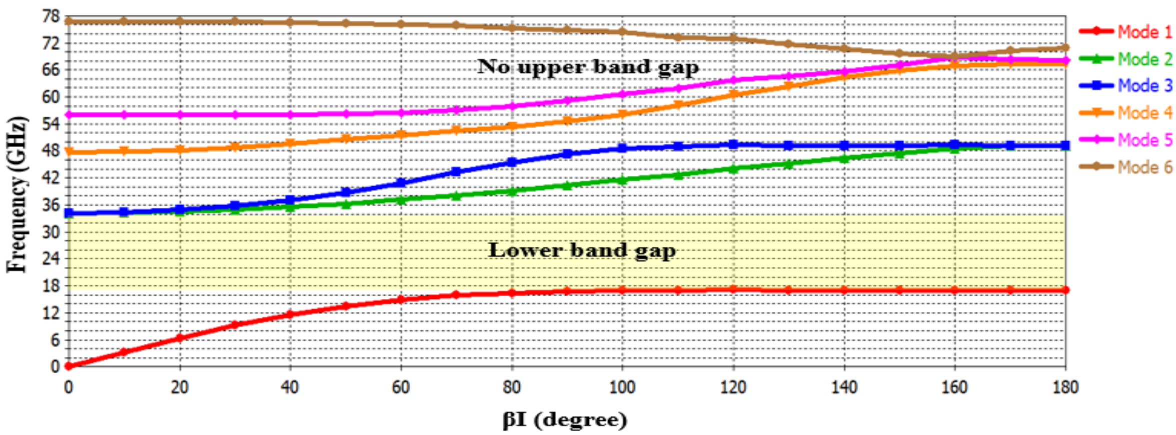

(a) Ɛ*r2* is 0.25 mm

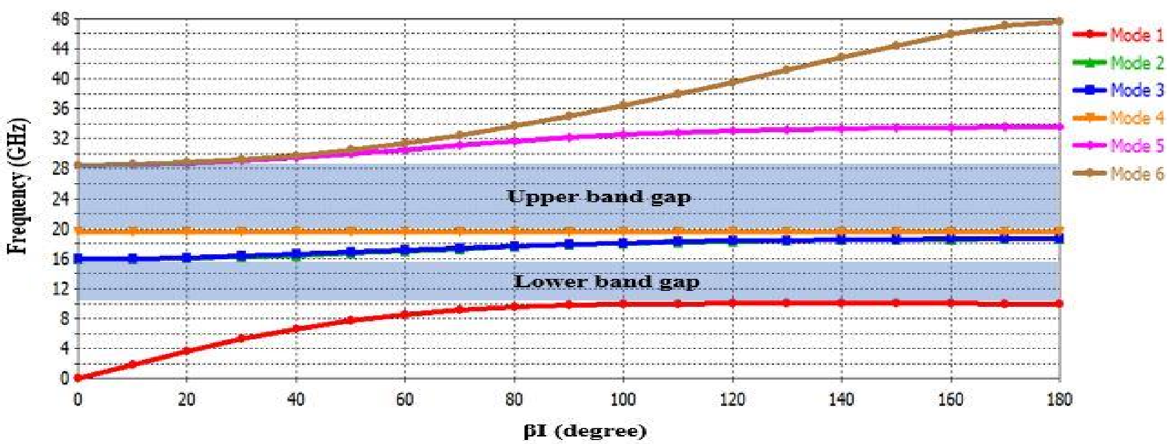

(b) Ɛ*r2* is 1.28 mm

Figure 3.17 Dispersion diagrams of the unit cell when the upper substrate thickness is (a) 0.25 mm and (b) 1.28 mm.

Table 3.2 Effect of upper substrate thickness *Ɛr2 (6.5)* on EBG

Upper substrate thickness (mm)	Lower EBG(GHz)	Upper EBG(GHz)
0.25	0	17-33
0.64	13-24	33-44
1.28	10.5-16	20-28

3.3.2.2 Lower Substrate Thickness RO 3003 (*Ɛr1 3.0)*

The lower layer substrate thickness is taken *Ɛr1* 0.75 mm as the optimized dimension. By fluctuating the thickness of the substrate, the EBG is varying, and frequency becomes switched. A wider dual-band gap is acquired when the thickness is small, so proper thickness is necessary to get the desired band gap—keeping the other parameters constant in the analysis. Figure 3.18 presents the layout of the dual-band unit cell when lower substrate thickness varies, and Figure 3.19 (a) and (b) illustrate the EBG of changing the lower substrate thickness. Table 3.3 shows the detailed output of lower substrate thickness and the acquired dual-band EBG output.

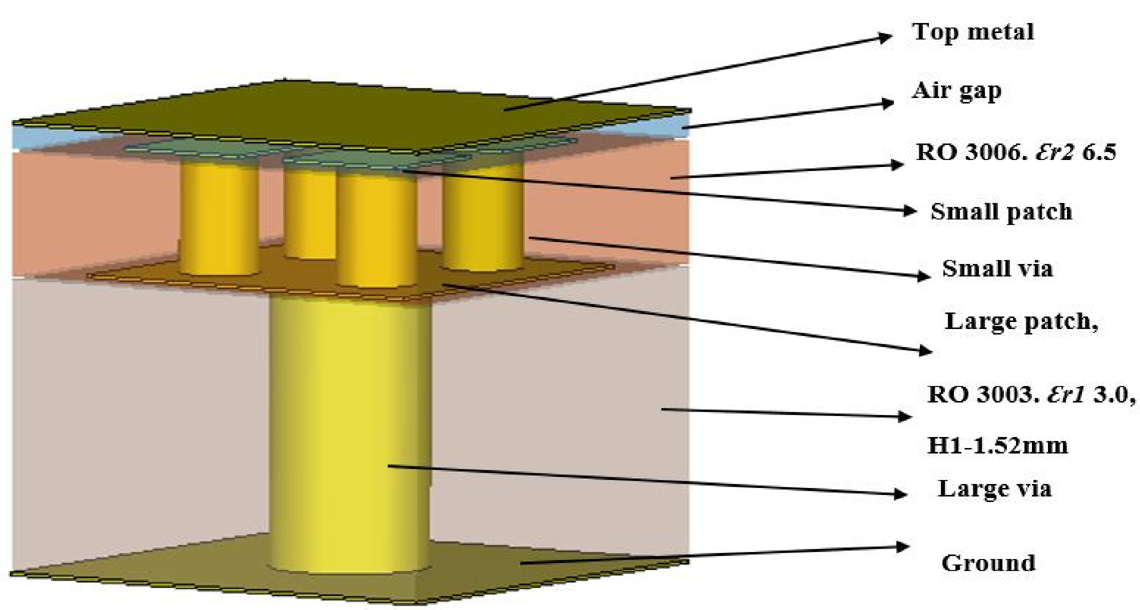

Figure 3.18 Geometry of the unit cell (lower substrate variation)

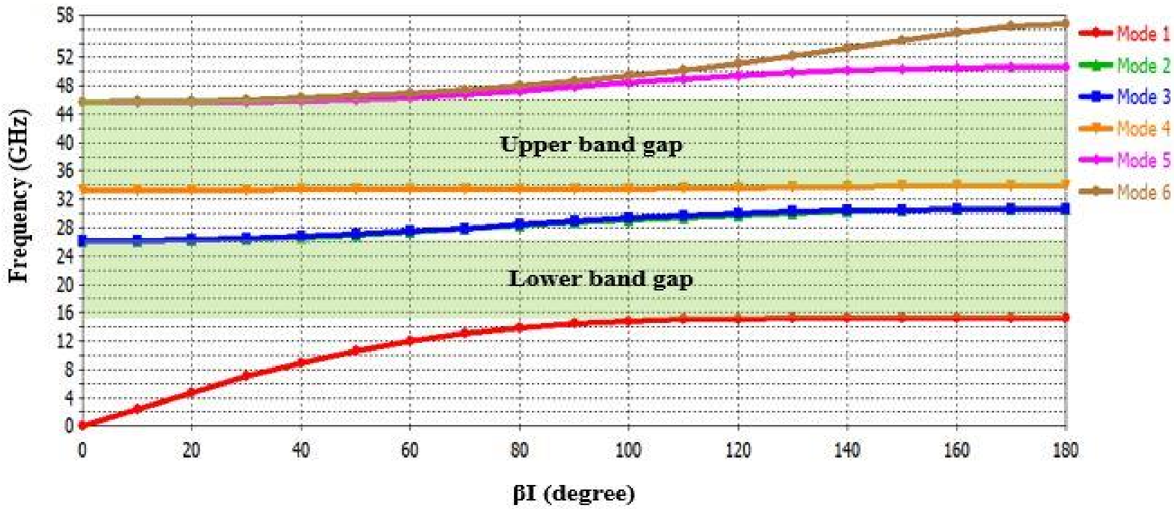

(a) $\mathcal{E}r1$ is 0.51 mm

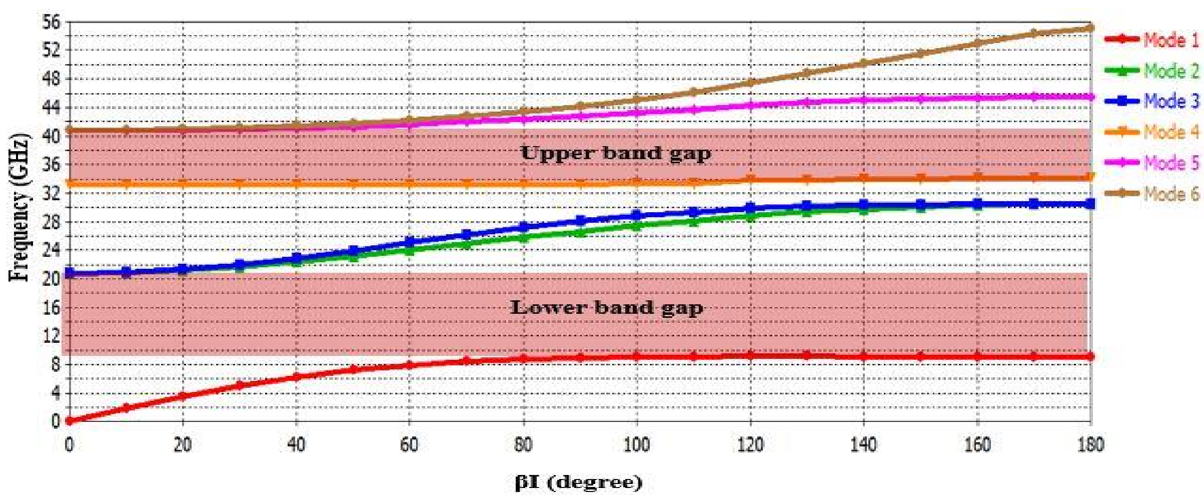

(b) $\mathcal{E}r1$ is 1.52 mm

Figure 3.19 Dispersion diagrams of the unit cell when lower substrate thickness is (a) 0.51 mm and (b) 1.52 mm

Table 3.3 Effect of lower substrate thickness $\boldsymbol{\mathcal{E}r1}$ on EBG

Upper substrate thickness (mm)	Lower EBG(GHz)	Upper EBG(GHz)
0.51	15-26	34-46
0.75	13-24	33-44
1.52	09-21	34-41

3.3.3 Effect of Large Via Radius

The large via radius or diameter is important to control the unit cell's EBG band gap. The inductance of the structure comes from the via. By changing the via radius, the EBG band gap varies, and frequency shifts. The optimized via radius is 0.3 mm. When the radius is small, the band gap becomes too narrow, so a proper radius is essential to get the expected outcome of the unit cell. Figure 3.20 illustrates the geometry of the unit cell, and Figures 3.21 (a) and (b) show the EBG of varying the via radius and other parameters remain steady. Table 3.4 details the via radius and the acquired dual-band EBG output.

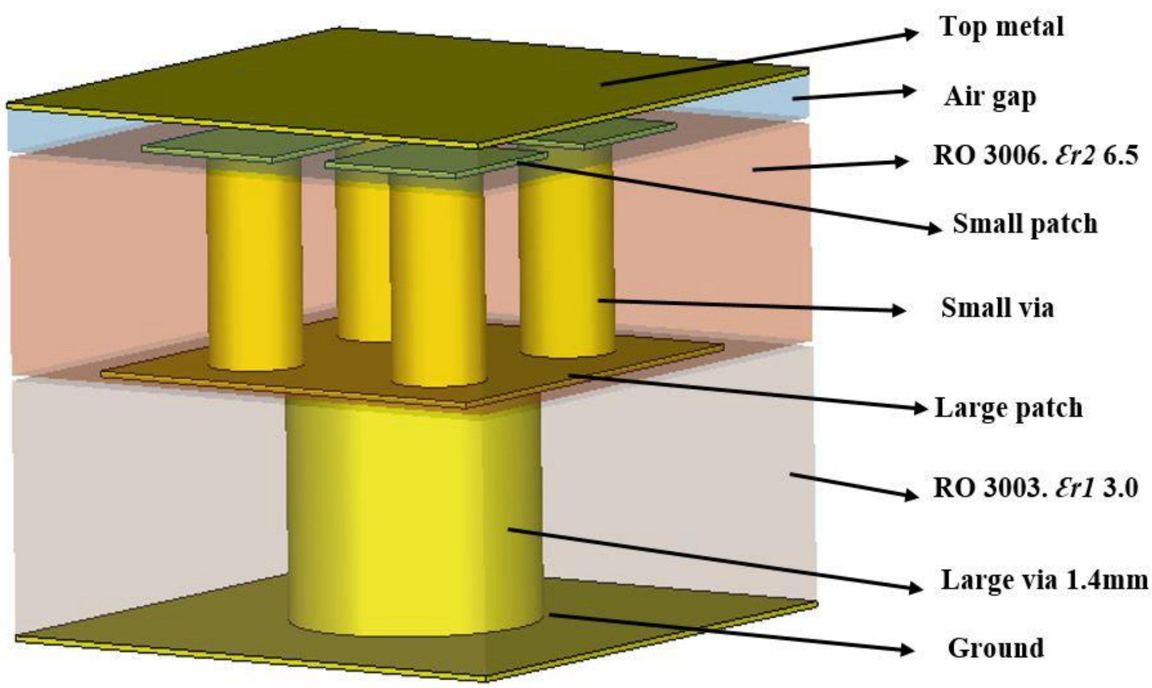

Figure 3.20 Geometry of the unit cell (Large via radius variation)

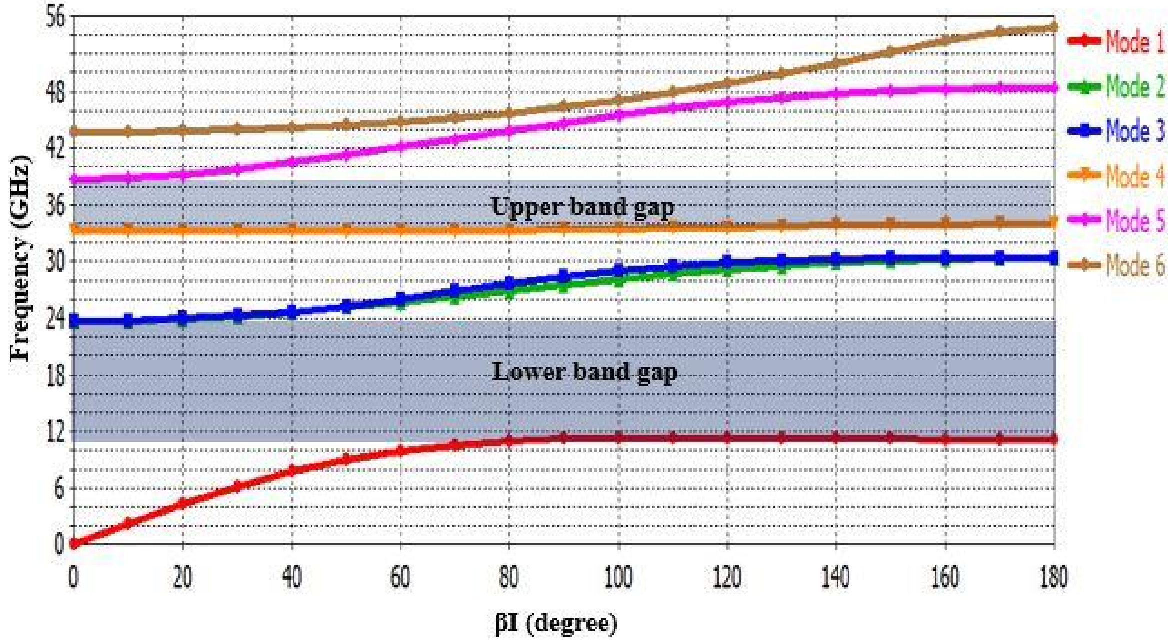

(a) Via radius is 0.2 mm

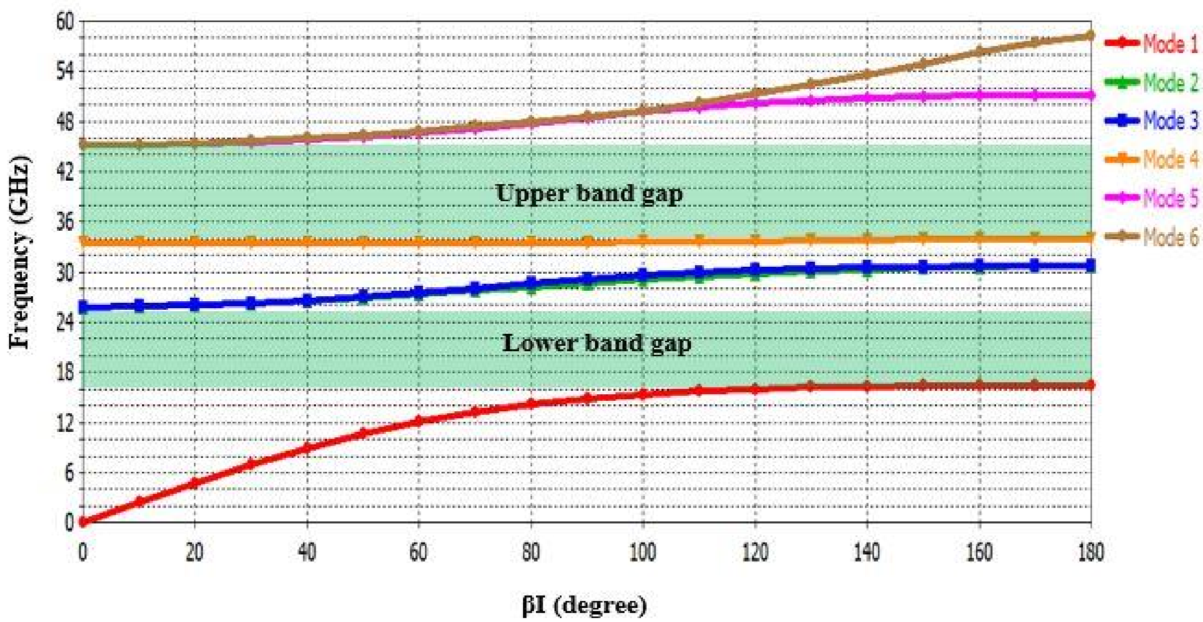

(b) Via radius is 0.4 mm

Figure 3.21 Dispersion diagrams of the unit cell, when large via radius is (a) 0.2 mm and (b) 0.4 mm.

Table 3.4 Effect of via radius on EBG

Via radius (in mm)	Lower EBG (GHz)	Upper EBG (GHz)
0.2	11-23.5	33-38.5
0.3	13-24	33-44
0.4	16-25.5	34-45

3.3.4 Effect of Large Patch Width

The large patch width has a vital effect on controlling the EBG band gap of the unit cell. The capacitance of the structure comes from the large patch width. By varying the large patch width, the EBG band gap changes and frequency shifts. The optimized large patch width is 1.4 mm. When the patch width is larger than the band gap becomes too narrow, so the proper patch width is

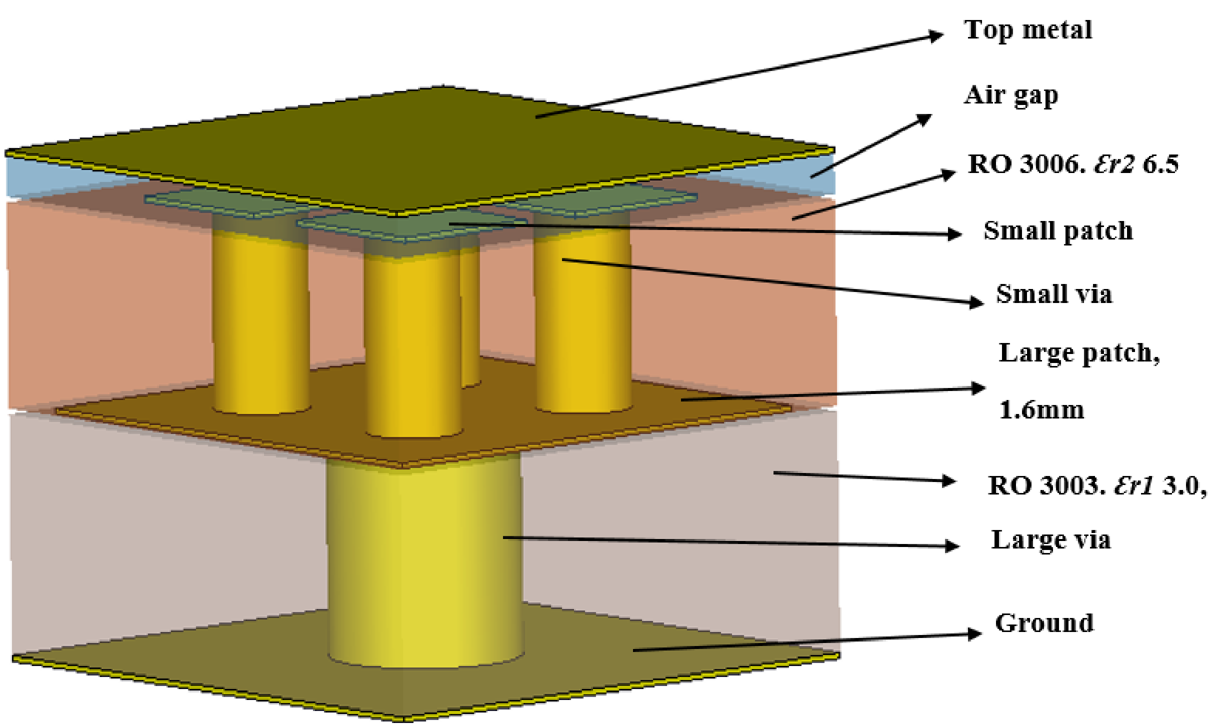

Figure 3.22 Geometry of the unit cell (Large patch width variation)

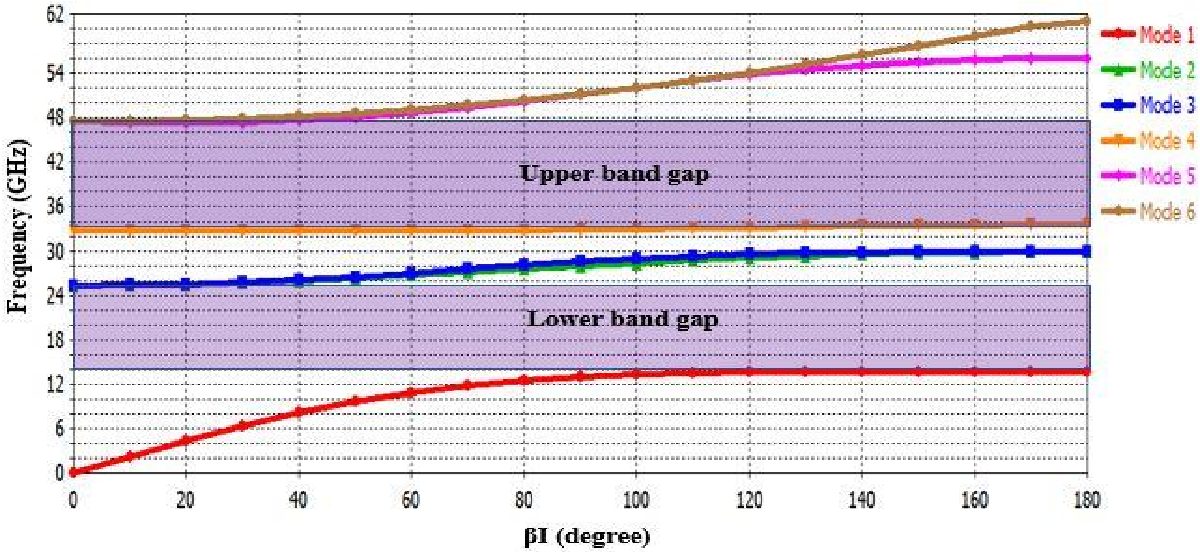

(a) Patch width is 1.2 mm

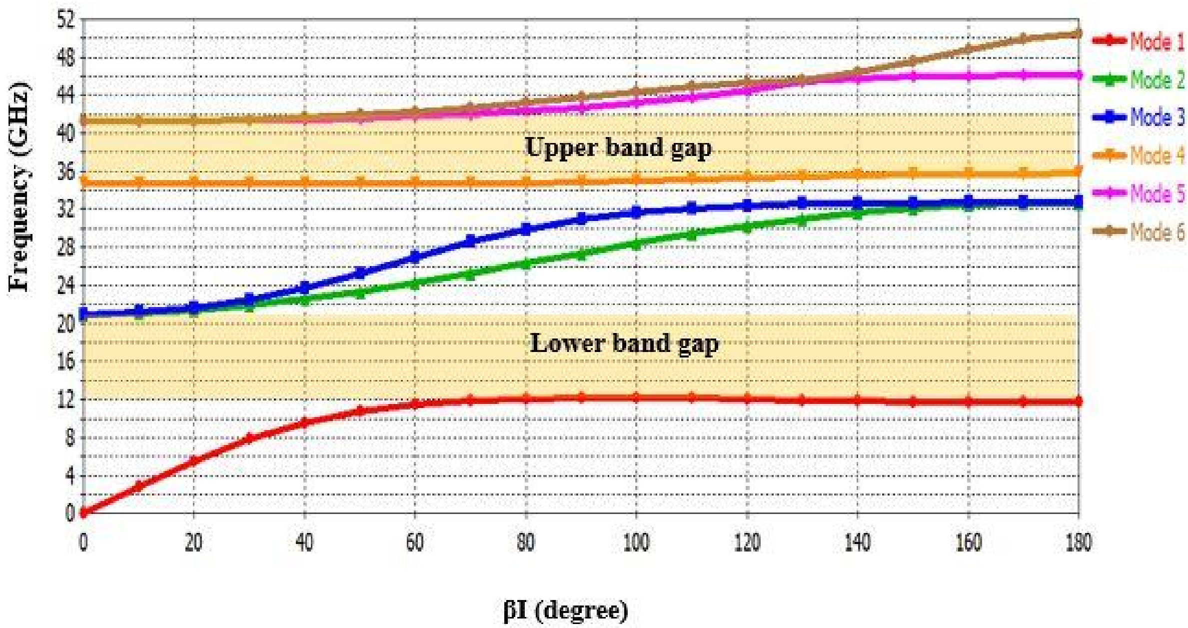

(b) Patch width is 1.6 mm

Figure 3.23 Dispersion diagrams of the unit cell when the large patch is (a) 1.2 mm and (b) 1.6 mm.

necessary to get the expected outcome of the unit cell. Figure 3.22 depicts the geometry of the unit cell, and Figures 3.23 (a) and (b) show the EBG of varying the large patch width and other parameters remain steady. Table 3.5 shows the large patch width details output and the dual-band EBG outcome achieved. Although a patch width of 1.2 mm provides a wider band gap for both bands than the selected patch width, the upper band of four small patches becomes congested and tough to accommodate on the top of a large patch if the width becomes 1.2 mm. Therefore, we select a 1.4 large patch width for the desired output.

Table 3.5 Effect of large patch width on EBG

Large patch width (mm)	Lower EBG (GHz)	Upper EBG (GHz)
1.2	14-25	33-47.5
1.4	13-24	33-44
1.6	12-21	35-41.5

3.4 Dual-band Unit Cell 4 Mushroom Patches Looking Downward (Air gap 0.127 mm)

Another proposed unit cell is sketched to acquire dual-band. Each unit cell layer is piled like a sandwich on top of each other. The unit cell geometry comprises double substrates with a single mushroom patch in the lower substrate connected to the ground plane by conducting vias. Four smaller mushroom patches are assigned in the second substrate; each is connected to the upper ground by conducting vias, but the upper patches face to the lower patch downward. Figure 3.24 depicts the layout of the proposed dual-band unit cell. The unit cell is 1.8 mm, with square patches on both layers. The lower substrate RO3003 with permittivity $\mathcal{E}r1$ of 3.0 and upper substrate RO3006 with permittivity $\mathcal{E}r2$ of 6.5, with a thickness of 0.75 mm and 0.64 mm, is used for the mushroom patch unit cell. To build the large patch, the width, via radius, top and bottom metal thickness is kept at 1.6 mm, 0.30 mm, and 0.0175 mm, as well as for the small patch width,

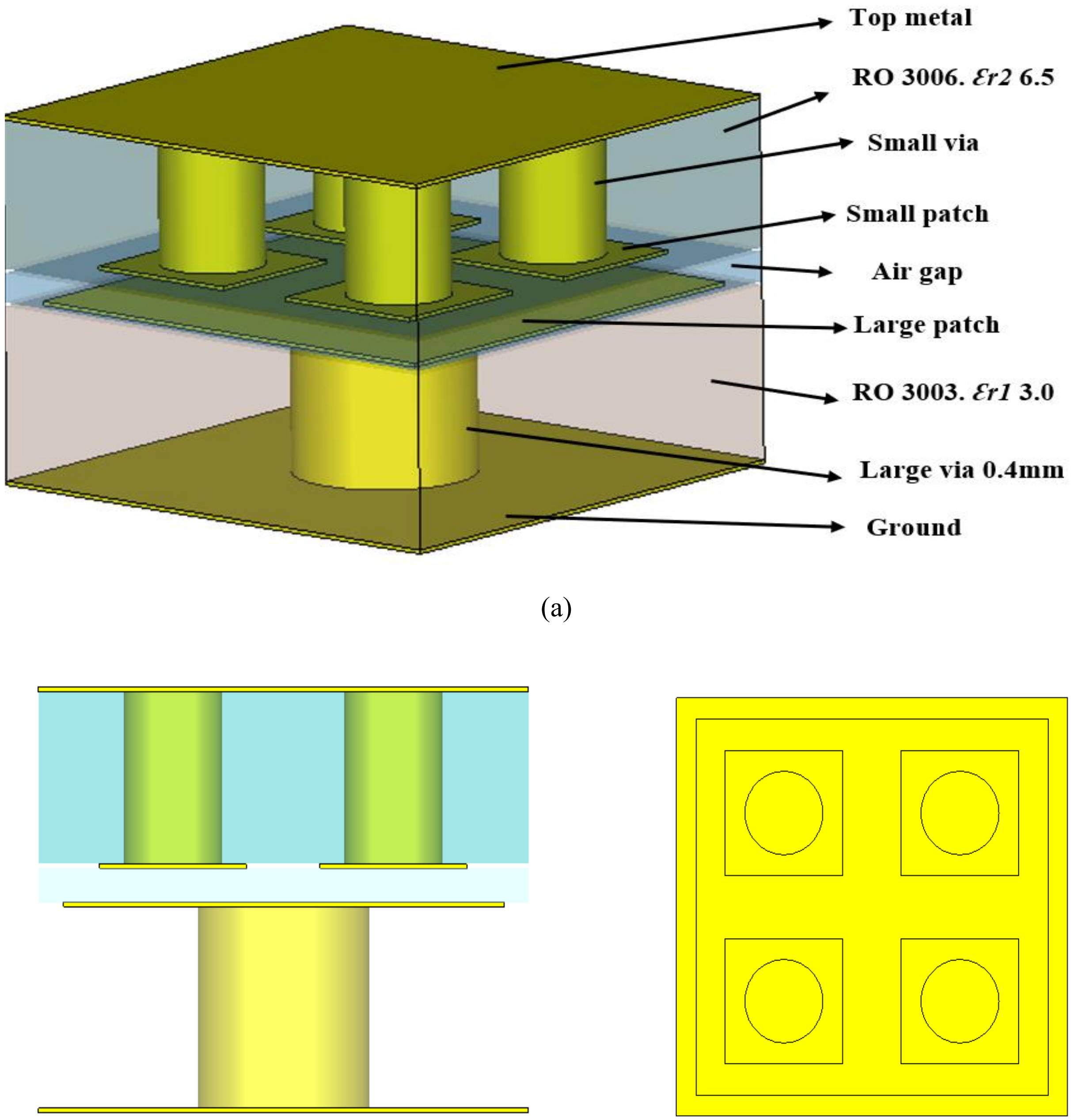

(a)

(b) (c)

Figure 3.24: Layout of upper mushroom patches looking downward of the unit cell (a) Mushroom patch with dimensions, (b) Cross section view, and (c) Top view of proposed mushroom patches.

small via radius are also kept at 0.45 mm and 0.15 mm. The air gap is placed between the two substrates, whose thickness is about 0.127 mm. The stopband, which specifies the operating bandwidth of the structure, can be used to assess the performance of the unit cell. The EBG surface behaves like a high-impedance surface inside this bandwidth.

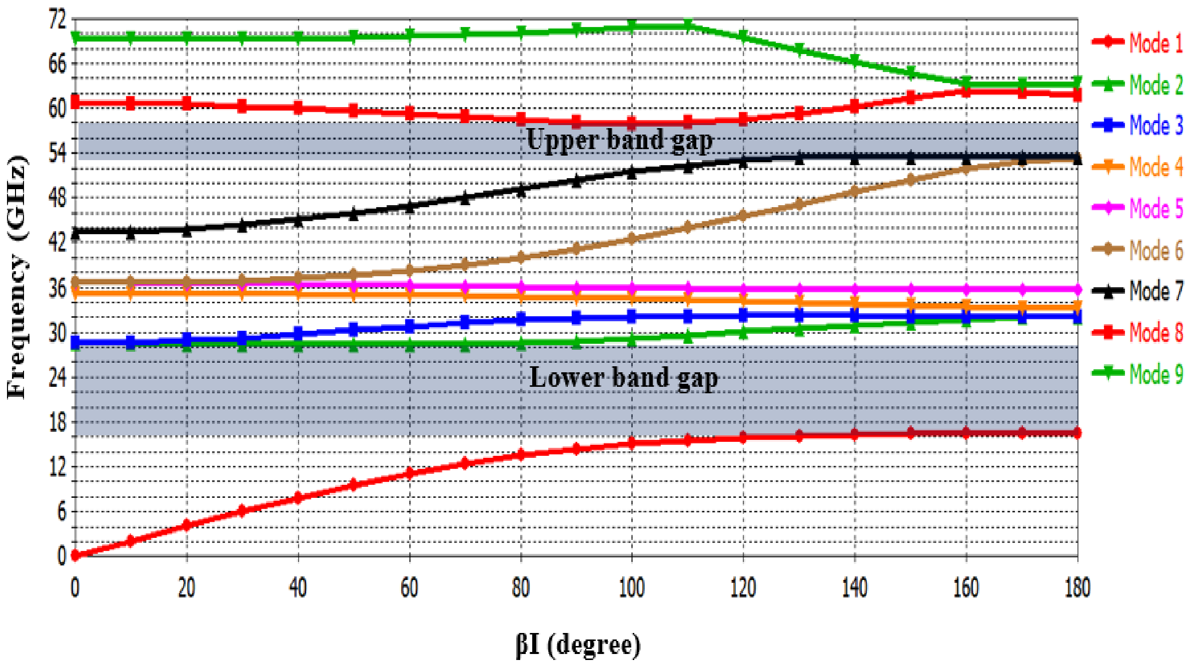

Figure 3.25: Dispersion diagram of upper mushroom patches looking downward of the unit cell where the band gaps are (16-28) GHz and (53-58) GHz, respectively.

To get the electromagnetic band gap (EBG), a dispersion diagram is often achieved using the Eigenmode solver of the commercial software CST Microwave Studio. Figure 3.24 illustrates the layout of the proposed dual-band unit cell looking downward. Figure 3.25 depicts a dispersion diagram of the proposed mushroom upper patches looking downward of the unit cell. Thus, the dispersion diagram of the proposed cell provides a dual-band, one for 16-28 GHz and another for 53-58 GHz; the upper band gap is a very narrow band, and the bold gray color shades provide the band gap for better visualization. Although this proposed designed unit cell provides dual-band, this is not a successful outcome for the desired dual-band gap.

3.4.1 Row of Cell Patches Looking Downward (Air gap 0.127)

The row of unit cells is the repetition of the same cells in 1D or 2D a finite number of times.

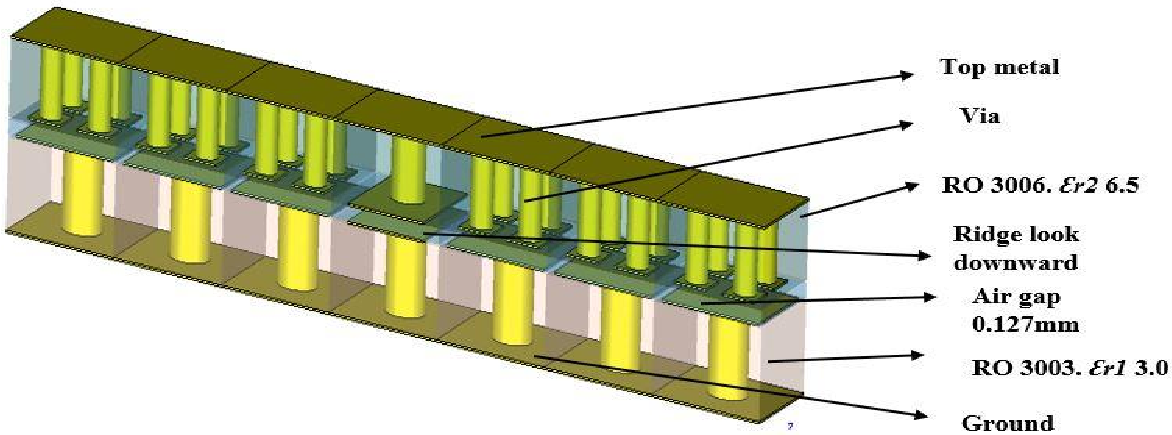

(a)

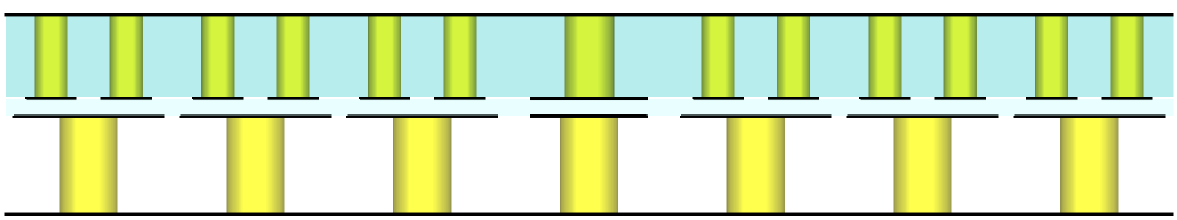

(b)

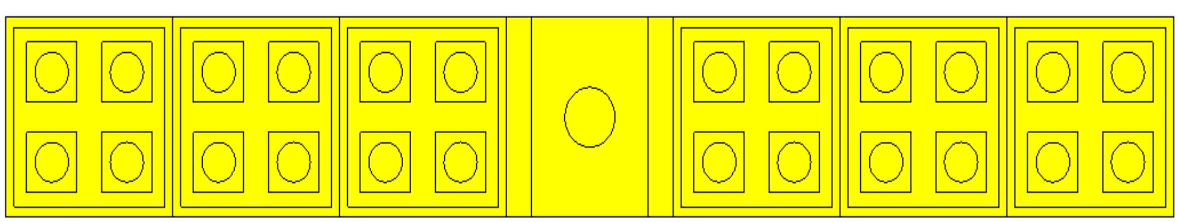

(c)

Figure 3.26: Geometry of a row of mushroom patch unit cells looking downward with a ridge in the central (a) Row of mushrooms with dimensions, (b) Cross-section view, and (c) Top view of a row of mushroom cells.

To create a mushroom row of cells, the middle patches are replaced by a ridge patch and periodic boundary conditions are applied for an acceptable outcome. The width and length of the ridge patch are 1.2 mm and 1.8 mm. Both ridge patch widths and lengths are the same. The dimension of the row of cells is the same as that of the mushroom patch, but an air gap of 0.127 mm is set up between the two patches where waves propagate through the ridge patches and air gap. Figure 3.26 presents the row of cells of mushroom patches looking downwards with dimensions (a), (b) the cross-section view, and (c) the top view of a row of mushroom patches looking downward.

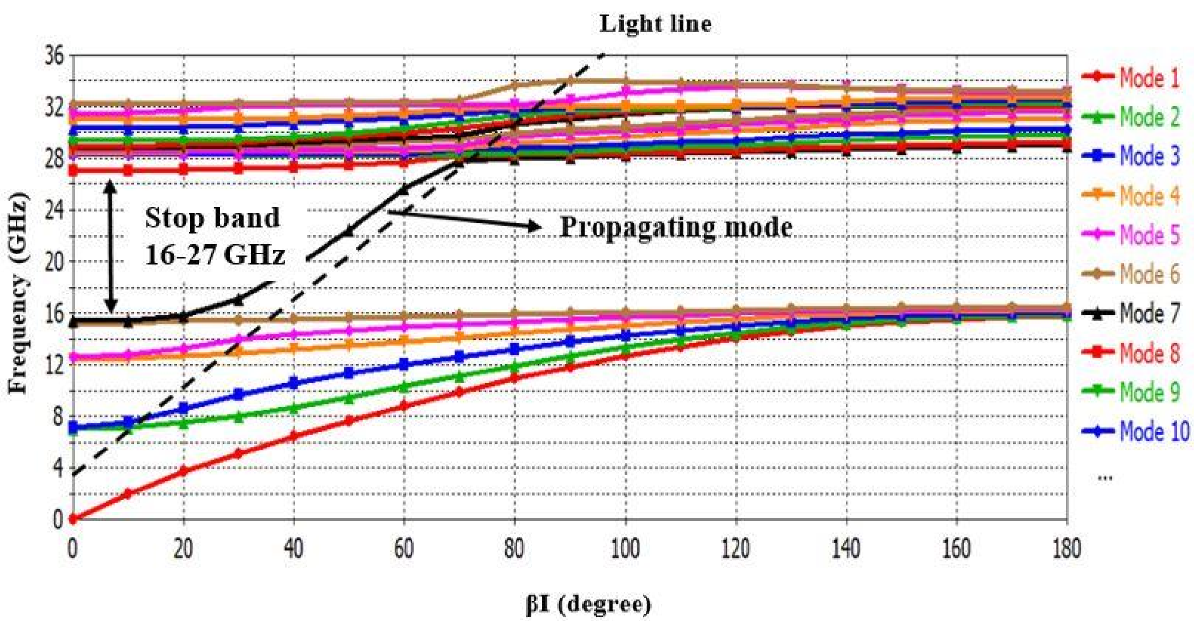

Figure 3.27: Dispersion diagram of a row of mushroom patch unit cells looking downward where mode no 7 is a propagating mode.

A quasi-TEM mode is generated within the ridge patch when the ridge is attached to the cell's row and propagates within the stopband. Figure 3.27 provides the dispersion diagram of the row of cells where 35 modes are demonstrated. As can be observed, only mode no 7, which is denoted by the black line, propagates within the band gap of 16-27 GHz, and there is no propagating mode for the upper band gap. Although designing a double-layer unit cell to look downward is to get a dual-band, this unit cell does not satisfy our goal of propagating two modes, so we will not further experiment with this unit cell.

3.4.2 Mushroom Patches Looking Downward (Air Gap Almost Zero 0.01 mm)

Another approach for getting a dual-band is to consider an almost zero air gap of 0.01 mm between

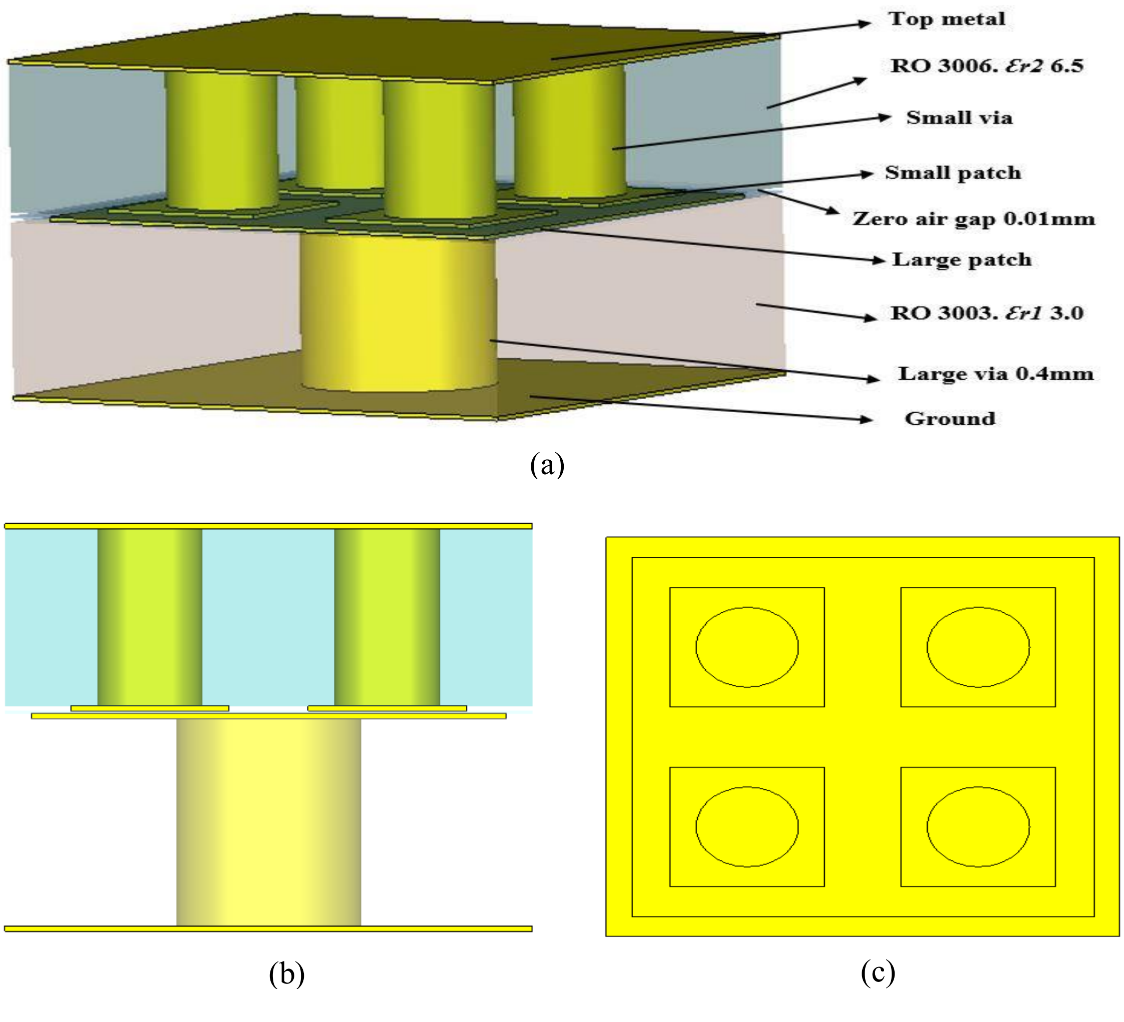

(a)

(b)

(c)

Figure 3.28: Structure of upper mushroom patches looking downward of the unit cell when zero air gap (a) Mushroom patch with dimensions, (b) Cross section view, and (c) Top view of proposed mushroom patches.

two patches of the dual layer that act as dielectric-filled SIW, where EM waves propagate through dielectric substrates. Keeping all other parameters constant, like mushroom patches, look downward, but the air gap is about 0.01 mm, which is almost zero air gap, and with the design, we get dual-band and dual propagating modes. Figure 3.28 portrays the structure of upper mushroom patches looking downward of the unit cell when zero air gap (a) Mushroom patch with dimensions, (b) Cross-section view, and (c) Top view of proposed mushroom patches looking downward at zero air gap.

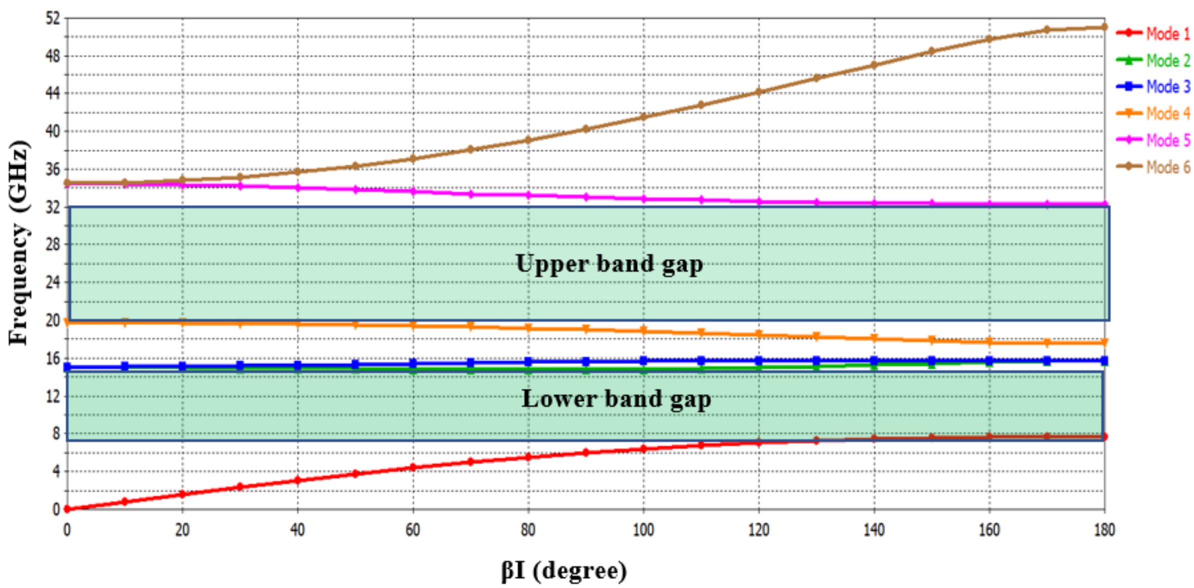

Figure 3.29: Dispersion diagram of upper mushroom patches looking downward of the unit cell at zero air gap where the band gaps are (07-15) GHz and (20-32) GHz bands, respectively.

Figure 3.29 displays a dispersion diagram of the proposed mushroom upper patches looking downward of the unit cell at zero air gap. As can be seen, the dispersion diagram allocates dual-band gaps through upper patches that look downward of the unit cell when the air gap is zero. One band gap is for 07-16 GHz and another for 20-32 GHz; the upper band gap is wider than the lower band. A bold green shade presents the band gap for better understanding.

3.4.3 Row of Cell Patches Looking Downward (Air Gap Almost Zero 0.01 mm)

The row of unit cells is the finite number of cells, and the ridge replaces the middle patch allows

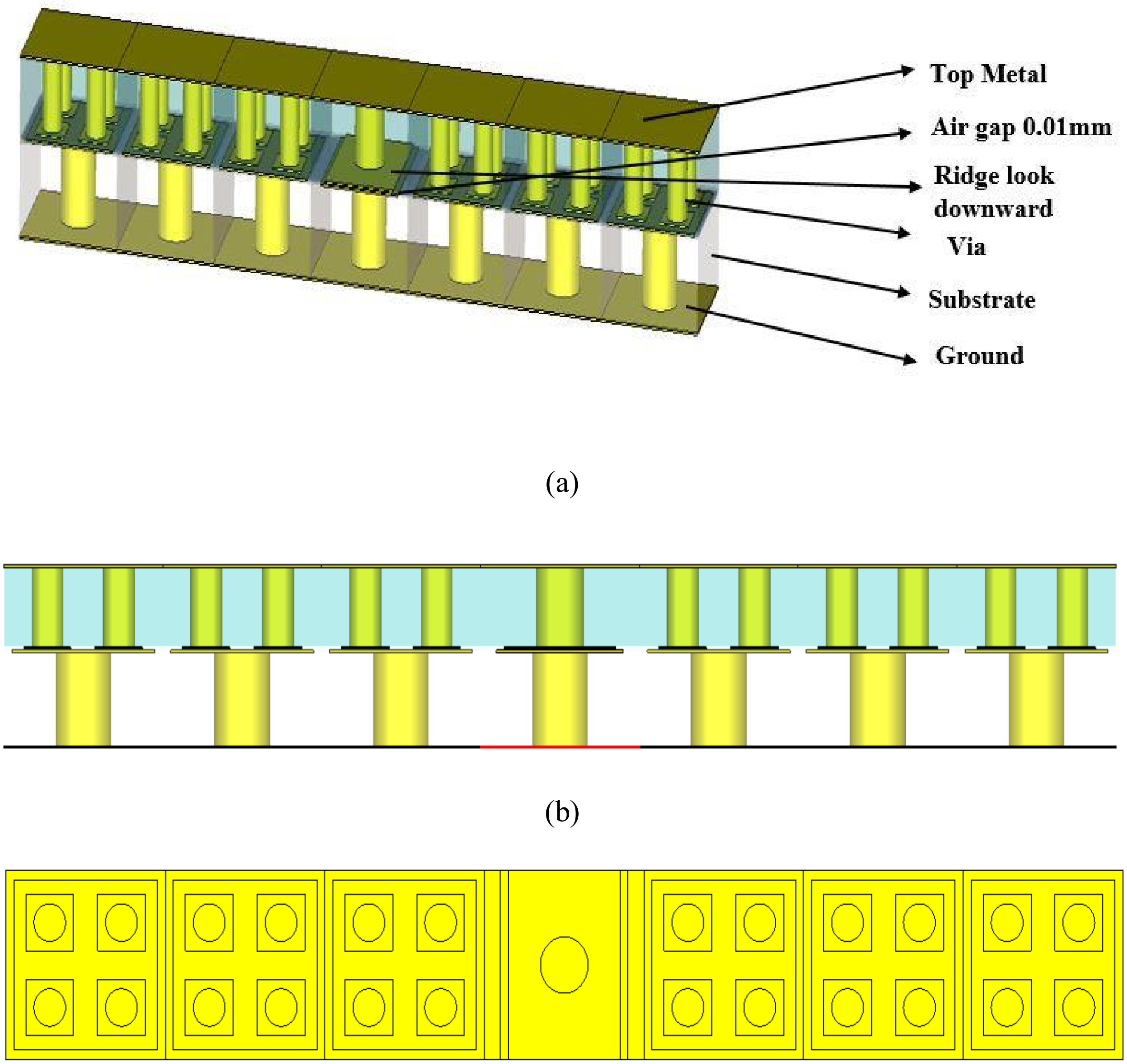

(a)

(b)

(c)

Figure 3.30: Layout of a row of mushroom patch unit cells with a ridge in the central (a) Row of mushrooms with dimensions, (b) Cross-section view, and (c) Top view of a row of mushroom cells looking downward at zero air gap.

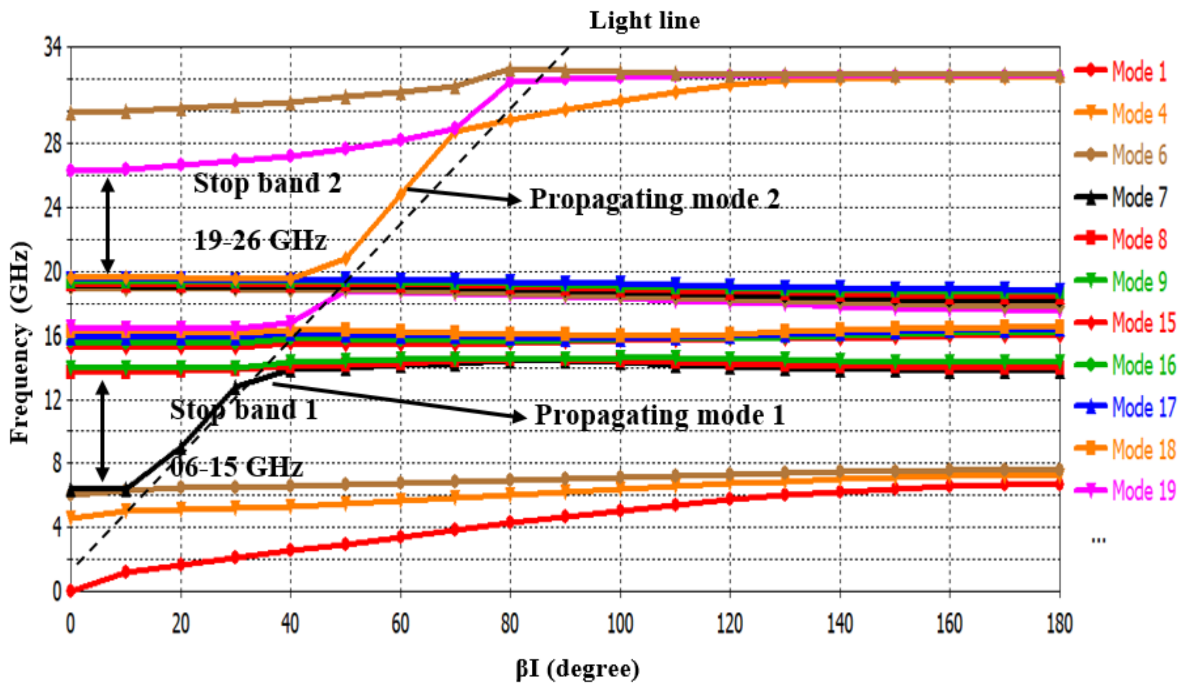

Figure 3.31: Dispersion diagram of a row of mushroom patch unit cells where mode no 7 and mode no 32 are propagating modes.

electromagnetic waves to propagate. Periodic boundary conditions are applied to get satisfactory results. The dimension of each row of cell is the same as the unit cell. The width and length of the lower ridge patch are 1.4 mm and 1.8 mm, and the lower upper ridge patch are 1.2 and 1.8 mm, respectively. In a row of cells, 3 cells are situated on both sides of the ridge patch. Waves propagate through the ridge patches in the dielectric substrates and act at the SIW waveguide, shown in the propagating mode in the dispersion diagram. Figure 3.30 presents the row of cells of mushroom patches at zero air gap with dimensions (a), (b) the cross-section view, and (c) the top view of unit cell patches looking downward. A Q-TEM mode is generated when a ridge is inserted in the cell's row and propagates within the band gap. Figure 3.31 illustrates the dispersion diagram of the row of cells where 40 modes are initiated. As can be noticed, two modes are established, mode no 7 denoted by the black line, and mode no 32, denoted by the orange line, are propagating with the two band gap, which are 06-15 GHz and 19-26 GHz. Although the upper band has a propagating mode, it does not cover the full band gap provided by the unit cell 19-32 GHz. This proposed design unit cell works as dielectric-filled SIW and ridge hybrid technology. However, we can use this unit cell for dual-band SIW filter design or millimeter-wave applications.

3.5 Dual-band 9 Mushroom patches Unit Cell

Dual-band can be obtained by another proposed unit cell with a double layer 9 mushroom patches unit cell. The configuration incorporates two layered substrates: RO3003 with permittivity ε_{r1} 3.0 on the bottom layer and RO3006 with permittivity ε_{r2} 6.5 on the upper layer piled on each other. The unit cell consists of one large mushroom patch in the bottom layer and 9 small mushroom patches in the upper layer. The small patches are connected with large through conducted vias, and the larger patch is linked to the ground with conducting via. The vias are utilized to suppress the surface wave to the substrate. The whole structure is similar to 4 patches mushroom cell, but the only difference is that 9 patches on the upper layer replace the 4 patches, and dimensions are different. The total unit cell size is 1.8 mm. Figure 3.32 displays the configuration of the proposed dual-band 9 mushroom unit cell. The upper and lower substrate thicknesses are 0.75 mm and 0.64 mm, respectively. To construct the large patch, the width, via radius, top and bottom metal thickness is kept at 1.6 mm, 0.3 mm, and 0.0175 mm, as well as for the small patch width, small via radius are also kept at 0.45 mm and 0.15 mm. The air gap between the top metal lid and upper layer patches is about 0.127 mm. The stop band determines the operating bandwidth of the full structure that provides the unit cell's performance. The EBG surface behaves like a high-impedance surface inside this bandwidth. Employing propagation, this band gap only supports

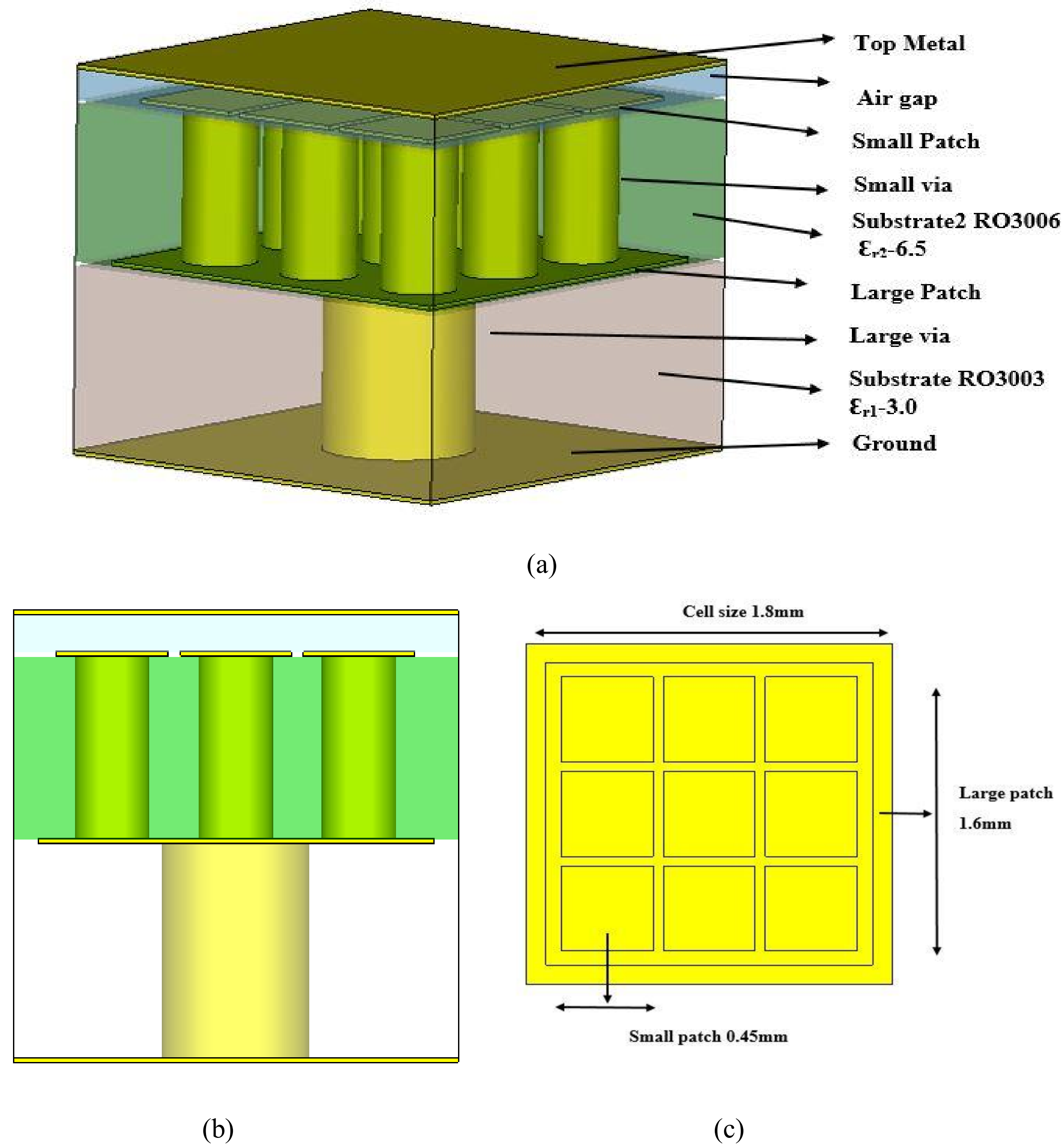

Figure 3.32: Configuration of dual-band 9 mushroom patches unit cell (a) Mushroom patch with dimensions, (b) Cross section view, and (c) Top view of proposed 9 mushroom patches unit cell.

Q-TEM waves and cancels other waves. The proposed unit cell allocates two wide band gaps that allow only Q- TEM waves. The periodic boundary condition is enough for this unit cell to analyze it. A dispersion diagram is essential to find the unit cell's electromagnetic band gap (EBG) using the Eigenmode solver of the commercial software CST Microwave Studio. Figure 3.33 shows a dispersion diagram of the proposed dual-band 9 mushroom patches unit cell. In the dispersion diagram, two wide band gaps were acquired, one for lower band 10-20 GHZ, from mode no 1 and mode no 2 and another for upper band 35-45 GHz, from mode no 9 and mode no 10. For better undersetting, the EBG band gaps are presented in bold yellow color in the dispersion diagram.

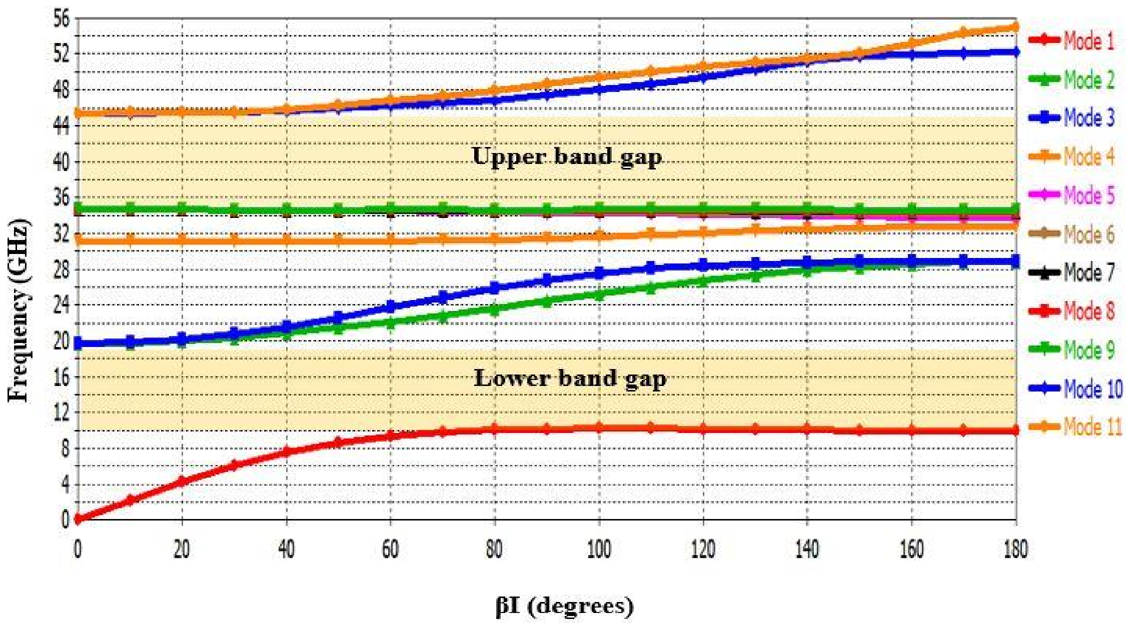

Figure 3.33: Dispersion diagram of a dual-band 9 mushroom patch unit cell where the band gaps are (10-20) and (35-45) GHz bands, respectively.

3.5.1 Row of Dual-Band 9 Mushroom Patches Unit Cell

The row of unit cells replicates the same cells in 1D or 2D a finite number of times. To build a mushroom row of cells, the middle patch is replaced by a ridge patch, and periodic boundary conditions are applied to get the desired result. The width and length of the ridge patch are 1.2 and 1.8 mm, respectively. The dimension of the row of cells is the same as that of the 9 mushroom patches. In a row of cells, 2 unit cells are on either side of the ridge patch. Electromagnetic waves travel through the ridge patch, shown in the propagating mode in the dispersion diagram. Figure 3.34 illustrates the row of cells of 9 mushroom patches with dimensions (a), (b) the cross-section

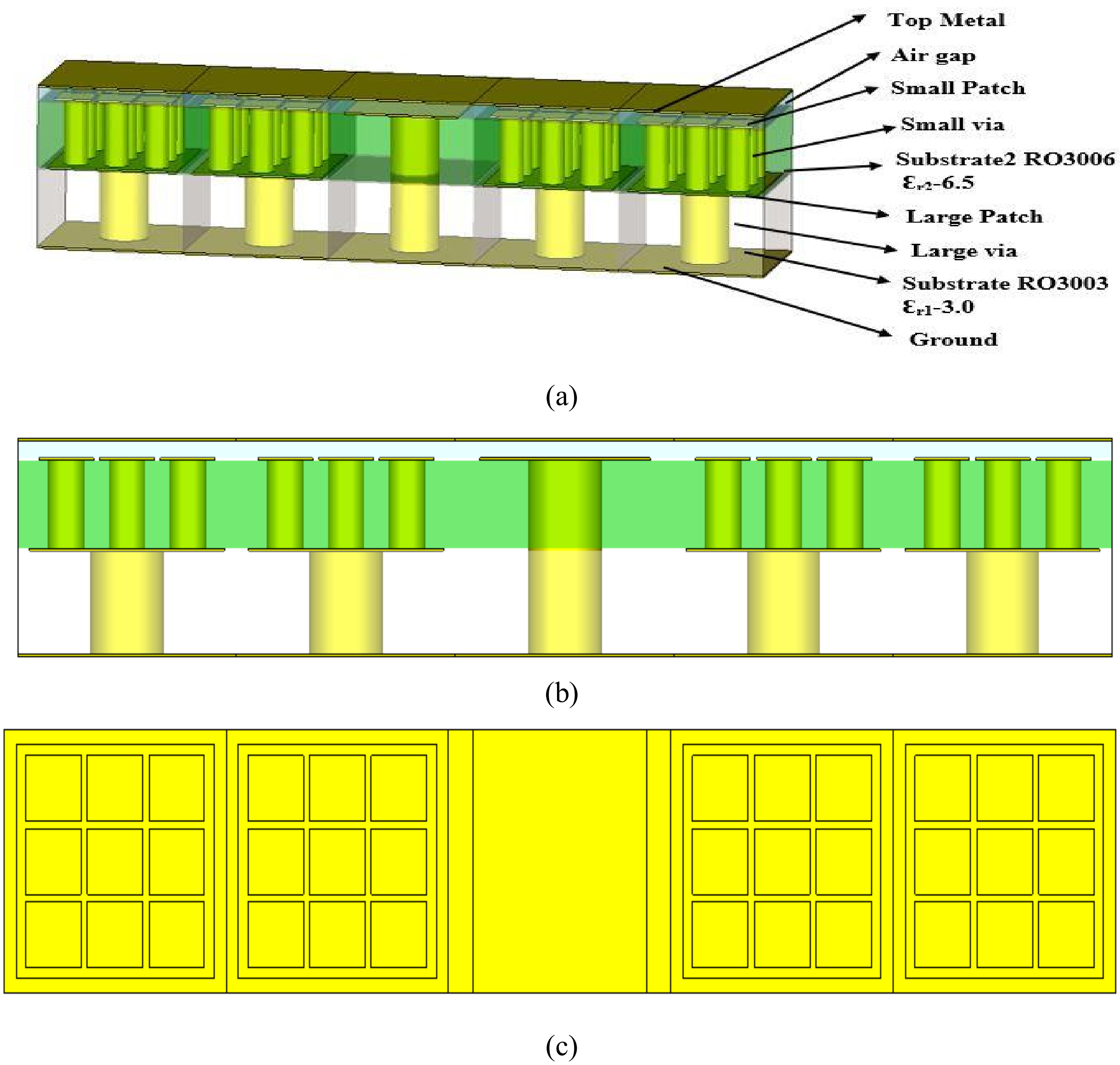

Figure 3.34: Structure of a row of cells of dual-band 9 mushroom patches (a) Row of finite cells with dimensions, (b) Cross section view, and (c) Top view of cell.

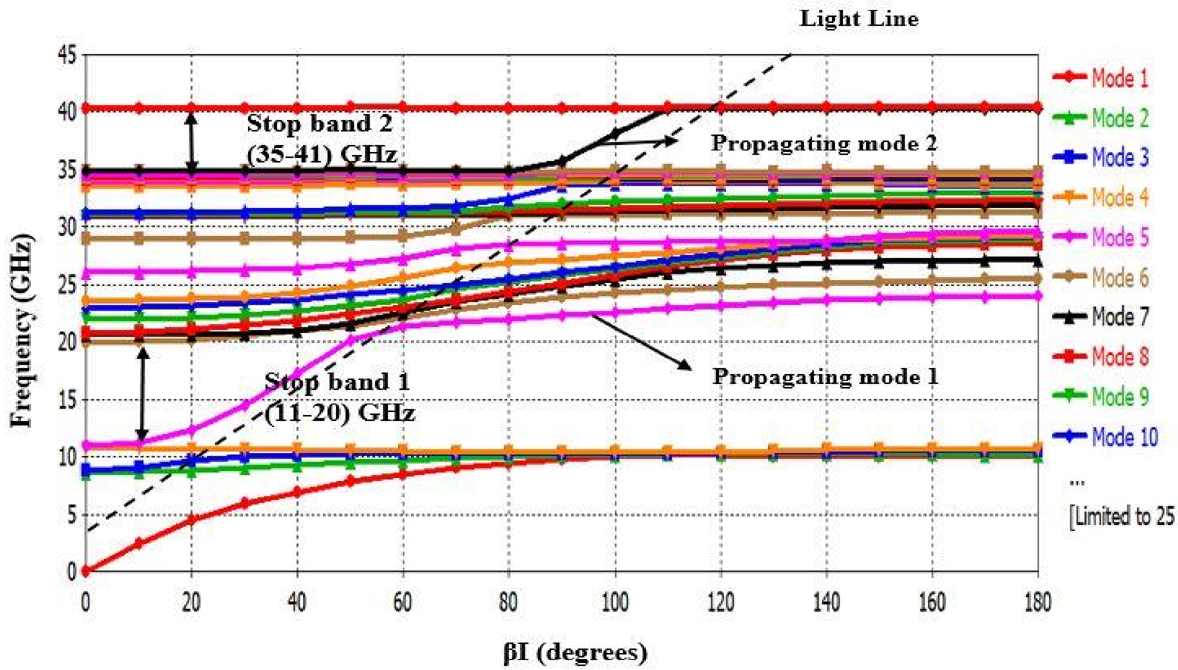

Figure 3.35: Dispersion diagram of a row of mushroom patch unit cells where mode no 7 and mode no 42 are propagating modes.

view, and (c) the top view of the row of 9 mushroom unit cells. The dispersion diagram presents the propagation modes related to the installed ridge within the EBG. Figure 3.35 portrays the dispersion diagram of a row of mushroom patch unit cells where mode no 5 and mode no 42 are propagating modes. As can be noticed, mode 1 propagates parallel to the light line at a lower frequency, but as the frequency escalates, the mode becomes slower, does not collaborate with the free space, and provides the band gap and propagating mode in higher frequencies. Two propagating modes can be observed in the dispersion diagram, indicated by mode 5 (pink line) within 10-20 GHz and mode 42 (black line) within 35-41 GHz. The first propagating mode can be observed between modes 4 and 6, and the second propagating mode can be observed between modes 41 and 43. However, the upper propagating band gap is supposed to be 35-45 GHz based on the unit cell's band gap, but the propagating mode, mode no 42, only travels between 35-41GHz, due to complex design and many structures and vias in the upper layer that may create some wave suppression in the upper band gap. Comparing the unit cell modes and the row cell modes, row cell modes are more due to the finite length of the cell that causes standing waves in the transverse direction of the ridge.

3.6 Result verification of proposed unit cell with another simulator

To verify whether the proposed unit cell design works perfectly, the model is constructed with another simulator, HFSS. All the dimensions are kept the same as the unit cell designed in CST software. A dispersion diagram is often obtained for a stop band in both Eigenmode solver in CST and HFSS software. One cell with a periodic boundary is sufficient to be considered for an infinite array of cells on the sides. Figure 3.36 depicts the dual band unit cell in HFSS software, (a) Full structure, (b) Cross section view and (c) Top view of unit cell. Figure 3.37 shows the dispersion diagram of the designed unit cell using HFSS. The modes variations with βI resemble the variation using CST. However, the lower band shows a frequency shift of the upper end of βI by 3 GHz. Thus, the HFSS lower band is 17-25 GHz. The upper band is 34-45 GHz. For the comparison of the results, the ideal parameters (article 3.2) are taken to design in both CST and HFSS simulators. Where the cell size is 1.8mm, the same substrates (Roger RO3003, RO3006) are taken with the thickness of 0.75mm and 0.64 mm respectively. The patch's widths are 1.4mm and 0.5mm with an air gap of 0.127mm. The via radius are 0.3 and 0.15 mm respectively. With the same parameters of the designed unit cell, both simulators provide dual bands but a little bit of frequency shift in the lower band is given by the HFSS simulator but almost the same in upper band. Therefore, the

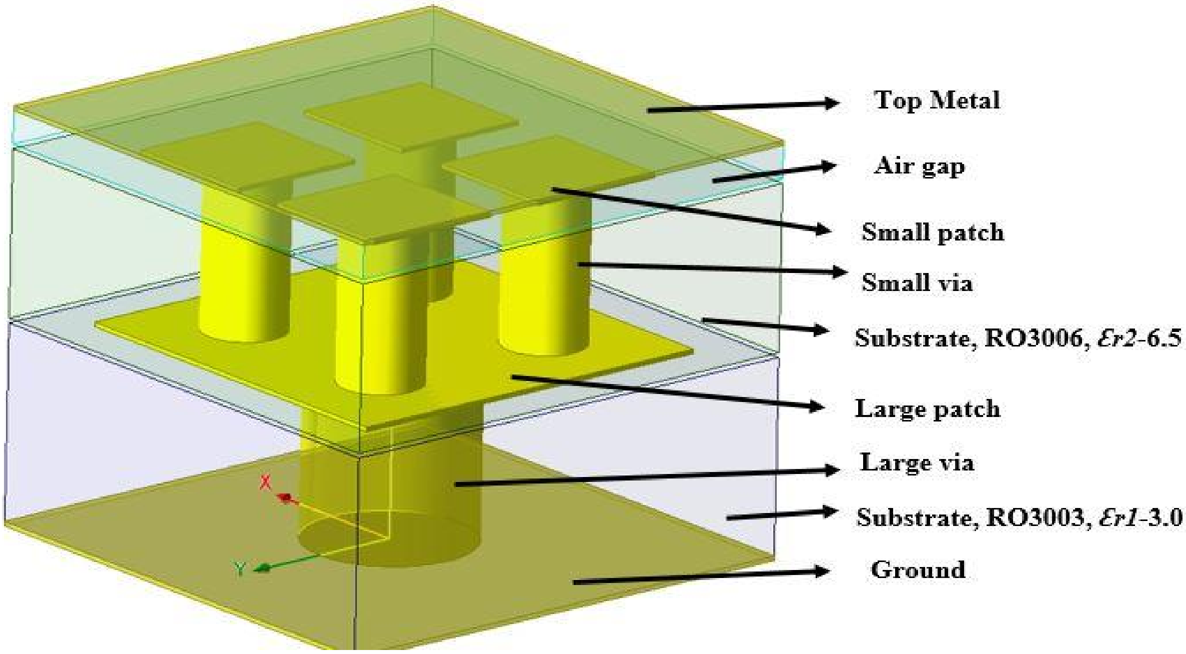

(a)

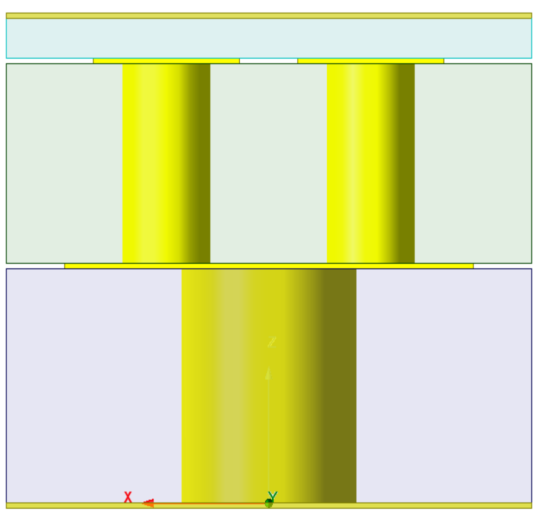

(b)

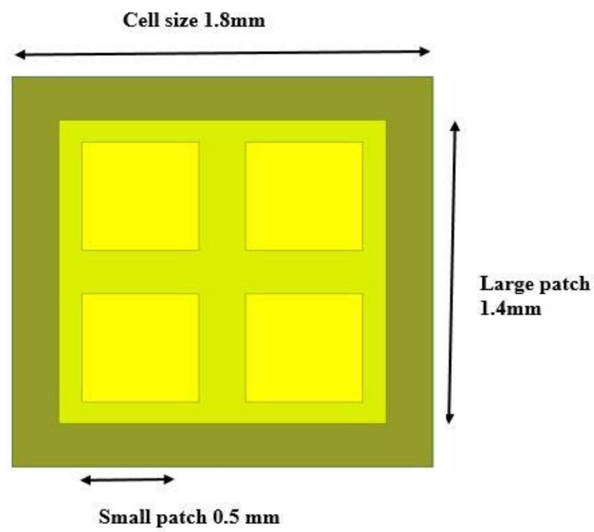

(c)

Figure 3.36: Geometry of dual-band 4 mushroom patches unit cell (a) Full structure, (b) Cross section view, and (c) Top view of the proposed unit cell in HFSS.

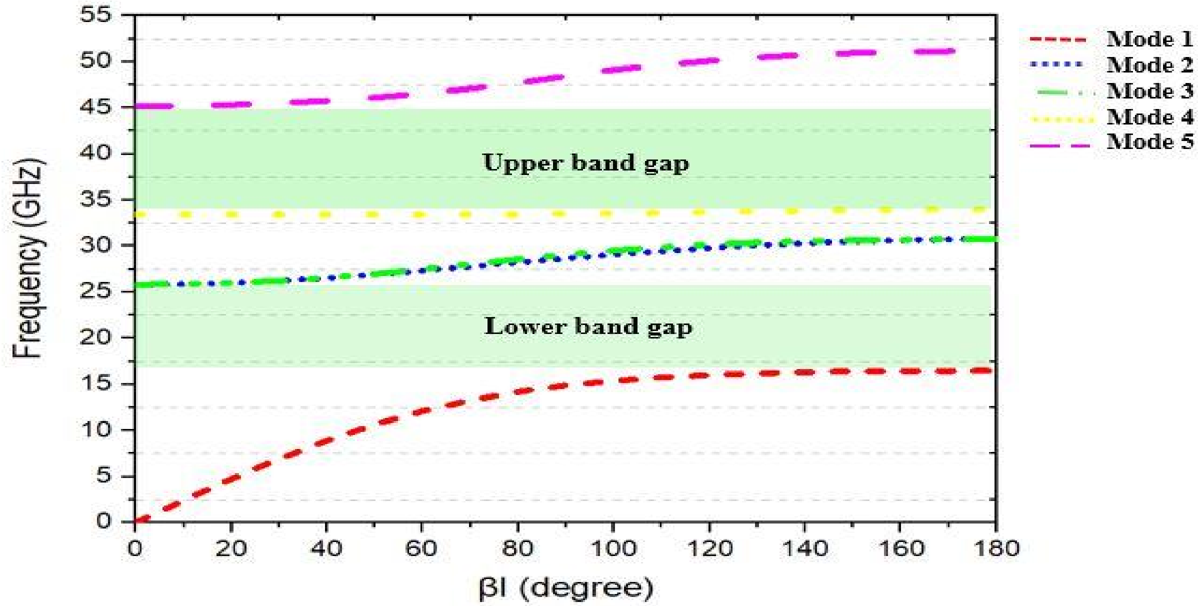

Figure 3.37: Dispersion diagram of a dual-band mushroom patch unit cell where the band gaps are (17-25) GHz and (34-45) GHz bands, respectively.

convergences of the CST solution are satisfactory for use in this study. Table 3.6 illustrates the comparison table of the results of EBG from the two simulators with the same parameters.

Table 3.6 Comparison table of EBG for designed unit cell in CST and HFSS Simulators.

Cell size 1.8 mm (same parameters)			
Simulator	**Lower band**	**Upper band**	**Mismatch**
CST	13-24 GHz	34-44 GHz	1. Lower band 3 GHz shift. 2. Upper band 1 GHz.
HFSS	17-25 GHz	34-45 GHz	

Although dual-band is achieved through double layer 9 mushroom patches unit cell, we consider 4 mushroom patches unit cell for our further experiments because both provide similar band gap and 9 mushroom patches unit cell doesn't offer any extra facility or benefit in our stop band with significant outcome. This design is verified with another simulator, HFSS, which is accurate. However, to avoid design complexity, simulation time, and fabrication cost, we chose a double-layer 4 mushroom patches unit cell in our further design process.

Chapter 4

Proposed Packaged Dual-band RGW Performance

The two parallel plates that make up the ridge gap waveguide are a top metal lid and a lower plate with a central metal ridge encircled by periodic unit cells [29]. The periodic unit cell can be realized with different-shaped patches connected with plated vias to suppress all the unwanted modes [30]. The unit cell consists of identical cells repeated a finite number of times in either 1D or 2D, creating an AMC surface with high impedance and not allowing wave propagation. The unit cell controls the bandgap of the whole structure [28]. CST microwave studio software designs the proposed unit cell and full works. An Eidgemode solver is used for unit cell analysis where periodic boundary conditions are applied for the desired outcome. It is important to note that in the Eigenmode solver, there are no ports for excitation where Maxwell's curl equations are used to calculate the problems for both electric and magnetic fields that provide the bandgap through the dispersion diagram. In order to design the waveguide and transition, the Transient solver of CST is used, where the finite integration technique (FIT) is developed to resolve the problem and implement the integral Maxwell's equation [44]. The PEC boundary condition is employed for designing the PRGW where $E_{tan}= 0$, and only the normal electric field exists. The H_{tan} produces a surface current because of the PEC boundary condition. The periodic patches function as an Artificial Magnetic Conductor (AMC) where no normal electric field exists. A Dual-band printed ridge gap waveguide is designed using the proposed unit cell. Four different types of PRGW are designed by changing the positions and conditions of the ridge, which are shown here with simulated results. After that, two 90-degree bend lines are presented with the proposed unit cell with result and field distributions. A 1x2 power divider with a dual-band AMC surface is exhibited. Finally, two couplers are proposed with the dual-band unit cell; one is designed for the lower band and another for the upper band

4.1 Printed Dual-band Ridge Gap Waveguide

The EBG mushroom cell surface can be fabricated as a packaging solution using printed circuit board technology [42]-[45]. This can be combined in the same substrate layer, making it more compact. The proposed RGW unit cell is constructed by two-layer substrates with an air gap layer on the top of the substrate to guarantee a gap height where waves propagate. A single square mushroom patch is in the bottom substrate, and four small square mushroom patches are placed in the upper substrate connected to a large patch and ground plate through metal vias. This proposed double-layer unit cell provides the desired band gap of RGW, and the band gap can be changed by varying the parameters of the unit cell based on our required frequency. A conducted metal strip on the top of the via of the upper layer here realizes a conducting metal ridge. This new technique is very capable and encouraging for researchers because of its low cost, compact size or packaged technique, lightweight, low loss, and outstanding performance compared to traditional microstrip lines and SIW. The printed version of gap waveguides is recognized as the printed ridge gap waveguide (PRGW). The printed version of the ridge gap waveguide has shown losses, bends, and numerical analysis using microstrip ridge transitions [45]. With printed circuit board (PCB) technology and packaging technique, a complete PRGW was created in this paper [46],[47]. The proposed RGW can operate two different frequency bands based on this unit cell. Four types of ridges are proposed by varying the ridge position and layer that provides users with shifted of both frequency bands in accordance with their requirements. In Chapter 3, the details of the unit cell were sketched with dimensions along with the promising criteria of the proposed dual-band PRGW with parametric studies. In Chapter 3, provide dual-band 9 mushroom patches unit cells with

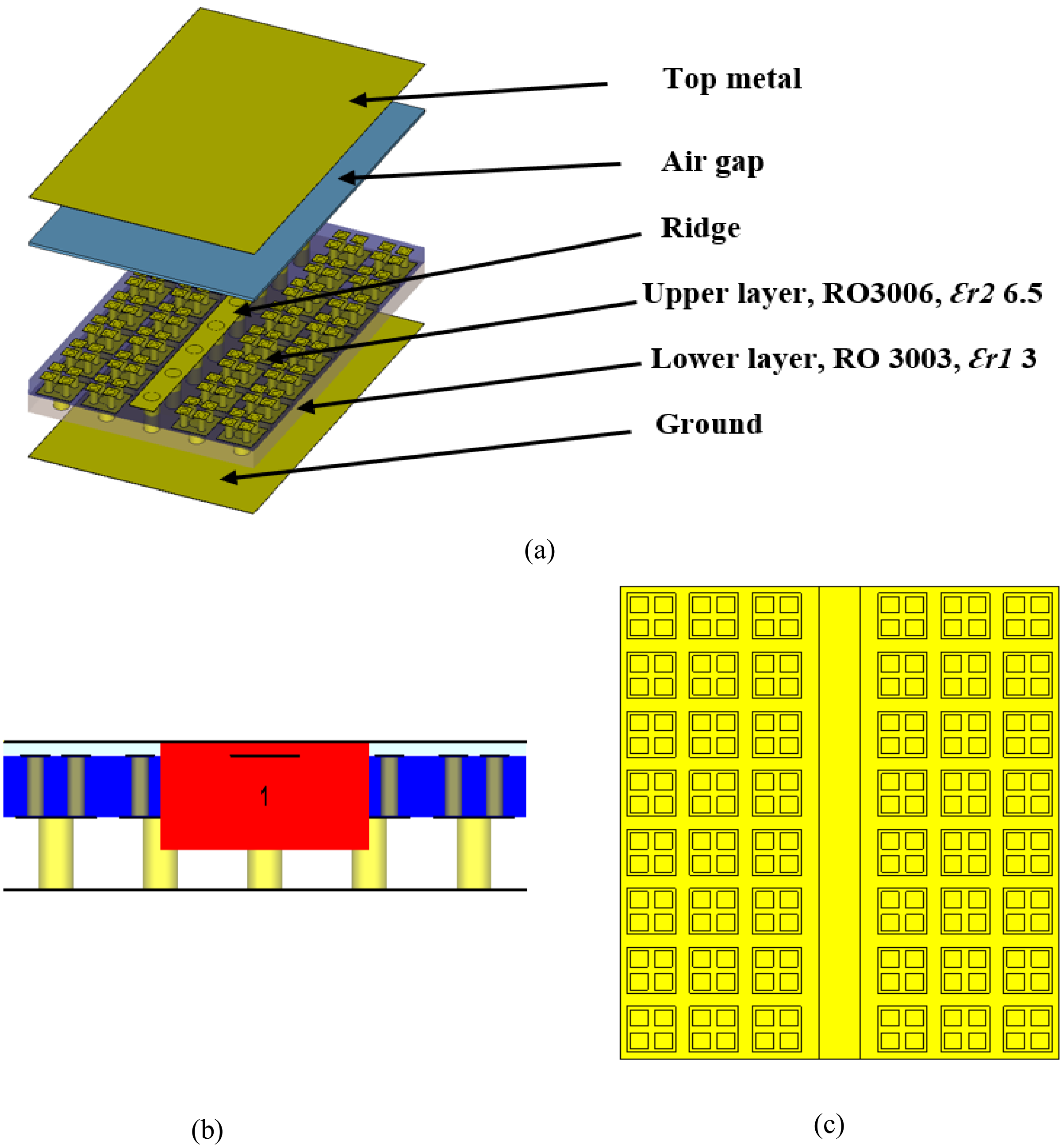

Figure 4.1: Geometry of the proposed dual-band ridge gap waveguide (a) Overall view, (b) Cross-section view, and (c) Top view.

dispersion diagram. In the previous chapter, the row of unit cells with propagating modes and the dispersion diagram of 4 and 9 mushroom patches unit cells are depicted in detail. Figure 4.1 presents the full geometry of the proposed dual-band PRGW: (a) the overall view, (b) the cross-section with port, and (c) the Top view. In terms of the proposed PRGW port excitation, the ideal wave port supplied by the simulator is used. It is important to mention that the definition of this port needs to be carefully evaluated to cover all the fringing fields surrounding the ridge, so a ridge cell with half of full of the neighboring cell would be a great choice for covering the fringing fields. The simulated S-parameters of PRGW are shown in Figure 4.2, which operate at 13-24 GHz and 34-44 GHz. It can be considered a passband of the proposed RGW as well. This plot demonstrates that 13 - 24 GHz and 33 - 44 GHz are vertically polarized ridge modes of stop band where the blue bold shades show the dual bands of proposed RGW. The width of the ridge line is 1.2 mm with an impedance of 31.5 Ω, where 50 Ω can be achieved by changing the ridge width or using an adapter.

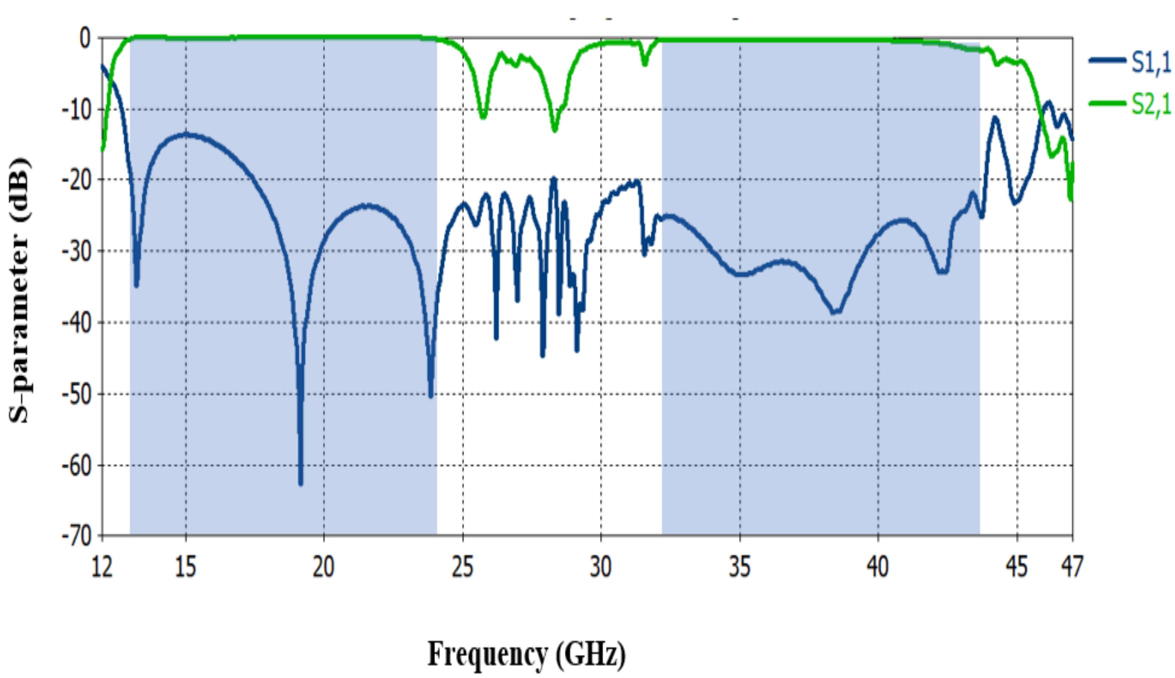

Figure 4.2: Simulated S-parameters of the proposed PRGW covering two frequency bands

A Q-TEM mode propagates along the metal ridge through the air gap. However, dual frequency bands are generated by the proposed dual-band ridge gap with outstanding matching except for the band between 25 to 33 GHz, which is out of band with some ripples.

4.2 Dual-Band RGW Microstrip Line Transition and Operating Modes

The ridge gap waveguide (RGW) is not a standard technology that can be implemented using conventional measurement tools. Hence, it must be linked to conventional transmission lines for performance to be excited and measured. For design purposes, the RGW is excited by the ideal

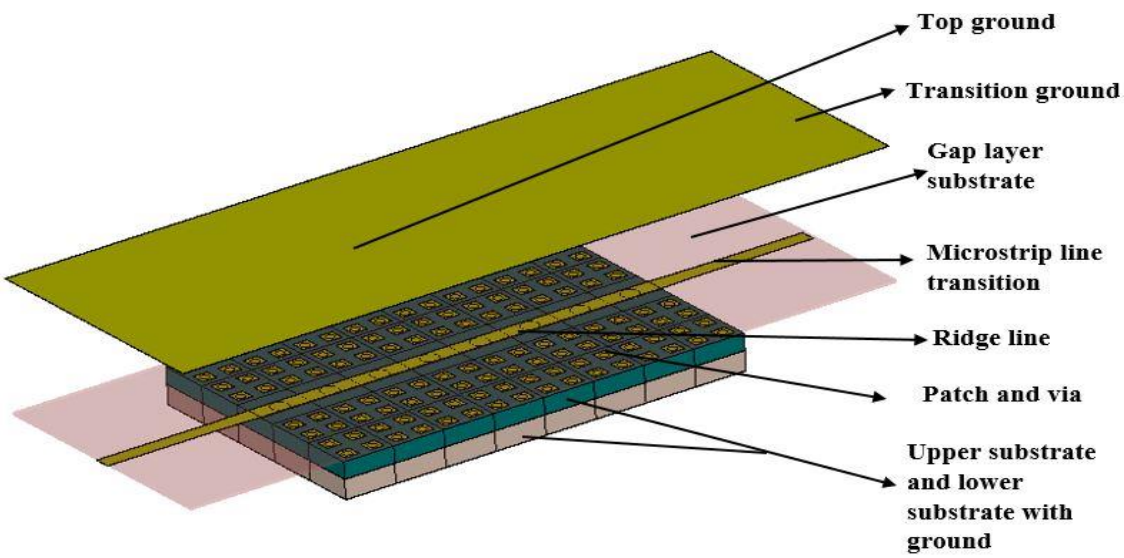

Figure 4.3: Microstrip layout to proposed dual-band ridge transition line.

wave ports supplied by the simulator. In the case of practical measurements, the waveguide is essential to feed with some standard transitions such as rectangular waveguide, coaxial, or microstrip transition [47]-[48]. Several experimental setups are required to test the guiding structure. Feeding the RGW with the microstrip line seems more useful since the microstrip supports the Q-TEM mode of propagation and is easy to design and fabricate. However, in our work, to enhance the dual-band RGW, a conventional tapered microstrip-ridge transition is considered, which is presented in Figure 4.3. In many articles, the microstrip-to-ridge transition has been inspected and published [49]-[50]. It is important to note that the fringing field should be

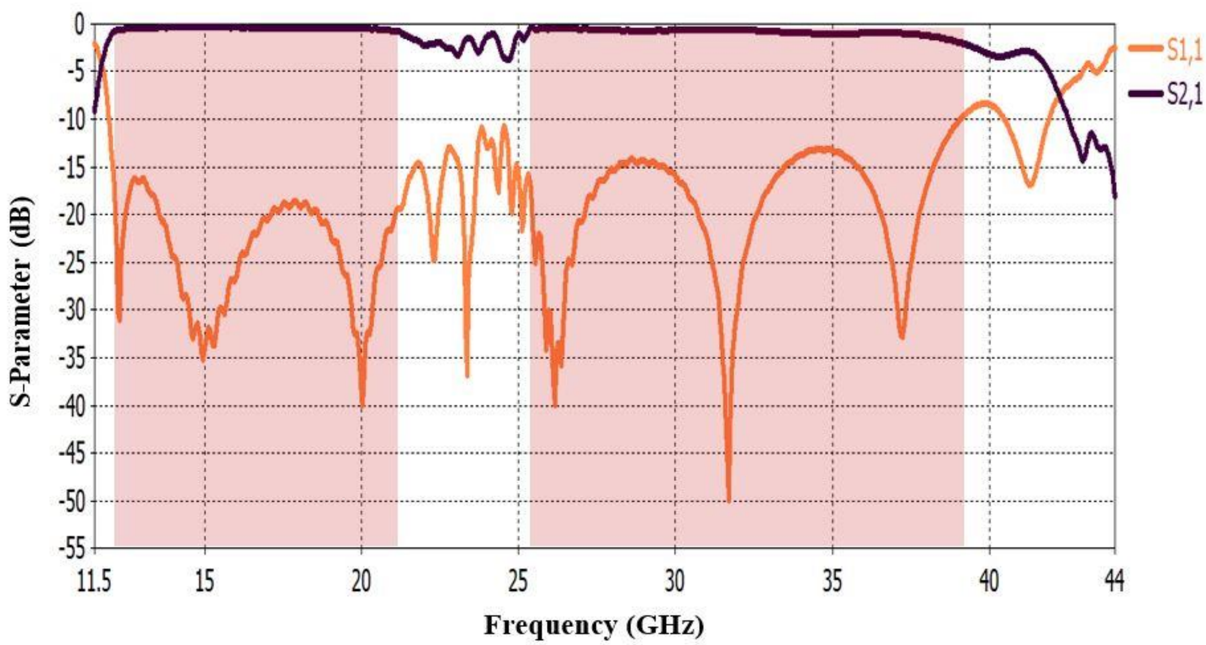

Figure 4.4: Simulated S-parameters of proposed PRGW with microstrip transition.

considered around the microstrip line while designing the transition. To make a quasi-TEM dielectric-filled RGW, a dielectric layer is added on the top of the ridge line in order to support the extended transition line, and then the top metal ground is set up. The Top ground plane should be extended up to two rows, and the strip line should be placed on the bottom part of the dielectric and connected with the ridge line on the top layer of the design. The width of the extended line is adjusted by changing it or tapering to match the 50Ω impedance of the microstrip. The added dielectric layer, the RT5880, with permittivity of εr 2.2, is used with the same thickness as the air gap, which is 0.127 mm. The transition line length is 5.5mm. Figure 4.3 illustrates the proposed

RGW with the transition to the microstrip line. Figure 4.4 depicts the simulated performance of the S parameters with the tapered microstrip transitions. The simulated performance is presented by the orange and purple curves and a bold orange shade covering the dual-band. The optimized line width is 0.65mm, the total length of the line is 19.9 mm to match 50 Ω, and tapering is used for good matching of the scattering parameter. It is noticed that within the frequency band, the S11 of the lower band is below -15 dB, and the upper band is almost -13dB with low insertion loss. The dual-band is 12-22 GHz for the lower band and 25.5-39 GHz for the upper band. The dual-band is shifted a bit to the lower side due to the addition of the transition. The performance of the upper-frequency band of the microstrip line deteriorates since it tolerates the cavity modes, which leads to surface waves. Due to the taper of the transition line, there will be leakage and diffractions; consequently, most of the signal will lose energy. This leakage of the transmission lines can reduce where the wave only travels within the ridgeline, and the unit cell of mushroom patches prohibits the wave propagation transverse to the direction of the ridge line [38].

The operating mode of PRGW is equivalent to a microstrip line that is quasi-TEM mode. A Q-TEM mode will arise due to a discrepancy in phase velocities between the two mediums. In this case, a portion of the waves propagates in the air, but the majority are contained within the dielectric substrate; as a result, quasi-TEM is created, and in the edges of the microstrip line, some fringing fields exist. Figure 4.5 shows the port modes of the proposed waveguide design: (a) E field distribution and (b) H field distribution. It is apparent in the Figure that the orientation of the ridge is in the Y direction, and the PEC boundary condition is applied in the Z-axis, so for the ground plane and ridge, according to the PEC boundary conditions, only the normal electric field component will exist here. Periodic boundary conditions are applied in the X and Y planes, which are high-impedance surfaces. The proposed dual-band PRGW at the port end of the Ez is the normal electric field perpendicular to the magnetic field Hx. Both Ez and Hx are transverse to the propagation direction, which is aligned in the Y direction. The E fields are vertically polarized, and the H fields are horizontally polarized. Due to medium changes, some fringing fields can be observed on both edges of the ridge line. There is no exact formula to calculate the characteristic impedance of the RWG. Some numerical analysis and analytical performance were done to get the approximate value of line impedance that was quite acceptable [30].

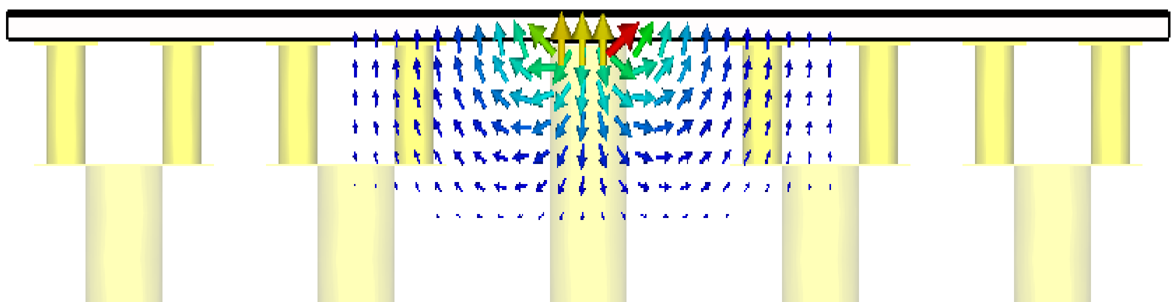

(a)

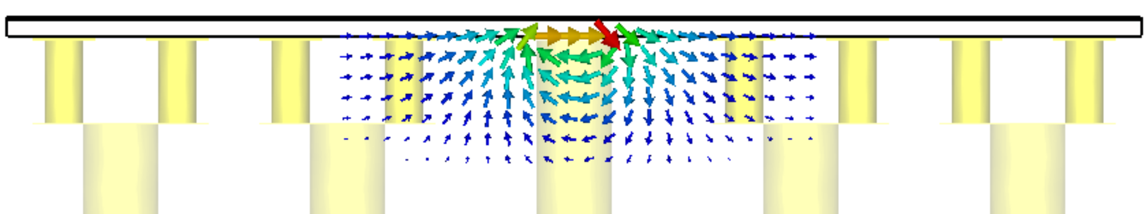

(b)

Figure 4.5 Field distribution from the port end (a) Electric and (b) Magnetic field.

4.3 Field Distribution along with RGW

The main object of periodic EBG unit cells is to cancel and neutralize the field propagation

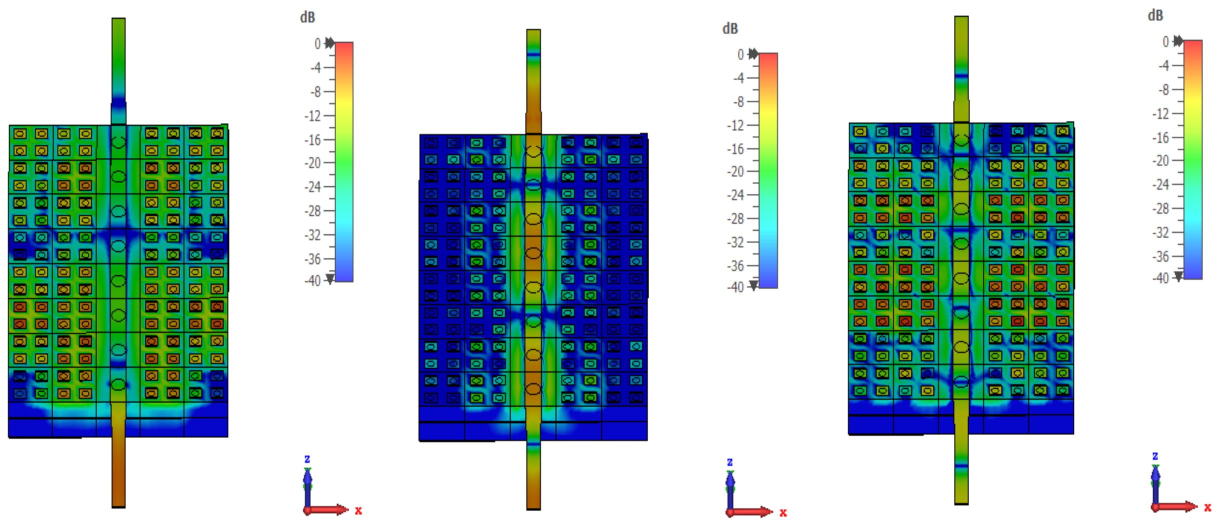

(a) 10 GHz (Out of band) (b) 15 GHz (In band) (c) 23 GHz (Out of band)

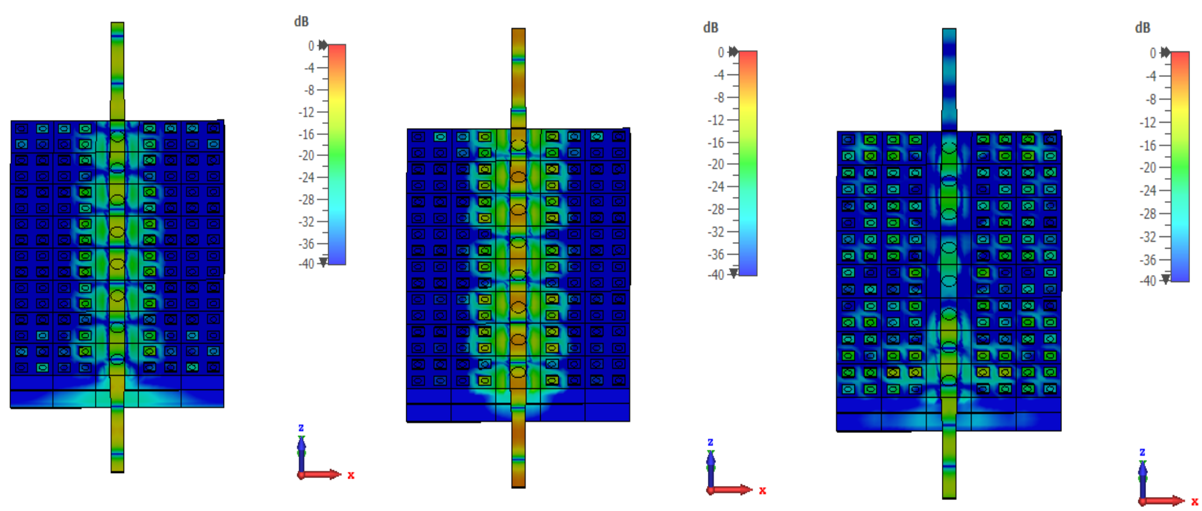

(d) 30 GHz (In band) (e) 38 GHz (In band) (f) 46 GHz (Out of band)

Figure 4.6: E-field distribution of the proposed dual-band ridge gap waveguide with microstrip transition at different frequencies. (a) 10 GHz, (b) 15 GHz, (c) 23 GHz, (d) 30 GHz, (e) 38 GHz, and (f) 46 GHz.

transverse to the ridge direction. If a magnetic boundary condition is applied, no fields will be propagation transverse to the ridge direction. One verification can be achieved of the EBG unit cell surrounded by a ridge through the study of field distribution. This simulation ensures that the ridge within the operating frequencies confines the electric fields. Using RGW as a guiding structure does not encounter cavity modes and surface waves within the two operating bandwidths of the waveguide over 12-22 GHz and 25.5-39 GHz, which are common for microstrip lines at higher frequencies. Figure 4.6 depicts the electric field distribution response of a periodic structure of different frequencies with or without the band gap. From the Figure, it can be observed that 10, 23, and 46 GHz are out of the EBG band, so fields are scattered all over the structure, while frequencies 15, 30, and 38 GHz are within EBG bands, so electric fields are densely bounded within the ridge line thus prohibit the leakage of the structure. Hence, before the lower cutoff frequency, after the upper cutoff frequency, and middle out of the frequency band, the EBG periodic unit cell does not work as an AMC surface, and the fields get scattered and decay the overall power transfer from one port to another; as a result, the transmission coefficient reduces badly. Thus, leakage occurs beyond and middle out of the band. The field intensity reaches nearly zero after three columns of mushroom patches on either side of the ridge, so designing up to two or three columns is better to avoid the structure's simulation time and complexity.

4.4 Four Different Designs of Dual-Band PRGW Using Proposed EBG Cell

The mechanism of RGW consists of a periodic structure distinct from the full ground plane by less than a quarter of a wavelength. It serves as a PEC-AMC parallel plate providing the stop band region surrounding the guiding ridge. The boundary conditions of the upper ground plane and the propagation medium's lower edge are different because of the PEC-PMC medium. The proposed dual-band RGW follows the same operating principle and conditions as a single-layer ridge. There are no dielectric losses like in coplanar waveguides or microstrip lines because they are constructed on a dielectric substrate and use air as the propagating medium. By changing the ridge layer and the position of the ridge state, four different types of RGW are proposed with the dual-band unit cell. The scattering parameters provide dual-band, but the frequency becomes shifted or the same as the band gap of the unit cell for both upper and lower frequency for four sorts of design, a great advantage of dual layer RGW. Four different types of RGW using dual-band EBG unit cells are given in the following section, with design and scattering parameters in detail. However, the proposed four different dual ridge gap waveguides provide four different scattering parameters, so one can pick any design based on the needs or requirements. Considering the four designs below, the single ridge in the upper layer provides the best possible scattering parameter as output with low insertion loss and the same frequency band as the proposed unit cell. As a result, we consider a ridge in the upper layer for further design of other components.

4.4.1 Ridge in Double Layer (Case-i)

The first design idea of RGW is using a ridge in both layers, the upper layer and the lower layer, but the port will connect in the upper layer. The ridge width is not the same; for the lower ridge width is 1.4 mm, and the upper ridge width is 1.2 mm, the lower ridge width is the same as the patch width. Above the ridge layer is an air gap where EM waves travel through the ridge line. The width of the ridge line is 0.75 λ in terms of wavelength. The characteristic impedance of the ridge gap waveguide is 31.5Ω. The upper ridge is connected with the lower ridge, and the lower, ridge is attached to the ground plane with metal vias. Figure 4.7 displays the dual-band RGW

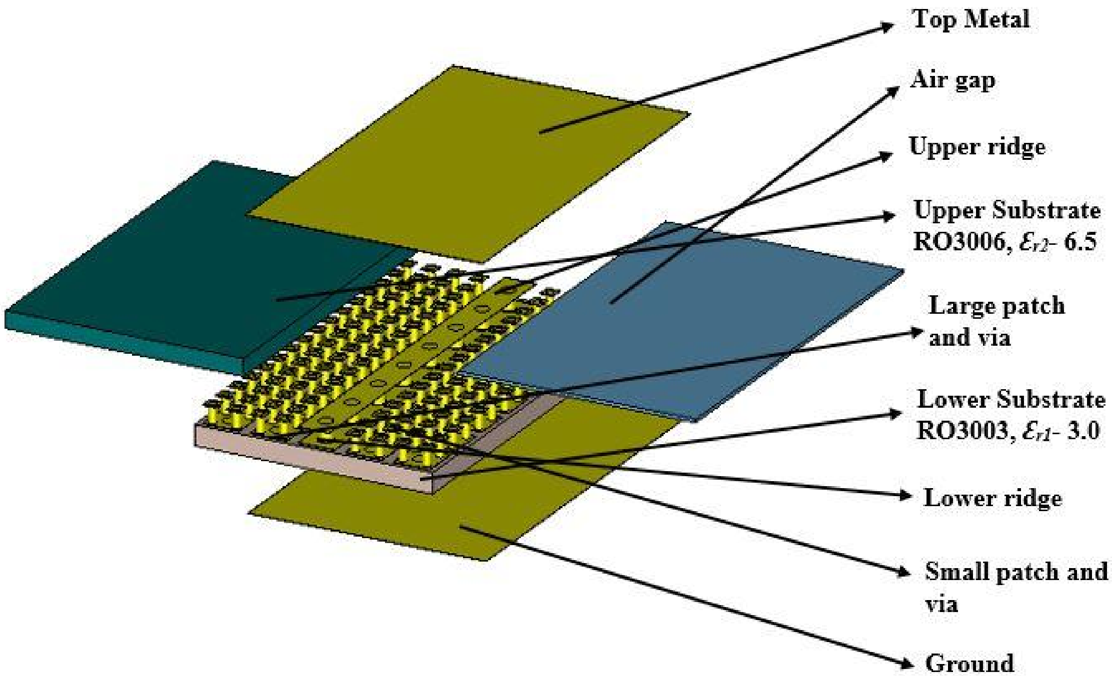

Figure 4.7: Dual-band ridge gap waveguide case-i, where the ridge is in the double layer.

where the ridge is located in both layers with different ridge widths. The upper ridge line is placed on top of the upper dielectric substrate RO 3006 with permittivity $\mathcal{E}_{r2}$ 6.5, and the lower ridge line is located on top of the lower dielectric substrate RO 3003 with permittivity $\mathcal{E}_{r1}$ 3.0. The scattering parameters are presented in Figure 4.8, where dual-bands 13-23 GHz and 35.5-47.5 GHz are generated with low insertion loss. The reflection coefficient, S11, is lower than -15dB for both layers precisely with outstanding match except out of band 23- 35 GHz with ripples. The scattering parameters are shown with bold green shades for better understanding. A few changes have been seen in frequency, where the lower frequency ends at 23 GHz instead of 24 GHz, and the upper frequency starts 35.5 GHz instead of 34 GHz and continues up to 47 GHz. The air gap height is kept at 0.127 mm. The full design is performed in the Transient solver of CST microwave studio.

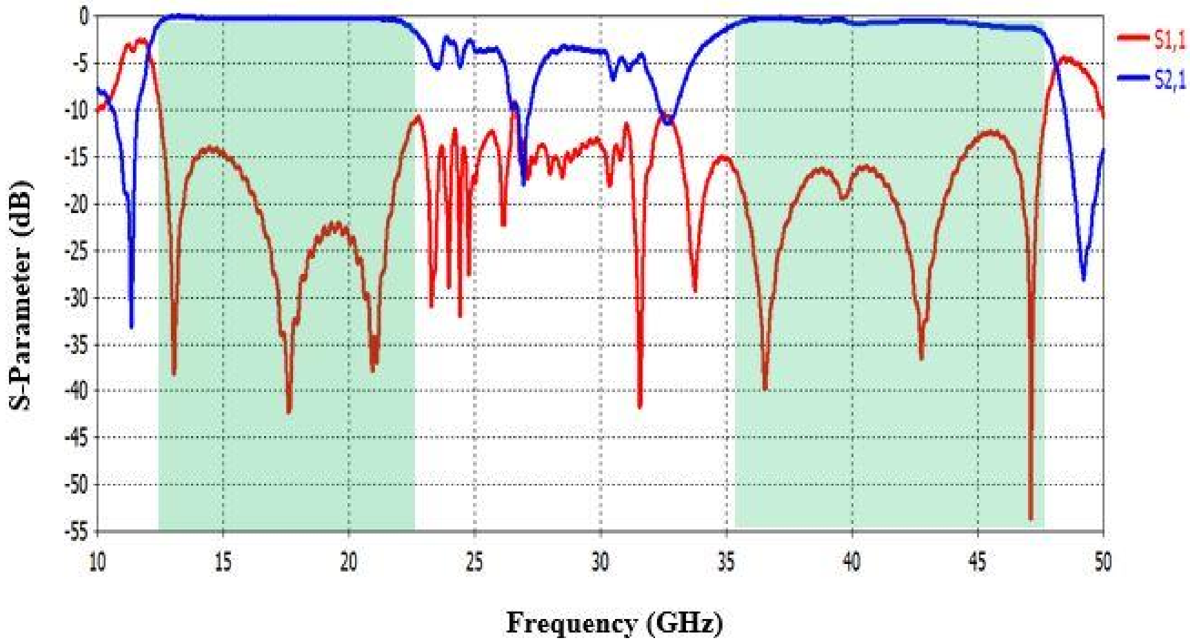

Figure 4.8: Simulated S-parameters of proposed PRGW for case-I, ridge in both layers.

4.4.2 Field Distribution

The E field distribution of double layer ridge gap waveguide is depicted in Figure 4.9. From the Figure at different frequencies, the E fields are confined within the ridge line for two different frequency ranges, and leakage occurs out of the frequency band. The undesirable radiation is blocked by the periodic cells. As can be noticed, the frequencies of 10, 28, and 50 GHz are out of EBG bands, so fields are disintegrated throughout the full configuration, whereas at the frequencies of 15 and 40 GHz are inside the EBG band so, electric fields are tightly confined within the ridge line and thus saves the power loss from the whole structure.

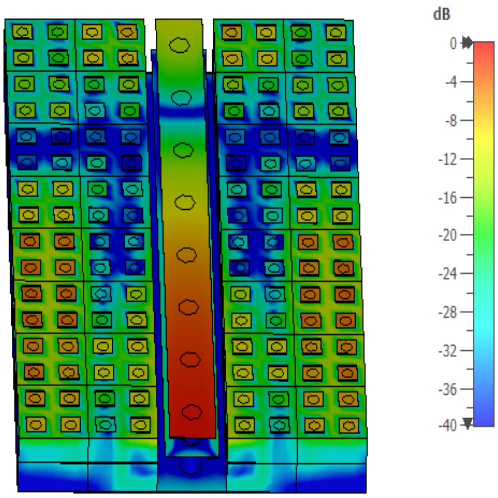

(a) 10 GHz (Out of band)

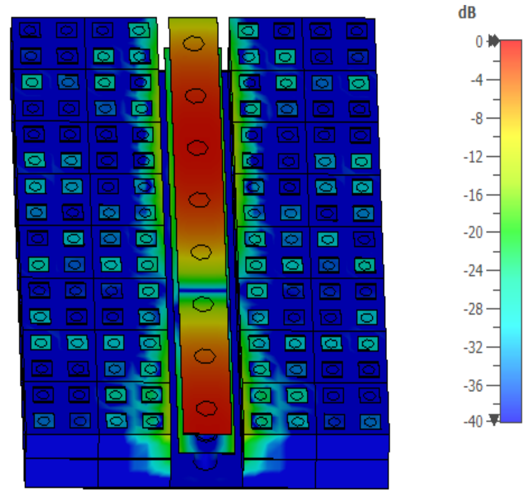

(b) 15 GHz (In band)

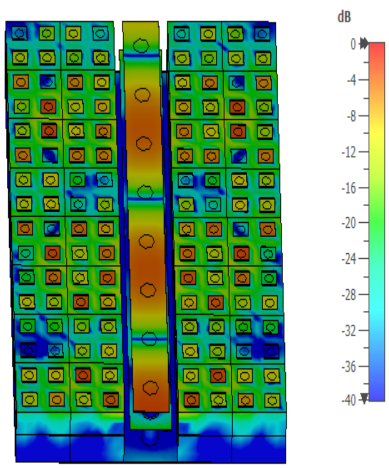

(c) 28 GHz (Out of band)

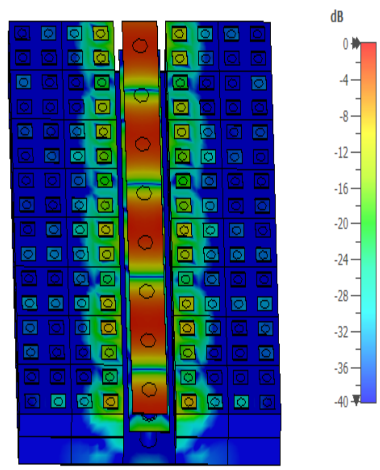

(d) 40 GHz (In band)

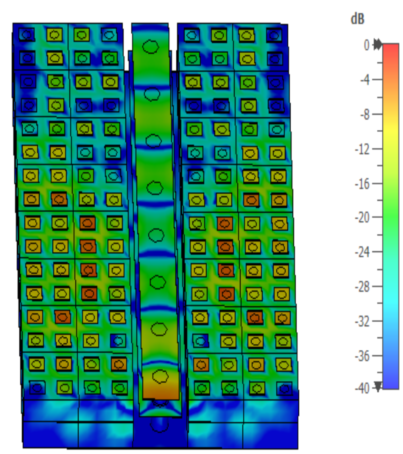

(e) 50 GHz (Out of band)

Figure 4.9: E-field distribution of the proposed dual-band ridge gap waveguide where ridge in the double layer at difference frequencies. (a) 10 GHz, (b) 15 GHz, (c) 28 GHz, (d) 40 GHz and (e) 50 GHz.

4.4.3 Ridge in Upper Layer and Patch in Lower Layer (Case-ii)

The second design concept of RWG is a ridge in the upper layer, and a periodic mushroom large

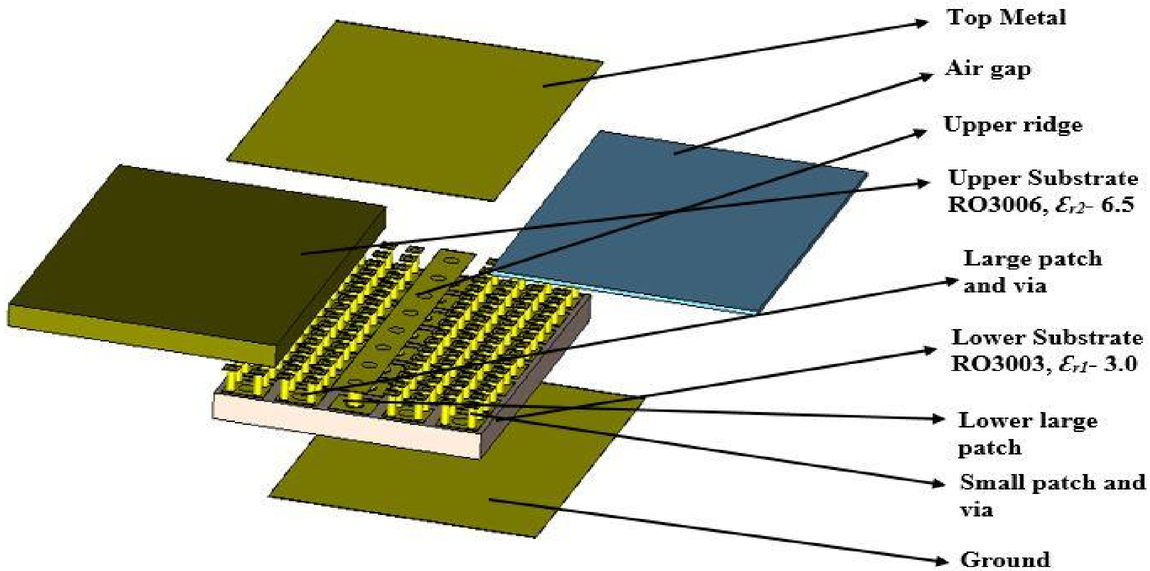

Figure 4.10: Dual-band ridge gap waveguide case-ii, where the ridge is in the upper layer and large patches in the lower layer.

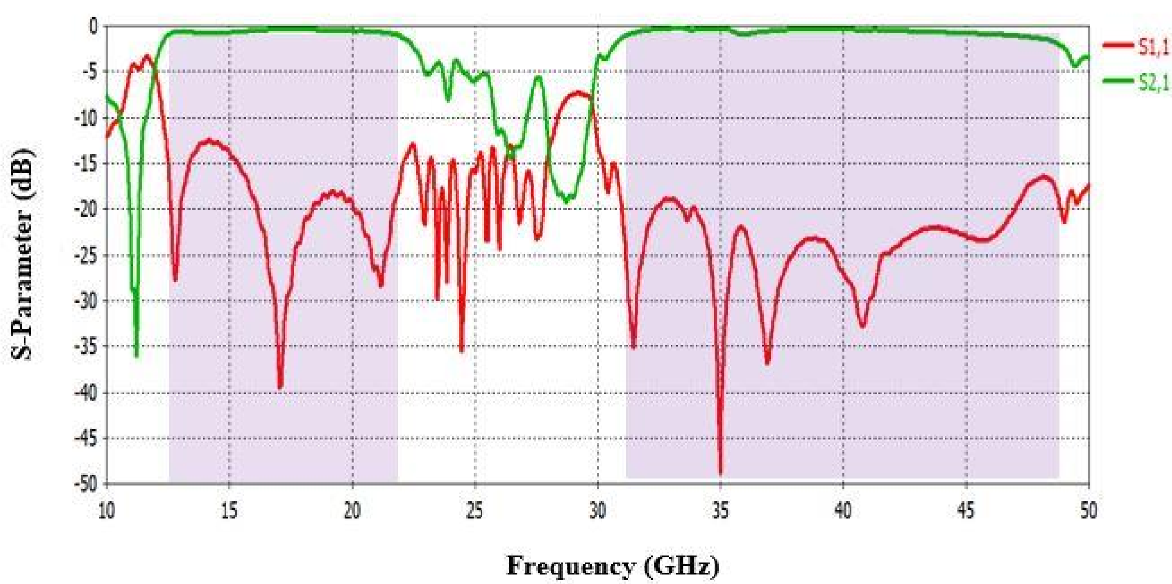

Figure 4.11: Simulated S-parameters of proposed PRGW for case-ii, the ridge is in the upper and the patches in the lower layer.

patch in the lower layer. The upper layer ridge line is linked to the bottom patch with conducting vias, and the discrete patch is connected to the ground through metal vias. The ridge width is kept for all four types of design at 1.2 mm, and the large square patch width is 1.4mm. The waveguide port is connected to the upper ridge line. Everything remains the same in the structure except the ridge condition. Figure 4.10 depicts the dual-band RGW where the ridge is in the upper and mushroom patches are in the bottom layer. The simulated S parameters are shown in Figure 4.11, where 13-22 GHz and 31-49 GHz are dual pass bands of the designed RGW. The scattering parameters of the case ii study of dual-band RGW are shown with the purple bold color shade for better reference. As can be seen, the insertion loss for both bands is less than -0.1dB, which is an excellent match. The upper band has 5 GHz, more coverage to be at 49 GHz instead of 44 GHz, which is beneficial and has a wider band gap for higher frequency applications such as Ku- and V-band. As a prominent outcome, the reflection coefficient, S11 is below -15 dB for both bands. The characteristic impedance of the ridge gap waveguide is 31.5 Ω, so the adapter can be used to match with 50 Ω.

4.4.4 Field Distribution

Figure 4.12 shows the E fields distribution of the RGW ridge in the upper layer and mushroom patch in the lower layer for case ii at different frequencies. The electric fields follow the ridge line, and the periodic EBG cells around the ridge line control any unwanted excitation from the line. As can be detected frequencies 10, 28, and 50 GHz are out of the EBG band, so fields are scattered all over the structure, while frequencies 15 and 40 GHz are within the EBG bands, so electric fields are very strong on the ridge, and saves the power loss of the structure.

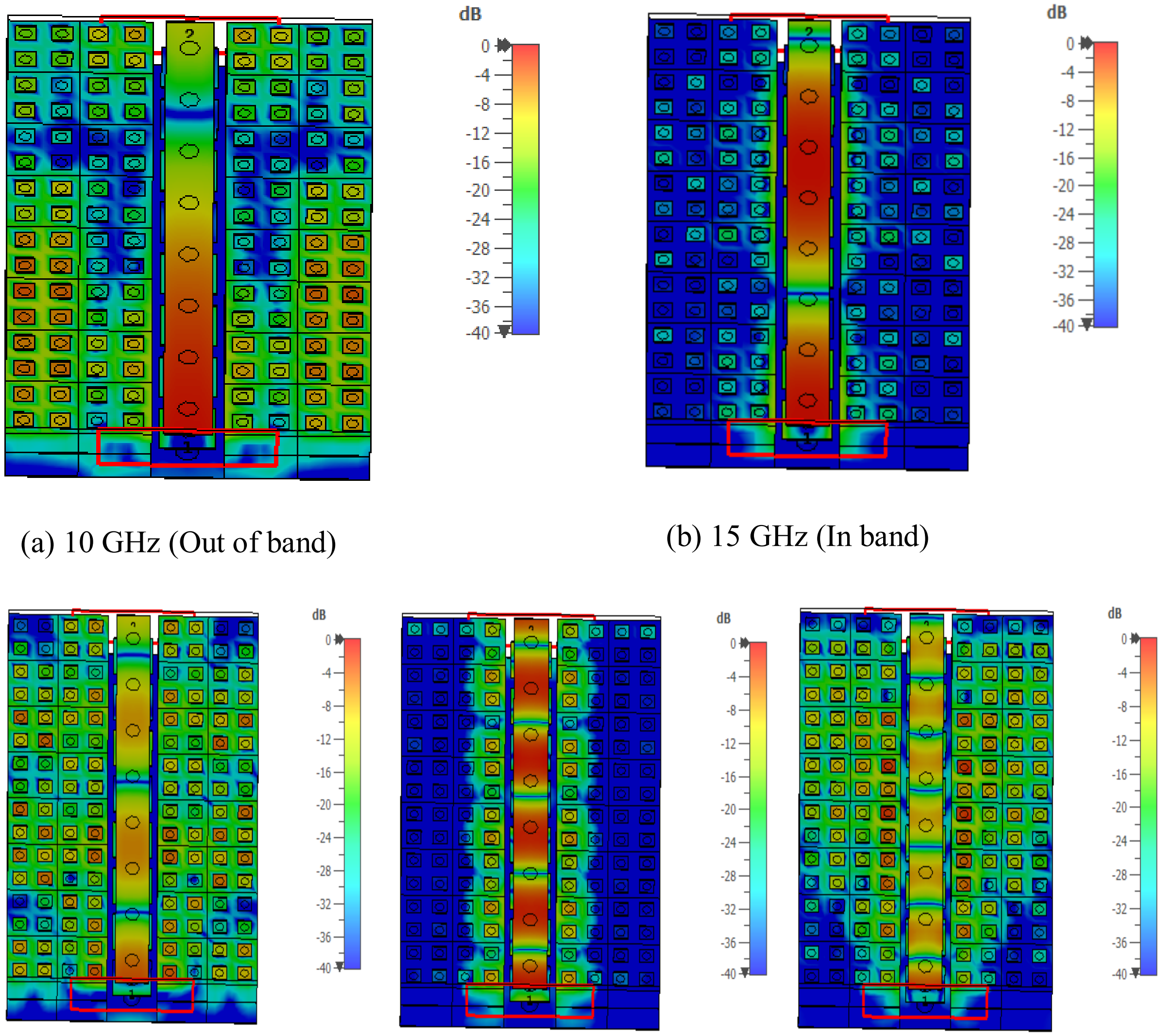

(a) 10 GHz (Out of band)

(b) 15 GHz (In band)

(c) 28 GHz (Out of band)

(d) 40 GHz (In band)

(e) 50 GHz (Out of band)

Figure 4.12: E-field distribution of the proposed dual-band ridge gap waveguide where the ridge is in the upper layer and the patches in the lower layer at various frequencies. (a) 10 GHz, (b) 15 GHz, (c) 28 GHz, (d) 40 GHz and (e) 50 GHz.

4.4.5 Single Layer Ridge in Upper Layer (Case-iii)

Another design scheme of dual-band RGW is one single ridge in the upper layer, and the lower layer is filled with a dielectric substrate. The ridge line connected with the ground plane directly through the conducting vias. The width of the ridge line is kept at 1.2 mm. The characteristic

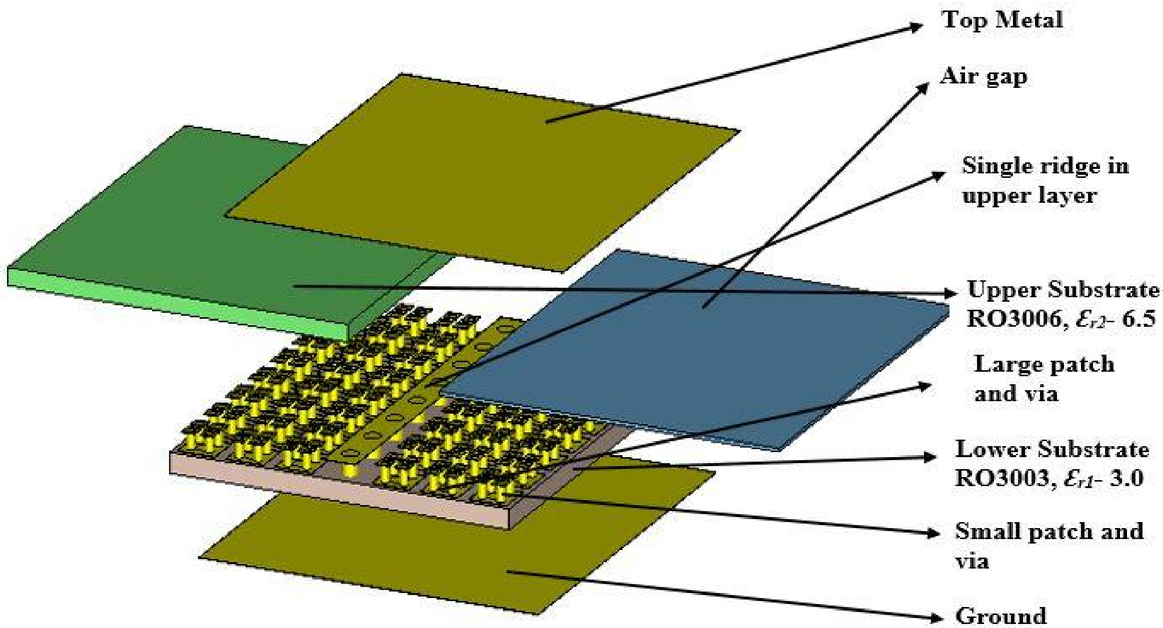

Figure 4.13: Dual-band ridge gap waveguide case-iii, where the ridge is in the upper layer.

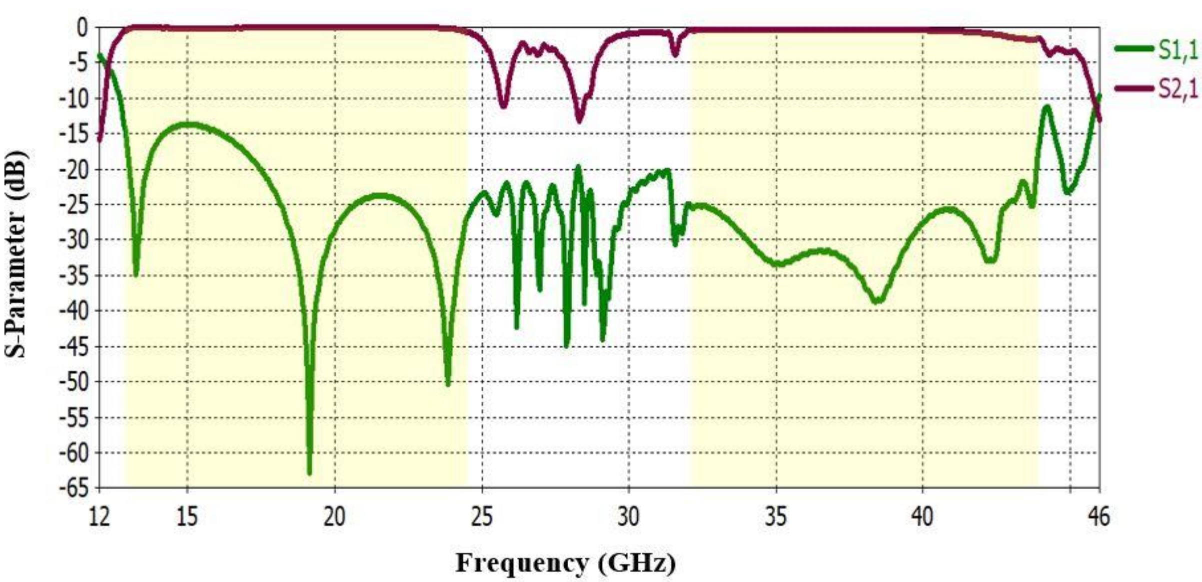

Figure 4.14: Simulated S-parameters of proposed PRGW for case-iii; the ridge is in the upper layer.

the impedance of the ridge gap waveguide is 31.5 Ω. The whole geometry of the single-layer ridge in the upper layer is shown in Figure 4.13. The EM waves travel in the ridge line of the upper layer through the air gap placed in the structure's top layer. The performance of this design is presented in Figure 4.14 through the scattering parameters where 13-24 GHz and 33-44 GHz are generated dual pass bands of the design. As can be perceived, the scattering parameters provide the best outcome from this design; passbands are below -15dB and ripple in the middle out of the band region. Low insertion loss is seen for both the lower and upper band, about -0.01dB, which is the same as the EBG unit cell with outstanding matching. The transmission and reflection coefficient of the RGW are displayed in the yellow bold color for better visibility. Therefore, we used this upper layer single ridge for further design.

4.4.6 Field Distribution

The E-field distribution behavior of the dual-band RGW is presented in Figure 4.15 at different frequencies. The EM waves travel along the ridge line. The fields are tightly bound around the ridge line, and the EBG unit cells suppress the leakage of the whole structure. The three-column ridge line and the EBG unit cells suppress the leakage of the whole structure. As can be seen, frequencies 10, 28, and 50 GHz are out of the EBG band, so fields are dissipated all over the configuration, whereas frequencies 15 and 40 GHz are within EBG bands, so fields are confined to the ridge densely within the stop band. The three columns on both sides of the EBG unit cell are good enough to restrict wave propagation around the line because the field strength becomes weaker and reaches almost zero.

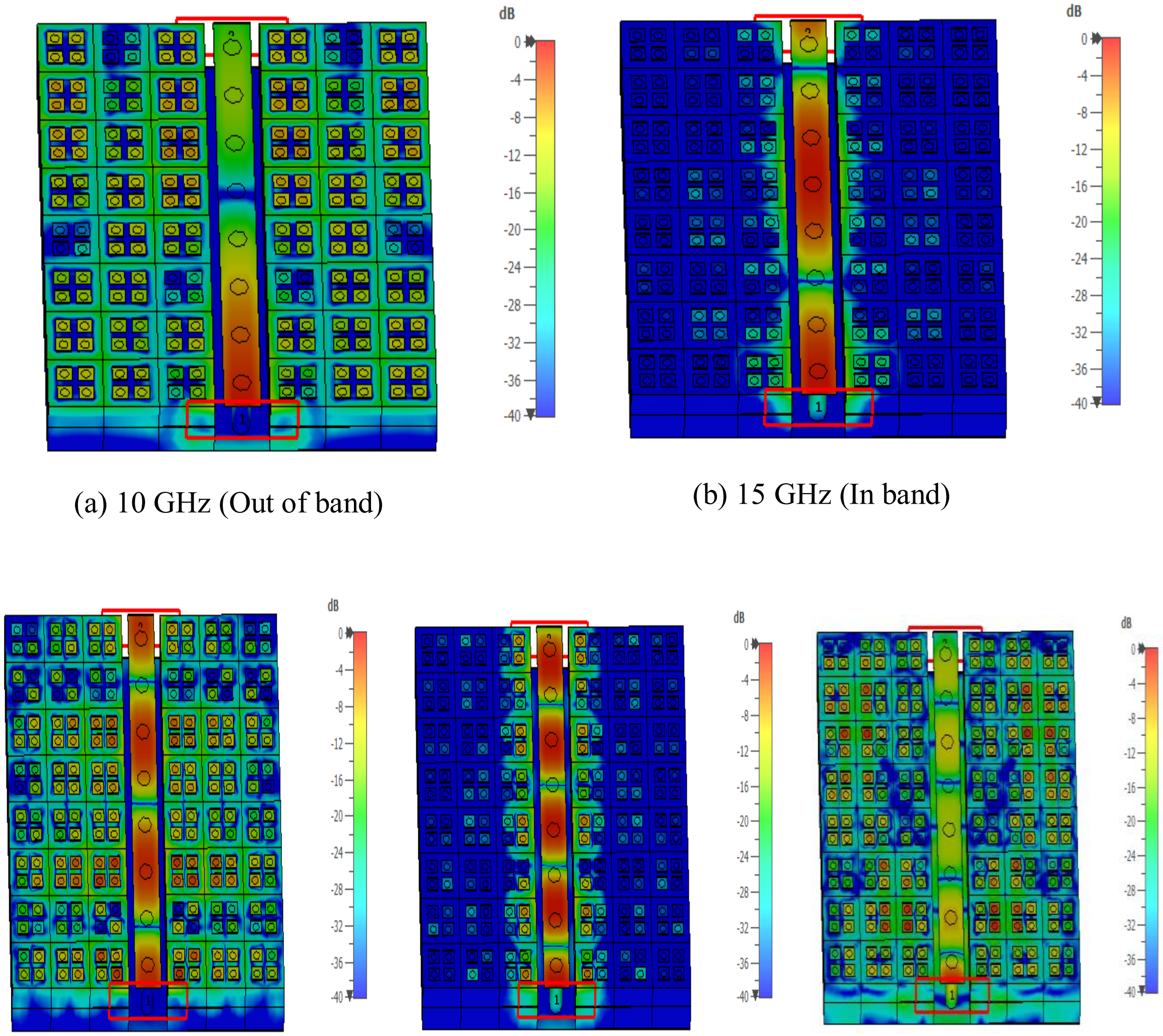

(a) 10 GHz (Out of band)

(b) 15 GHz (In band)

(c) 28 GHz (Out of band)

(d) 40 GHz (In band)

(e) 50 GHz (Out of band)

Figure 4.15: E-field distribution of the proposed dual-band ridge gap waveguide where a single ridge in the upper layer at different frequencies. (a) 10 GHz, (b) 15 GHz, (c) 28 GHz, (d) 40 GHz and (e) 50 GHz.

4.4.7 Single Layer Ridge in Lower Layer (Case-iv)

The last design layout of the dual-band RGW is the ridge line in the lower layer, and the upper layer is loaded with dielectric substrate, as shown in Figure 4.16. The width of the ridge line is

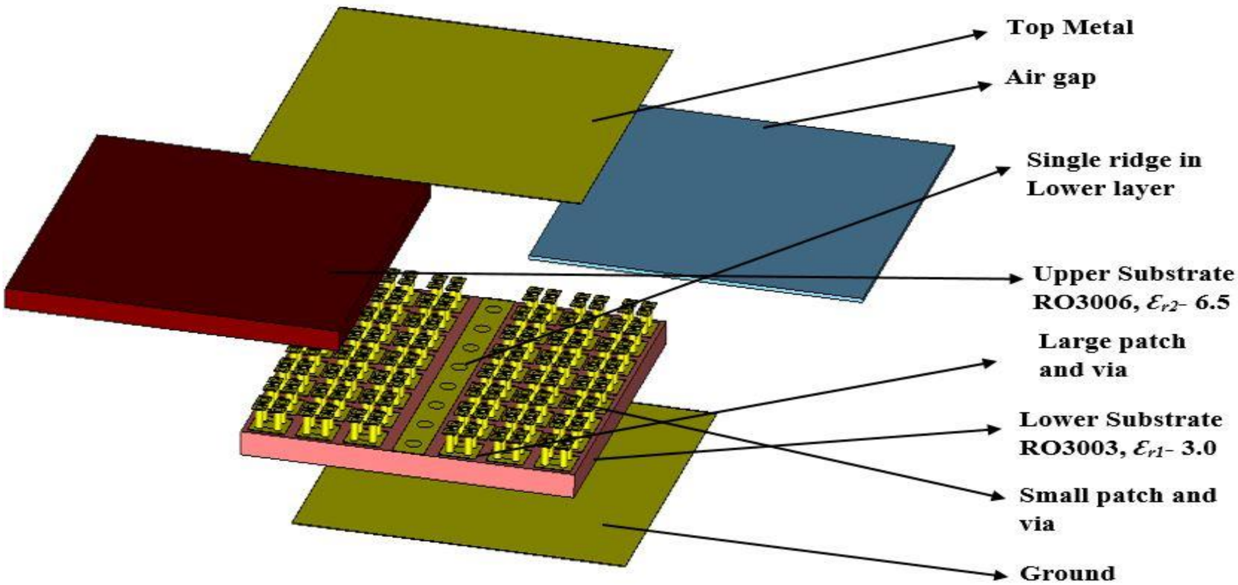

Figure 4.16: Dual-band ridge gap waveguide case-iv, where the ridge is in the lower layer.

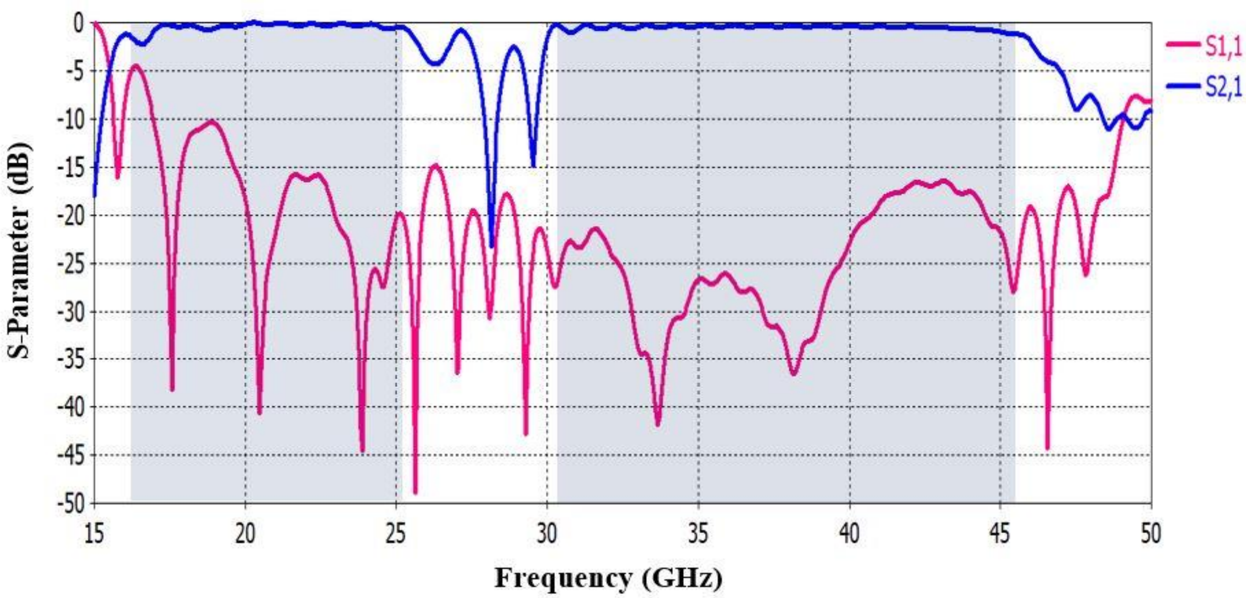

Figure 4.17: Simulated S-parameters of proposed PRGW for case-iv, ridge in the lower layer.

kept fixed at 1.2 mm, and the ridge is in the lower layer. The ridge line is attached to the ground plane through conducting vias. The simulated S parameters are portrayed in Figure 4.17, which provides a dual-band for ridge lines 16-25.5 GHz and 30.5-46 GHz with perfect matching.

As can be observed, the lower band is shifted to the layer with a higher frequency for 13 to 16 GHz, which is a narrow band, and the upper band covers 4 GHz more than the lower frequency that the unit cell provided. The upper band is wider in this design, which is another advantage for higher frequency applications such as V- and K-band. The insertion loss is low in this design concept, about -0.01 dB. The transmission and reflection coefficients of the RGW are displayed in a bold gray color for better perception. The reflection S11 of the lower ridge is almost -15 dB for both bands. Some ripple is seen from 25.5 to 30 GHz, which is out of the band of our design. The characteristic impedance can be matched to 50 Ω by changing the ridge width or using the adapter.

4.4.8 Field Distribution

The E-field distribution along the lower ridge is presented in Figure 4.18. It is evident that at the different frequencies, the E fields behave differently. For example, inside the band gap, the E-fields are confined strongly along the ridge line. On the other hand, before and after the band gap, the E fields are scattered throughout the periodic cells and lose the signal's power. However, the periodic AMC mushroom surface is only excited on its surface at a certain frequency band within the stopband and terminated the propagation strongly in the gap region out of the band. As can be noticed, frequencies 10, 28, and 50 GHz are out of the EBG band, so fields are dissipated all over the configuration, whereas frequencies 20 and 40 GHz are within EBG bands, so fields are bounded tightly around the ridge. As a result, it helps to stop leakage of the propagating waves and provides the best performance of the full structure.

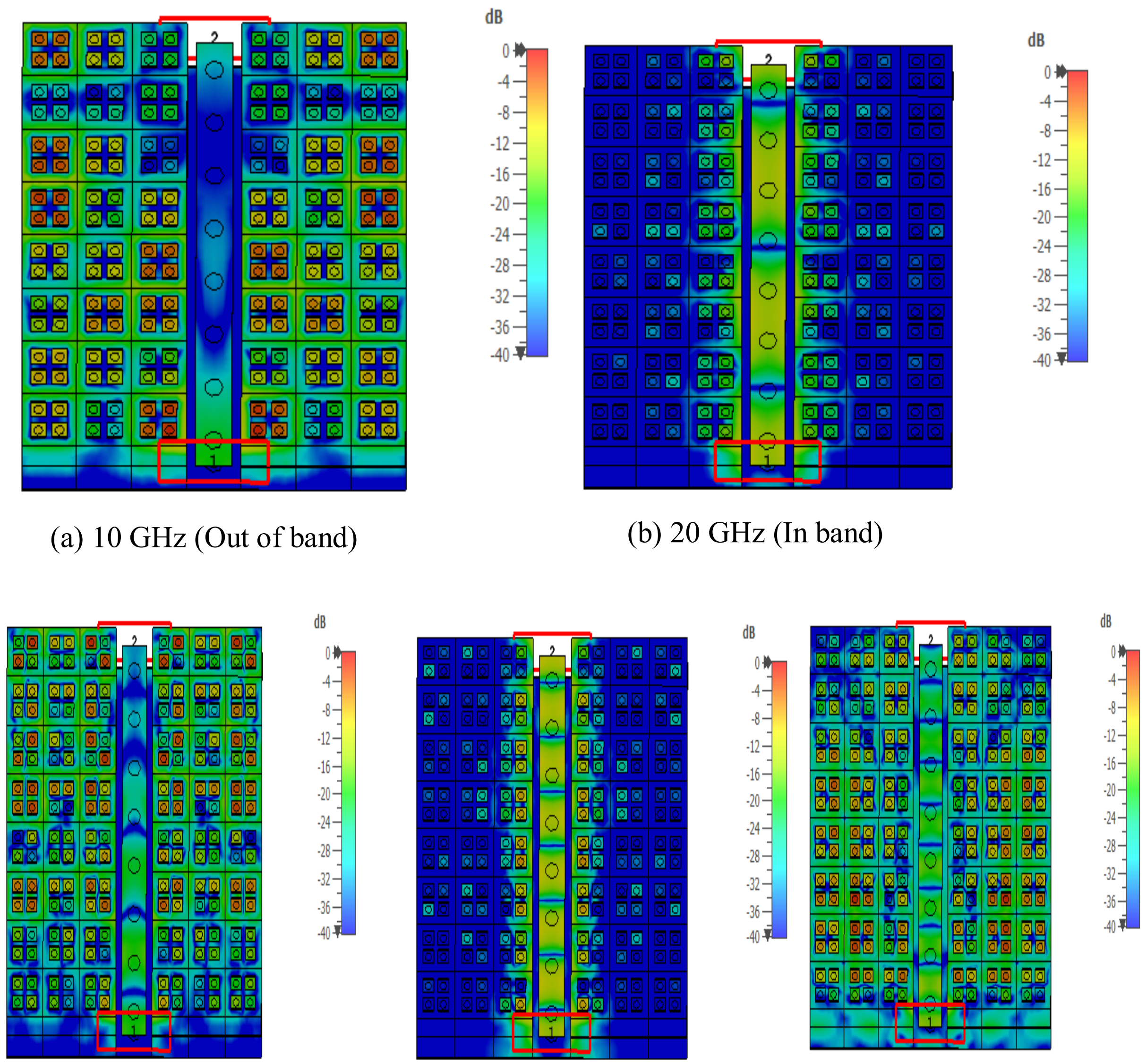

(a) 10 GHz (Out of band)

(b) 20 GHz (In band)

(c) 28 GHz (Out of band)

(d) 40 GHz (In band)

(e) 50 GHz (Out of band)

Figure 4.18: E-field distribution of the proposed dual-band ridge gap waveguide where ridge in the lower layer at various frequencies. (a) 10 GHz, (b) 20 GHz, (c) 28 GHz, (d) 40 GHz and (e) 50 GHz.

Table 4.1: Comparison of proposed different types of dual-band ridge gap waveguide

Unit Cell Band Gap, Lower band-13-24 GHz, and Upper band-34-44 GHz				
Ridge gap types	**Lower band (GHz)**	**Upper band (GHz)**	**Mismatch**	**Comments**
Ridge in a double-layer	13-23	35.5-47.5	Lower band-1 GHz less Upper band-3.5 GHz more	Suitable for Ku- and K-band
Ridge in the upper layer and patches in the lower layer	13-22	31-49	Lower band-2 GHz less Upper band-5 GHz more	Suitable for Ka bands
Single ridge in the upper layer	13-24	34-44	Lower band-0 GHz Upper band-0 GHz	The best result as a Unit cell provided, suitable for further design.
Single ridge in the lower layer	16- 25.5	30.5-46	Lower band-3 GHz less Upper band-3.5 GHz more	Suitable for V bands

4.5 Packaged Two 90-Degree Bend Lines

In printed technology, the mushroom types' EBG surface can be used as packaging where the same substrate layers are combined, similar to microwave circuits. The validation of EBG pins cells for packaging passive microstrip transmission line circuits was presented with the electric field distribution along the bends microstrip packed line with smooth metal lid here [51]-[52]. Later, many other papers were published regarding bend lines surrounded by various EBG cells. This EBG surface is an AMC surface with a flat surface parallel to the metal plate. The AMC surface is high impedance, so no waves travel in this surface, but by installing a ridge that could be a

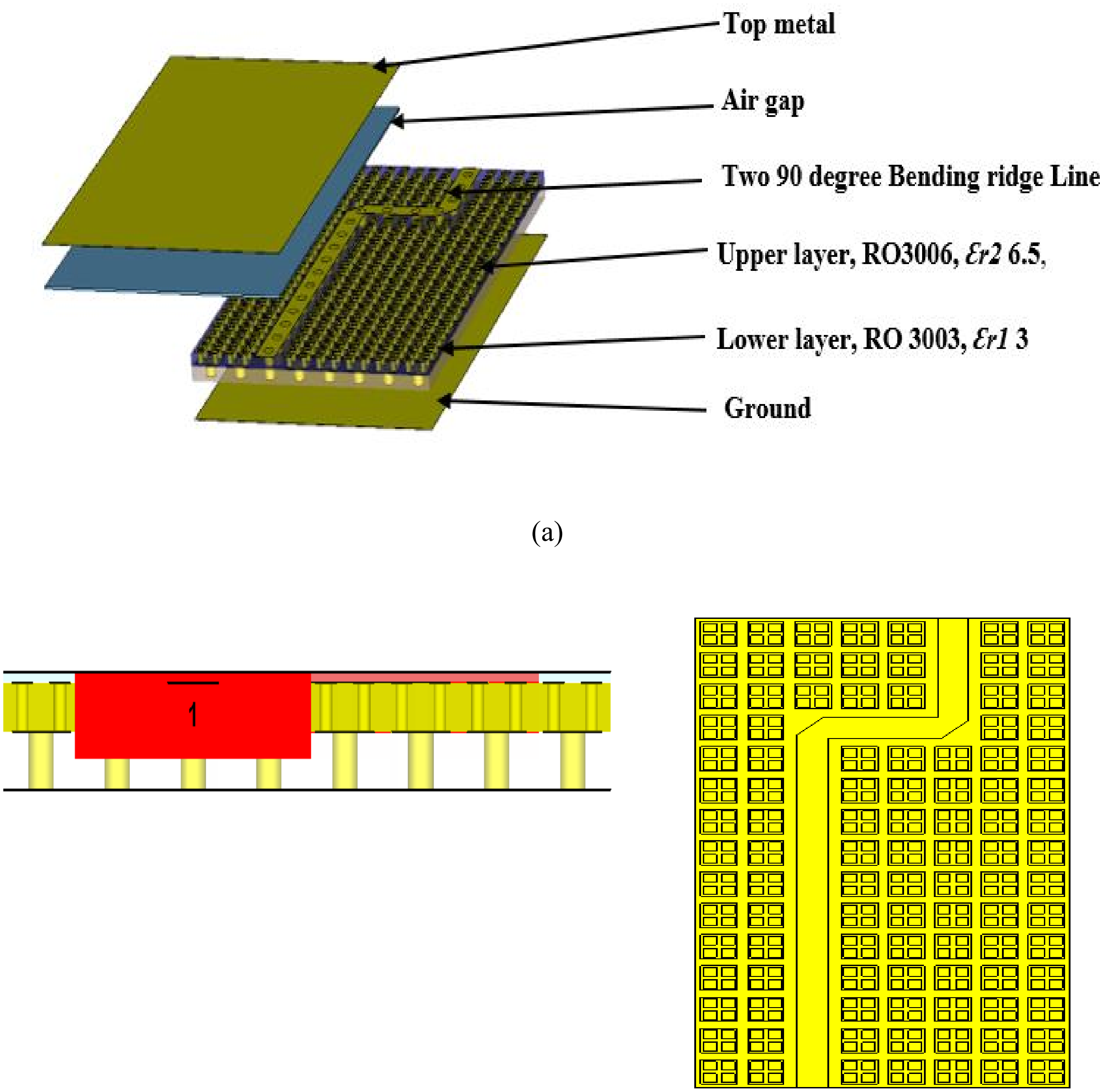

(a)

(b) (c)

Figure 4.19: Layout of the proposed dual-band ridge gap waveguide with two 90-degree bend lines. (a) Overall view, (b) Cross-section view, and (c) Top view.

straight line or bends line then, a quasi-TEM mode is demonstrated and propagated within the two stop bands of this design and all other higher order mode are forced to be cut off by the EBG mushroom cells. A full wave analysis as straight-line dual-band PRGW has been presented in the previous section with four varieties of ridge line positions and their effects. Any microwave circuit will naturally contain several discontinuities, for instance, a splitter, power divider coupler, bend transmission line, and a feeding network for antenna arrays. However, studying the discontinuity of the strip-ridge bend is crucial since it provides design suggestions and knowledge about active or passive microwave components. Dual-band can be achieved through two 90-degree bend lines

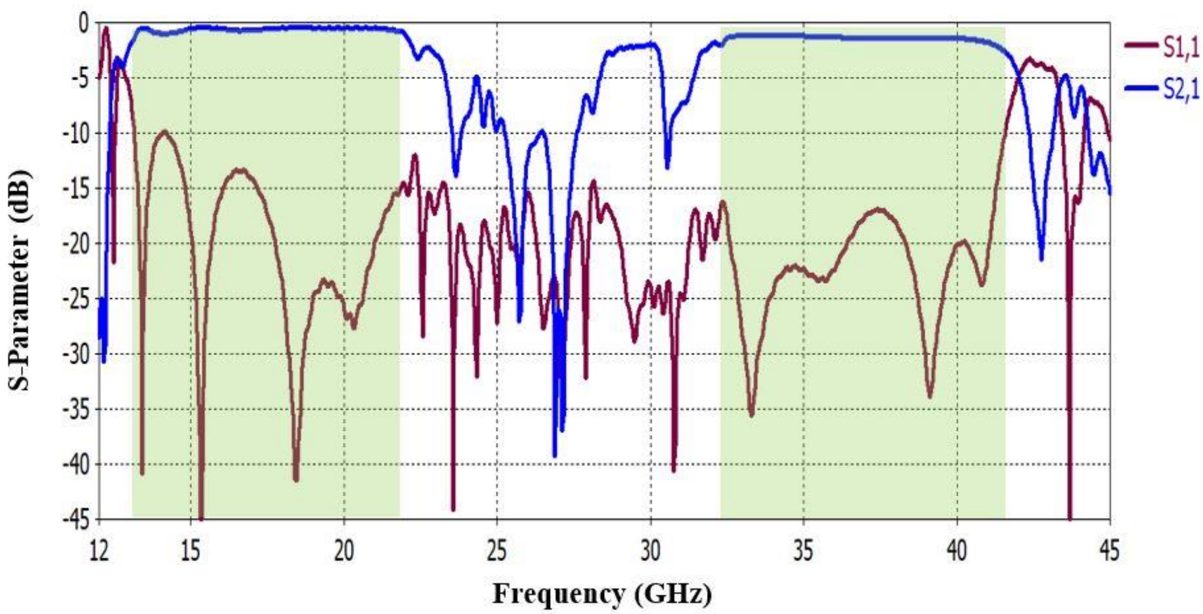

Figure 4.20: Simulated S-parameters of the proposed dual-band PRGW with two 90-degree bend lines.

using the proposed dual-band EBG cell. The ridge line is located in the upper layer of the structure, and the line is directly connected to the ground plane with the metal vias. The width of the ridge line is kept constant as a straight line of 1.2 mm with the characteristic impedance of the bend ridge gap waveguide at 31.5 Ω. Some modification is necessary on the two sides of the bend line to improve the performance of the proposed design. Chamfering the bend line greatly influences excellent matching of the full design. The bend lines cover three consecutive cells on both sides of the bend line, and 11 cells cover the straight line. Figure 4.19 illustrates the layout of the proposed dual-band PRGW with two 90-bend lines. The whole structure follows the packaging technique, thus reducing the size of the structure and becoming compact. The simulated scattering parameters as reflection and transmission coefficients of two 90-degree bend lines are revealed in Figure 4.20. As can be observed from the scattering parameters, double bands acquired for the lower band start from 13 to 22 GHz, and the upper band starts from 32 to 42 GHz, which is similar to the proposed EBG unit cell but slightly less bandwidth of 1.5 GHz in the lower band. The performance of the overall result of the bend line in terms of insertion loss is higher in contrast with the straight line. The insertion loss of the bend line is -1 dB for the lower band, and for the upper band, it is about -1.5 dB. The reflection coefficient is better for both bands below -10 dB, but some ripples can be found and ignored in the middle band due to the out-of-band from 23 to 32 GHz. For better understanding, the bandwidth coverage area is shown in light green, in a bold shade. Table 4.2 provides a comparison between the proposed dual-band ridge with two 90 bend lines and the previous works that show single layer mushroom patch ridge with two 90 degree bend lines figure with simulated results [38]. Another paper in [53] shows ridge with two 90-degree bend lines using an EBG pin cell in gap waveguide technology.

However, compared to the straight line, the two 90-degree bend lines exhibit a larger insertion loss in the upper band due to the discontinuity of the line. The proposed two 90-degree bend lines provide a wide dual band with fantastic matching for both bands.

Table 4.2: Comparison of proposed dual-band ridge two 90-degree bend lines with previously published works.

Ref	Type	Figure	Coverage bandwidth	Insertion loss
Proposed work	Double-layer mushroom patch EBG cell	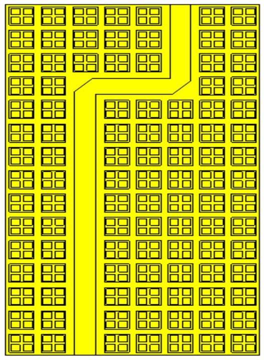	Lower 13-22 GHz Upper 32-42 GHz. 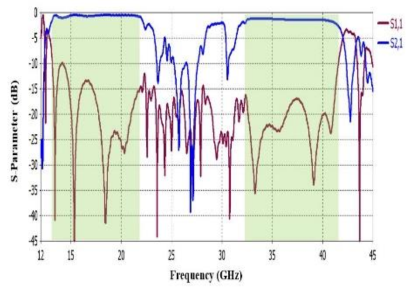	1 dB for both band
[38]	Single-layer mushroom patch EBG cell	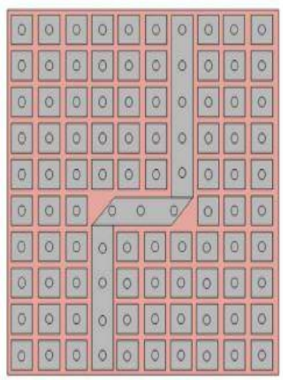	Band 5.3-11.3 GHz. 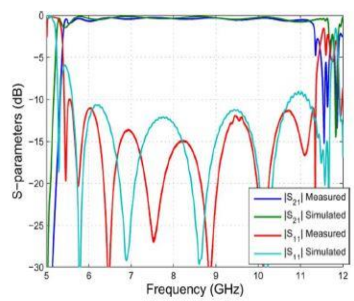	0.5 dB
[53]	Single-layer metal pin EBG cell	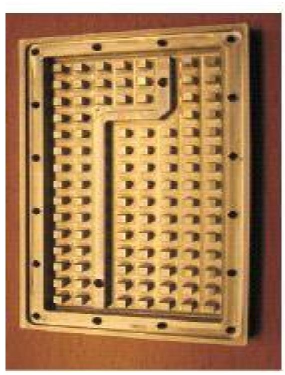	Band 13-16.3 GHz. 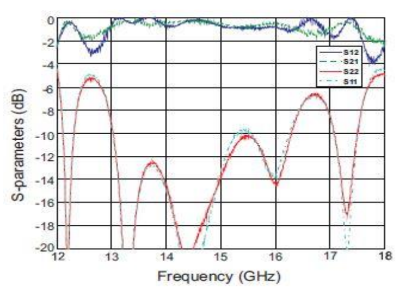	1 dB

4.5.1 Field Distribution of Packaged Two 90-degree Bend Lines

The E-field distribution provides the polarization and direction of the field. Figure 4.21 depicts the

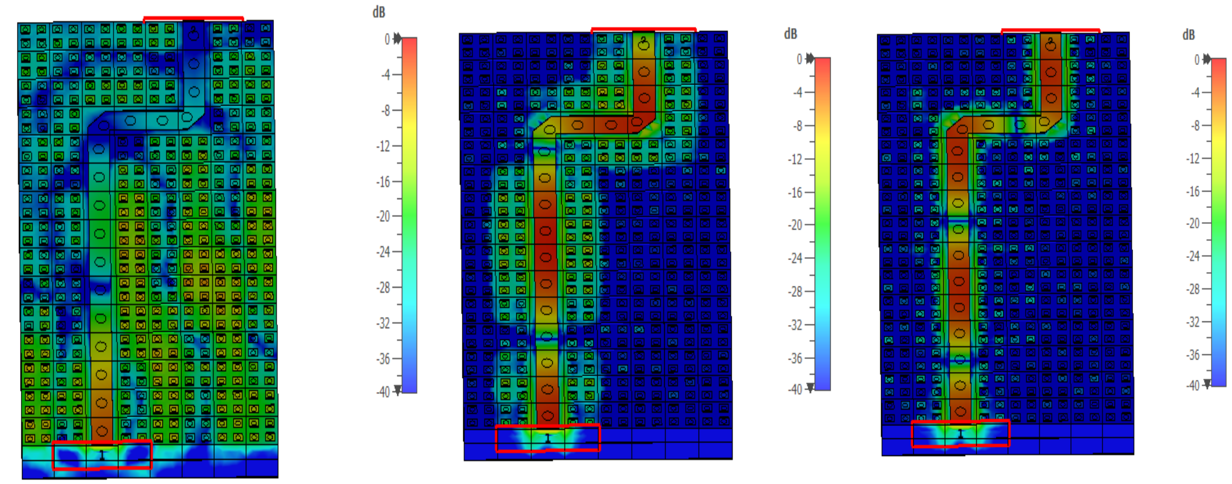

(a) 10 GHz (Out of band) (b) 15 GHz (In band) (c) 20 GHz (In band)

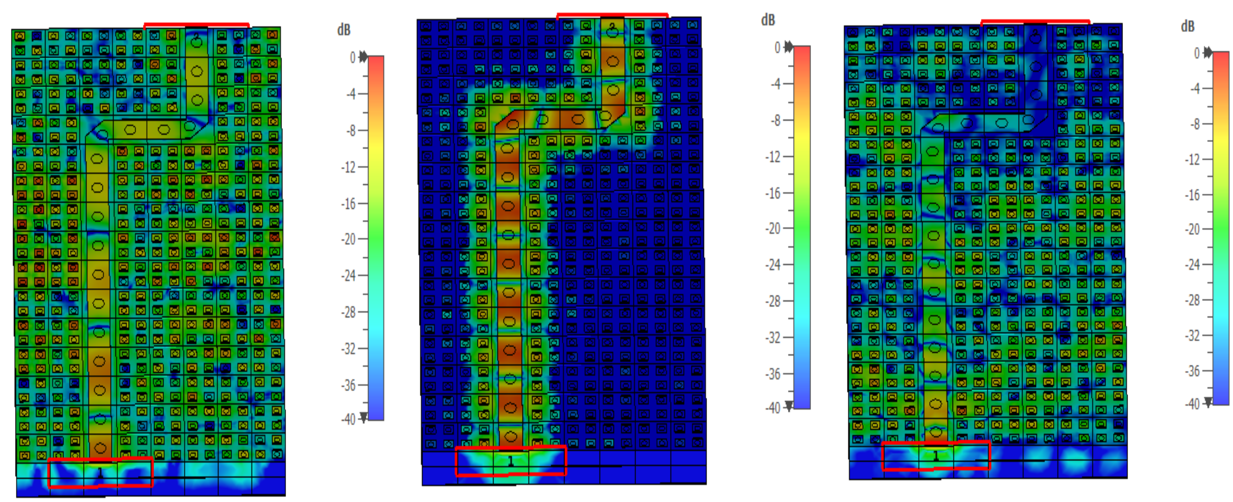

(d) 25 GHz (Out of band) (e) 40 GHz (In band) (f) 50 GHz (Out of band)

Figure 4.21: E-field distribution of the proposed dual-band ridge with two 90-degree bend lines at different frequencies. (a) 10 GHz, (b) 15 GHz, (c) 20 GHz, (d) 25 GHz, (e) 40 GHz ,and (f) 50 GHz.

electric field distribution behavior inside the bends RGW line at different frequencies inside the two bandwidths. As seen from the field distribution, the waves travel along the discontinuous line where the texture structure around the line prohibits any unwanted excitation from the bend regions. As observed, the fields are precisely confined to the ridge line in the two frequency bands. Before the lower cutoff frequency band from 13 to 22.5 GHz and after the upper cutoff frequency band from 33 to 43 GHz for both bandwidths, the EBG unit cells do not work as AMC surface, and fields are scattered throughout the whole area of the structure. From the Figure, the frequencies 10, 25, and 50 GHz are out of the EBG band, so fields are scattered all over the structure.

In contrast, frequencies 15, 20, and 40 GHz are within EBG bands, so electric fields are densely bounded within the ridge line, thus preventing the structure's leakage. Naturally, after three columns of mushroom patches on both sides of the bends line, the field intensity becomes fragile and nearly zero. The ridge in the bends line works perfectly as the ridge straight line where the fields follow the bends line. The two 90-degree bend lines perform admirably and accurately in the dual intended bandwidth.

4.6 PRGW Technology-Based Feeding Network

The gap waveguide technology offers some advantages for high-frequency antenna applications due to its planar profile and is suitable for low-loss feeding networks for array antennas. Using superstrate or meta-materials can be difficult to build, although constructing an array is not difficult, and it can be quickly developed and integrated. Designing microstrip arrays in the mm-wave region can be difficult because of the large dielectric losses at higher frequencies. In this research work, a dual-band feeding network is built using a Printed Ridge Gap Waveguide (PRGW). The feeding network, power divider, and antennas can easily be constructed in the printed technology because the field travels in the air instead of the substrate, consequently causing low dielectric losses. The line width can be raised to reduce conductivity losses, and there is no difficulty with surface wave excitation, which affects ordinary microstrip feed networks. However, there is no need for good electrical contact between the feeding network and the antenna block. To combine the benefits of both technologies, hybrid arrays attempt to link a microstrip array with a waveguide feed network. However, these structures have fewer losses in the feed network; they are large and have integration issues with mm-wave planar circuits. On the other hand, texture structures such as mushroom patches with conducting vias allow particular frequency bands to propagate and prohibit waves traveling for other modes that create a bandgap. In addition, the periodic AMC surface can be used below the microstrip feeding line and make manufacturing simpler and cheaper at high frequency because the layer containing the uniform periodic surface can be re-used for other similar designs at the same frequency of operation.

In the past, microstrip line power dividers, SIW power dividers, and ridge gap power were proposed for wideband or higher band applications. A 3-way fork power divider consisting of three 90^{o} microstrip lines using left-handed transmission lines (LHTLs) to compact the size for a 5 GHz band of operation was proposed in the paper [54]. Feeding networks and power dividers can be designed in SIW technology and have gained popularity over the last few years, and many articles have been published with the proposed work. A power divider using an SIW bandpass filter was developed for a WLAN application that replaced a conventional power divider, and adding an SIW bandpass filter was implemented in this paper [55]. A SIW filtering power divider for good isolation was proposed and published in some papers [56]-[57]. Low losses and high radiation efficiency are more attractive reasons for using SIW antenna at higher frequencies, and many designs have been proposed [58]-[59]. Many articles proposed wideband power dividers and side lobe reduction using ridge gap technology here [60]-[61]. RGW technology is promising for low loss and compact design for power dividers, and its popularity is increasing daily. In this thesis work proposes a dual-band 1x2 feeding network based on PRGW technology that can be used for dual frequency applications or array antenna design.

4.6.1 A 1x2 Power Divider Based on PRGW

This part proposes the design of a dual-band 1x2 power divider using PRGW technology. The design is implemented through the Transients solver of CST microwave studio software. The whole structure has two layers with two different dielectric substrates. The feeding lines and the small mushroom patches are printed on the same upper substrate of the top layer of the structure, and on the bottom layer, there are large patches with another dielectric substrate that are also printed. The line is connected to the ground plane with conducting vias. The design uses a bend in the line and three transformer sections to accomplish the desired result. To get the required result, three chamfers are utilized. Some small patches must be removed to create cavities or relocated that do not remarkably affect the result. Figure 4.22 illustrates the structure of the proposed dual-band 1x2 power divider network. The chamfering is about 1.0 on both bent sides.

The simulated performance of scattering parameters is presented in Figure 4.23. The 1x2-power divider indicates the uniform power distribution that provides dual-band. The reflection coefficient is below -12 dB for the lower band from 16 GHz to 24 GHz and -13 dB for the upper band from 32.5 to 42.5 GHz. The insertion loss is about -4 dB for the lower band and -5 dB for the upper band. A light blue bold color shade indicates the scattering parameters for better visibility. The line width is about 1.2 mm. The line impedance of the power divider is 31.5 Ω, but 50 Ω can be acquired by changing the line width or using an adapter.

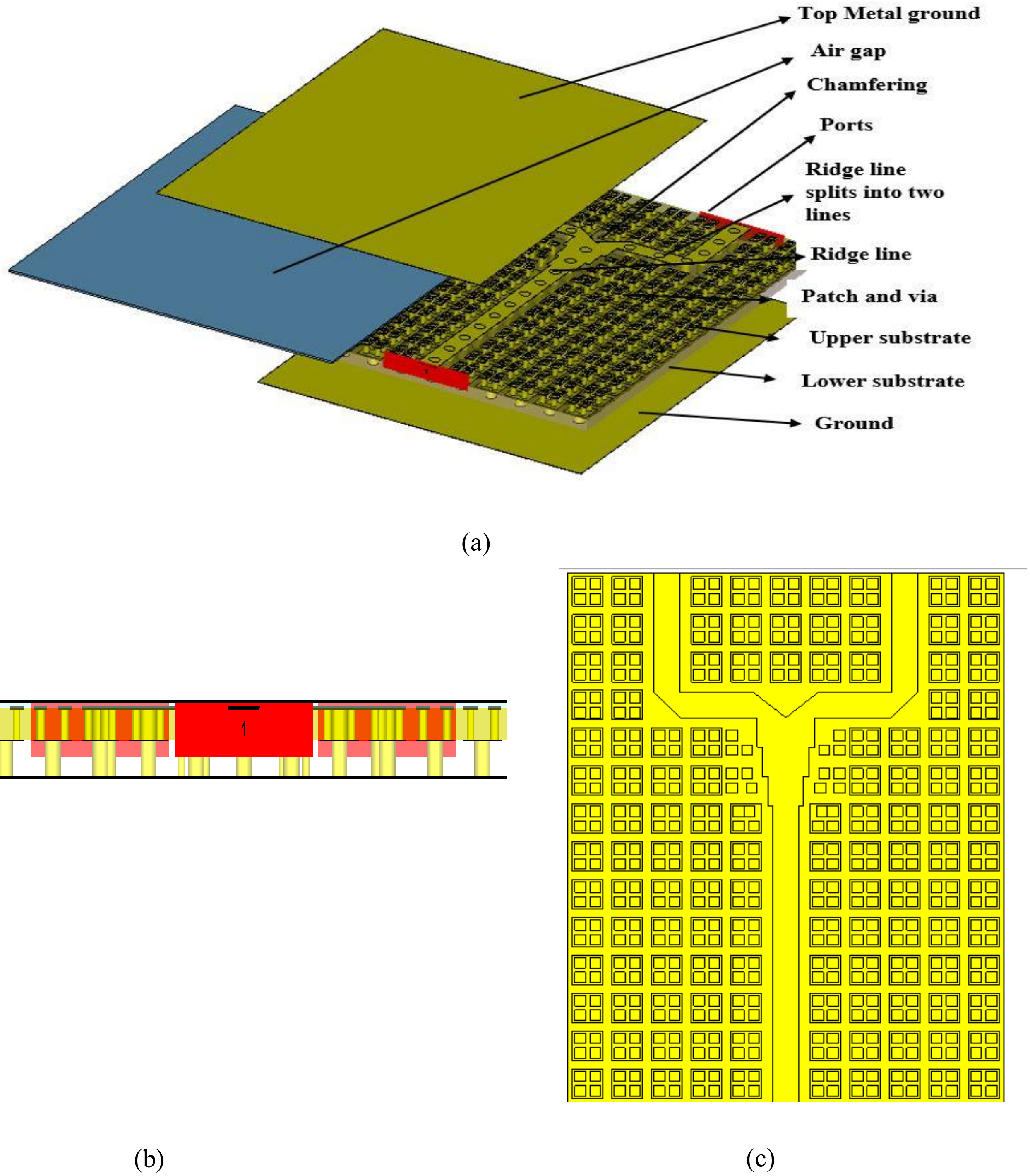

(a)

(b) (c)

Figure 4.22: Full Structure of dual-band PRGW 1x2 Power divider, (a) Full layout, (b) Cross-section view, and (c) Top view.

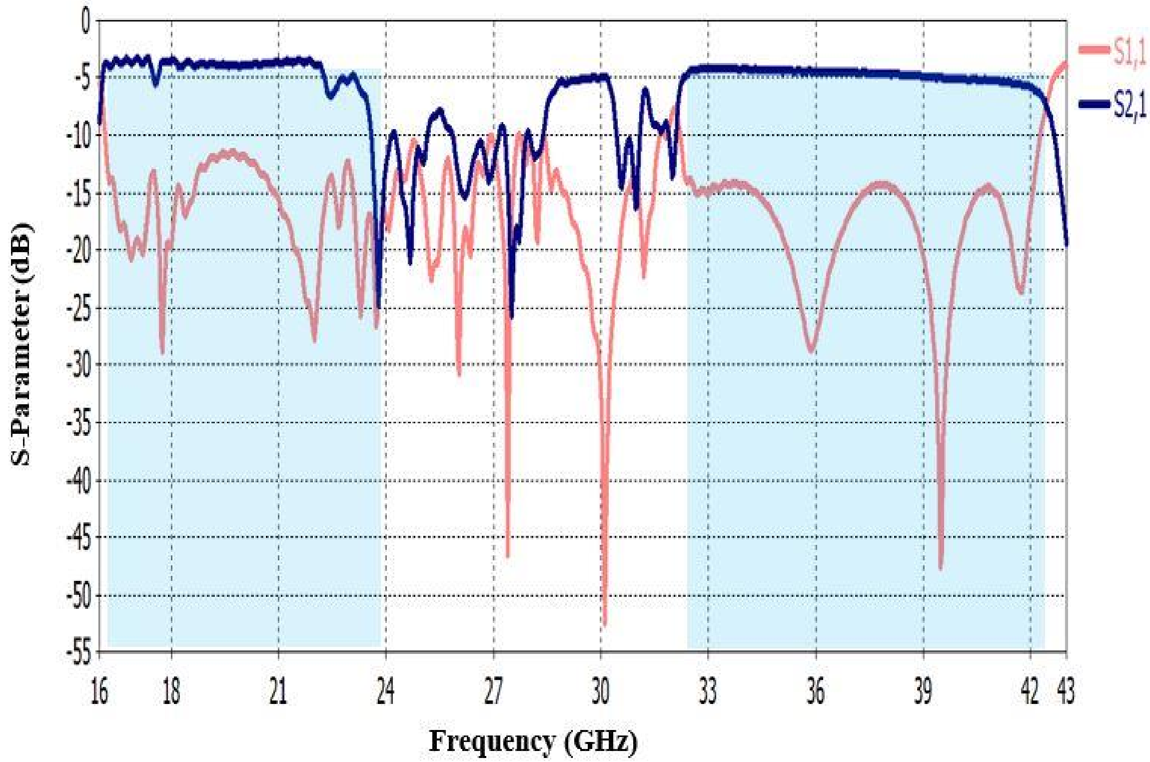

Figure 4.23: Simulated S-parameters of the proposed dual-band PRGW power divider.

Table 4.3 depicts a comparison between the proposed dual band power divider and the previous works that show single layer power divider with EBG metal pins unit cell in gap waveguide with the figure and simulated results [62]. In paper [63] illustrates ridge with multi vias mushroom patches in double ridge gap waveguide technology with scattering parameters.

Therefore, the antenna array can be designed using this dual-band power divider with low insertion loss as a perfect matching outcome

Table 4.3: Comparison of proposed dual-band power divider with previously published works

Ref	Type	Figure	Coverage bandwidth	insertion loss
Proposed work	Double layer mushroom patch EBG cell	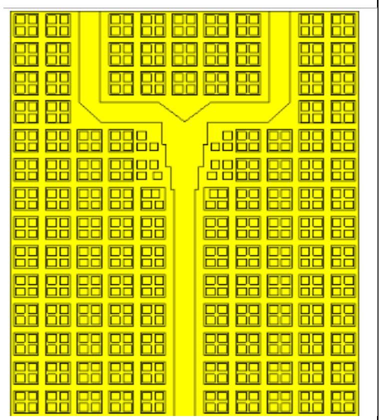	Upper band 32.5-42.5 GHz Lower band 16-24 GHz 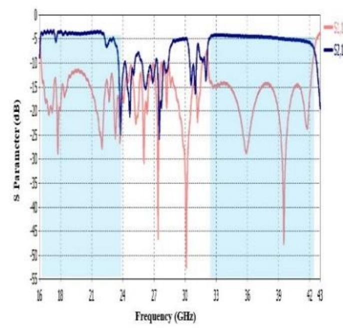	5.0 dB
[62]	Single layer metal pins EBG cell	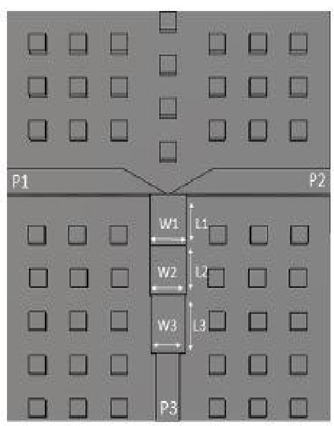	Band 19-40 GHz 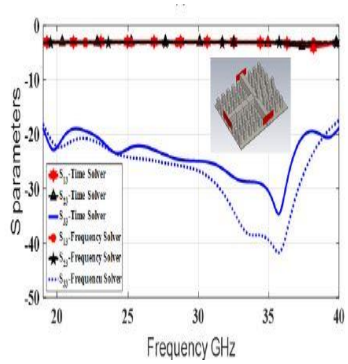	4.0 dB
[63]	Single layer multi vias mushroom EBG cell	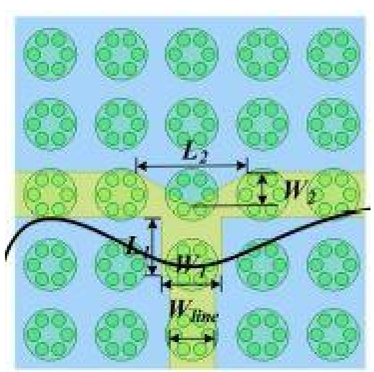	Band 35-45 GHz 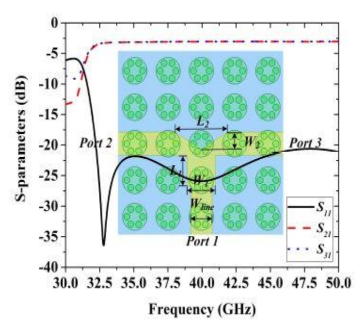	4.0 dB

4.6.2 Field Distribution of 1 x 2 Power Divider Based on PRGW

The E-field distribution provides the E-field traveling along the line through the air gap at different

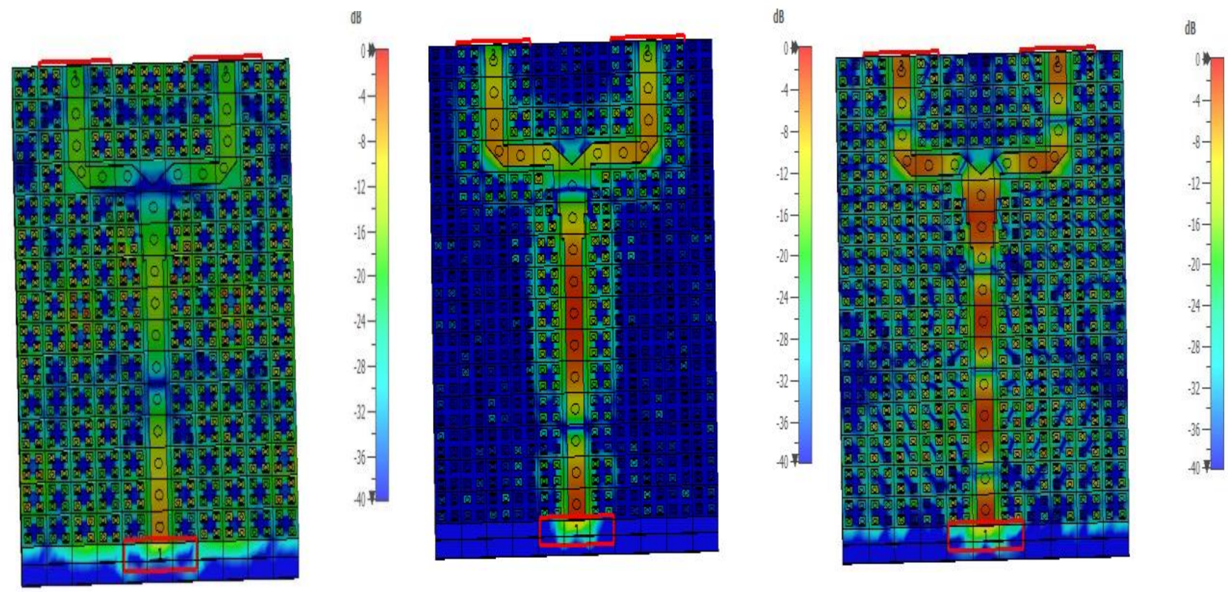

(a) 10 GHz (Out of band) (b) 20 GHz (In band) (c) 27 GHz (Out of band)

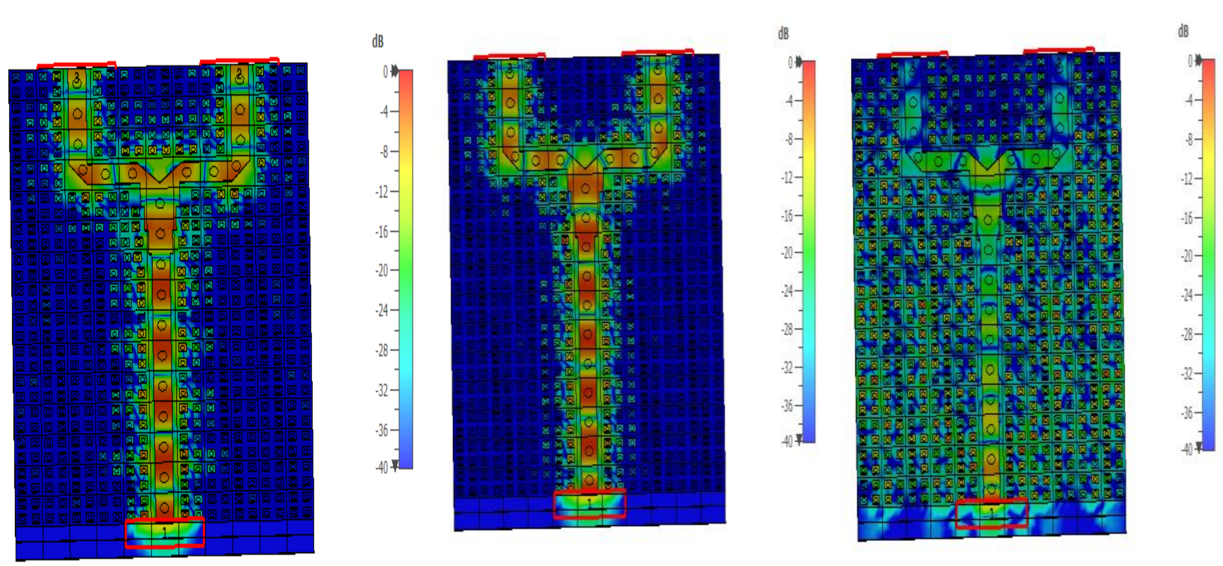

(d) 35 GHz (In band) (e) 40 GHz (Out of band) (f) 50 GHz (Out of band)

Figure 4.24: E-field distribution of the proposed dual-band 1x2 power divider at different frequencies. (a) 10 GHz, (b) 20 GHz, (c) 27 GHz, (d) 35 GHz, (e) 40 GHz , and (f) 50 GHz.

frequency points, as shown in Figure 4.24. The electric fields are enclosed predominantly within the ridge line at that frequency band gap provided by the unit cell. As can be seen at frequencies 10, 27, and 50 GHz, electric fields are spread all over the structure because it is out of stop band, periodic mushroom cells are not working as AMC surface, and unwanted radiation is not blocked by the EBG mushroom cell. On the other hand, frequencies 20, 35, and 40 GHz are inside the band gap, electric fields are more densely bounded along the ridge line, and undesired radiation is suppressed by the EBG mushroom cells. Using 2-3 columns of periodic cells between the two lines can terminate the mutual couplings between the elements. The EBG mushroom cells eliminate the unwanted excitations of the total structure, thus boosting the total power transfer from one port to another. This saves the signal strength and leakage of the structure.

4.7 Coupler Design Based on PRGW

Broadband quadrature hybrid microwave directional couplers are one of the most essential types of passive microwave circuits. As they are utilized in microwave smart beam switching subsystems, they primarily divide or combine signals with proper phase. For future 5G communication systems in the millimeter wave frequency that require intelligent subsystems, for example, beam switching. Beam-switching networks are necessary because of the improved quality and reliability of wireless communication links [64]-[65]. Beam-switching subsystems and their accompanying components must meet various technical requirements, including low loss, small size, and cheap cost.

The hybrid coupler was developed in various forms, including coupled lines and branch lines [66]-[67]. In the last few decades, hybrid couplers were introduced in various configurations and were implemented based on traditional guiding technologies such as rectangular waveguides and stripline or microstrip lines [68]-[79]. Unfortunately, these guiding structures suffer from severe losses such as dispersion or radiation loss at millimeter waves. On the other hand, they can be accomplished by modern guiding structures, for instance, substrate-integrated waveguide SIW. The realization of directional couplers using SIW was proposed through the literature, and later, the advanced implementation versions were published using SIW [70]-[76]. The ridge gap waveguide is one of the potential guiding structures appropriate for high-frequency band applications. This technology was first introduced in 2009 by a research group in Sweden by Dr. Kildal [13]. The fundamental concept of the RGW was developed from hard and soft surfaces presented in the early 1980s [17]-[18]. In addition, research has been initiated, and the printed version of RGW, called PRGW, was developed in 2012 [42]. PRGW technology offers numerous advantages over SIW technology. One of the most suitable reasons for choosing this technology is minimal signal distortion, as the propagating mode is a quasi-TEM mode, and another is low loss at mm-wave frequency due to wave travels inside the air gap [77]. Many microwave components, such as filters and antennas, were deployed due to this technology's increasing popularity [78]-[79]. The design and implementation of directional couplers was invented using RGW presented in the literature [32]. However, the PRGW couplers were performed with few trails, but the design limitation in terms of bandwidth was reported here [80]-[81]. Many articles about the bandwidth enhancement of directional couplers with design procedures and performance based on PRGW for 5G communication were published in these papers [82]-[83].

A quadrature hybrid direction coupler based on PRGW has been proposed using a dual-band unit cell. Although a dual-band coupler could not be acquired through a dual-band EBG unit cell, two couplers are proposed. One is designed for lower bands and another for upper bands separately here through the proposed dual EBG unit cell. The proposed coupler is accomplished based on the fundamental concept of the branch line coupler structure. The paper here inspires the coupler's design idea [84]. The length of the branch-line and parallel intervals in the proposed branch-line coupler are both $\lambda_g/4$ (where λ_g is the center wavelength of the passband). There are three steps to follow in order to design the proposed coupler. Firstly, designing a unit cell with proper dimensions surrounding the ridge to suppress any wave propagation, thus stopping power leakage within the desired frequency ranges 13-24 and 34-44 GHz, already done in previous chapter 3. Secondly, an accurate strip line model for the PRGW line was selected, built with the pre-designed unit cell shown in Chapter 4 in the previous section. Finally, calculate and optimize the coupler section dimensions as well as the required electrical characteristics of the operating bandwidth or band of interest. All the designs are performed through the Transients solver of CST microwave studio software. The lengths of the branch-line and parallel intervals are L and W, respectively, but they are not exactly equal to the $\lambda_g/4$. Some optimization is required in terms of coupler dimensions to get the desired bandwidth efficiently.

4.7.1 Proposed Couper for Lower Band

We intend to achieve the coupler size for the lower band $1.78\lambda g/4$ x $1.48\ \lambda g/4$ at the center frequency of 20 GHz. The proposed coupler covers the three rows of cells around the middle

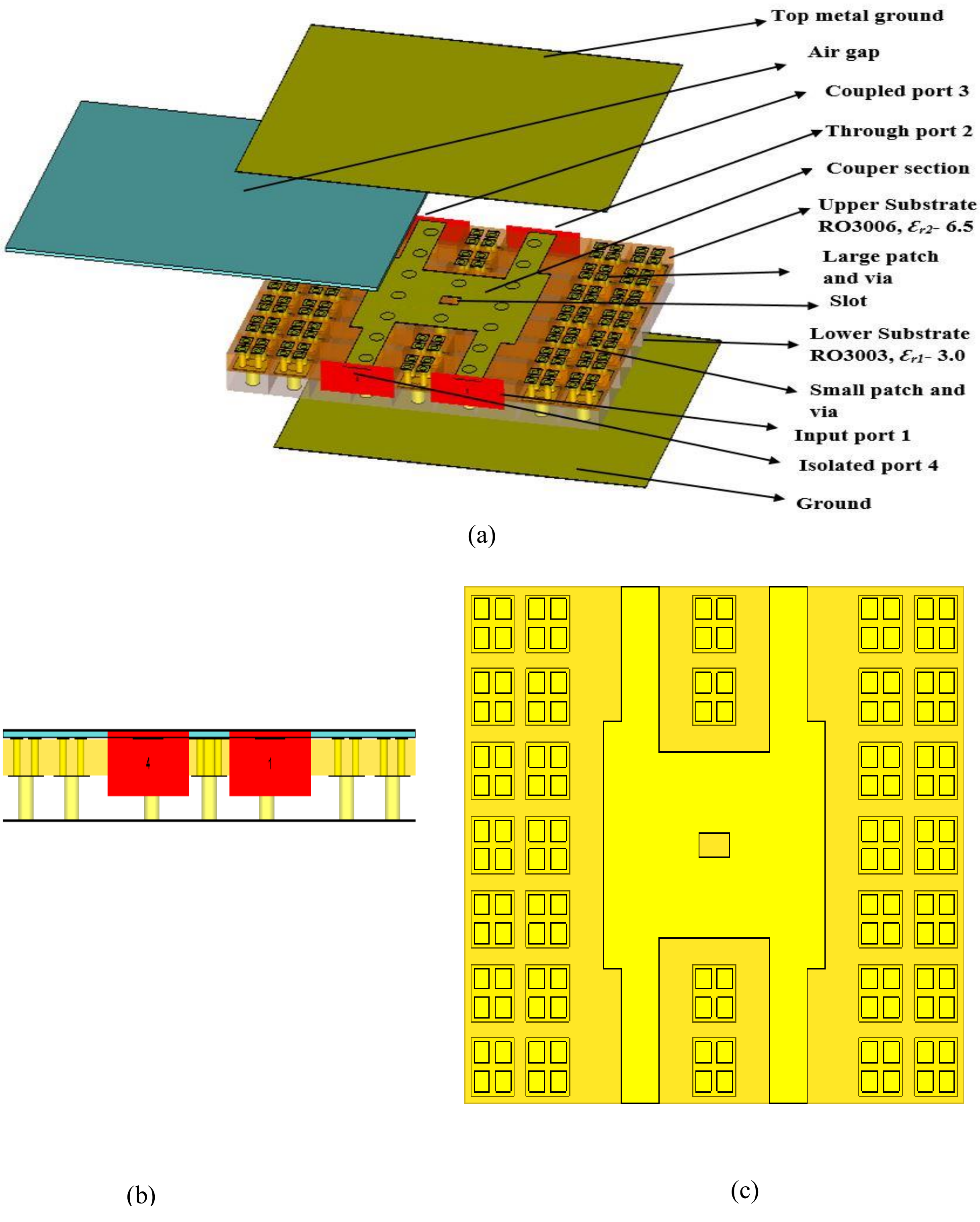

Figure 4.25: Proposed coupler for lower frequency band, (a) Full geometry, (b) Cross-section view, and (c) Top view.

junction. To get the expected outcome, a slot is installed in the middle of the coupler, which is length & width 0.9x0.8 mm. The coupler is accomplished based on PRGW technology that is well suited for higher frequency bands application, for instance, low loss due to the wave propagation inside the air gap. However, the dual-band PRGW supports a quasi-TEM mode with minimal dispersion. The proposed coupler is designed for a lower frequency band that allocates the passband from 14 -26 GHz at the center frequency of 20 GHz, which can be achieved from our design, and the band cover bandwidth is presented in the green bold shade for better understanding. The proposed coupler design for the lower band with dimensions (a), (b) the cross-section view, and (c) the top view are shown in Figure 4.25. The optimized coupling section length and width are 7.2mm and 6.0mm, respectively. The coupler is placed on the upper substrate and the structureis connected to the bottom ground plane with large metal vias. An air gap is accommodated on the top of the coupler where the wave can propagate. There is a cavity on both sides of the coupler to get an excellent matching level. Figure 4.26 presents the simulated S-parameters of the proposed coupler that works for lower frequency bands of 14-26 GHz. As observed from scattering parameters, the phase difference between the coupled and through ports is $90^{o} \pm 10^{o}$. The isolation is more than -10dB matching level between the input and the isolation port over the fractional bandwidth of 60% at center frequency 20 GHz. However, the amplitude imbalance for both the through and coupled ports is about -7 ± 2 dB over 18.6% of the operating frequency band. The width of the arms is 1.2 mm, which provides 31.5Ω line impedance. The frequency is shifted to a higher frequency, up to 26 GHz instead of 24 GHz. This coupler is suitable for Ku and K band applications.

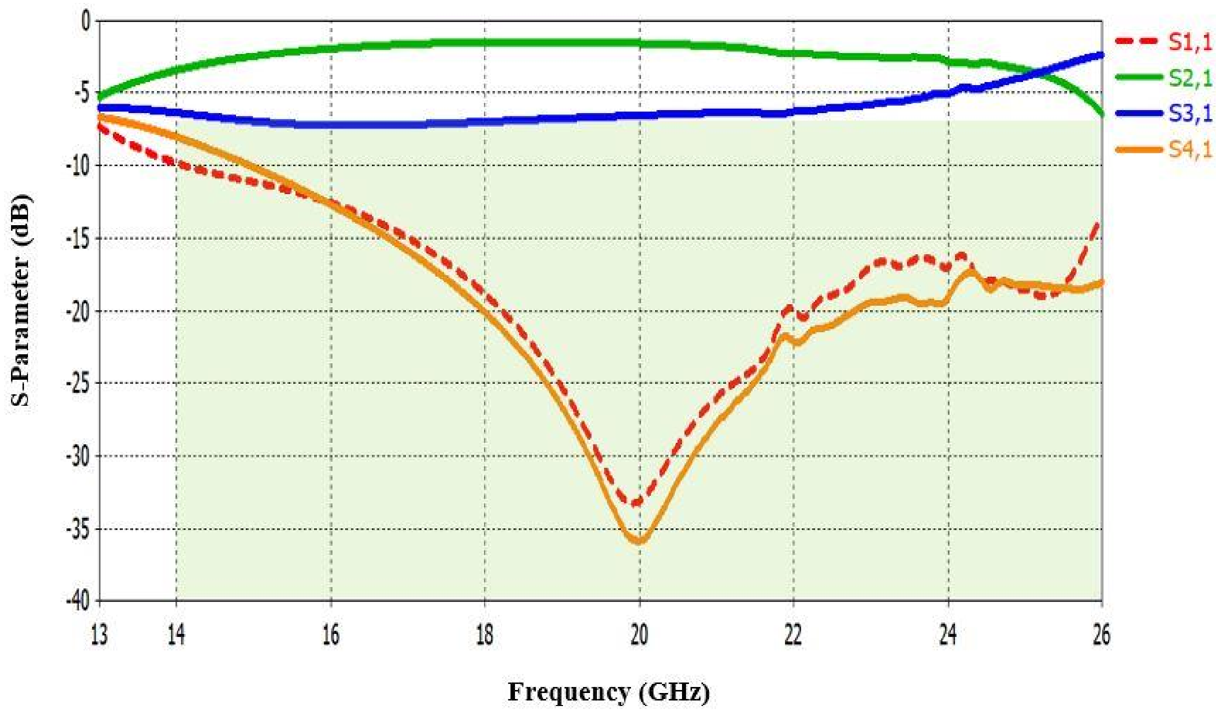

Figure 4.26: Simulated S-parameters of the proposed coupler for lower frequency band 14-26 GHz.

4.7.2 Field Distribution of Lower Band Coupler

The electric field distribution of the proposed coupler that supports the lower band is portrayed in Figure 4.27 at frequencies 10, 18, 22, and 30 GHz. As can be seen, the coupler works significantly within the frequency band at 18 and 22 GHz where port 4 is isolated. No electric field is traveling through this port, or very little is propagated within this isolated port, and the EBG unit cell also acts excellently, suppressing the electric field throughout the structure and only traveling within the coupler. On the other hand, the frequencies 10 and 30 GHz are out of the coupler band, so the electric field is scattered all over the structure. Isolated port 4 is not working, and field travels within this port. Moreover, the coupler works perfectly with a 14-26 GHz frequency range with good matching and isolating levels.

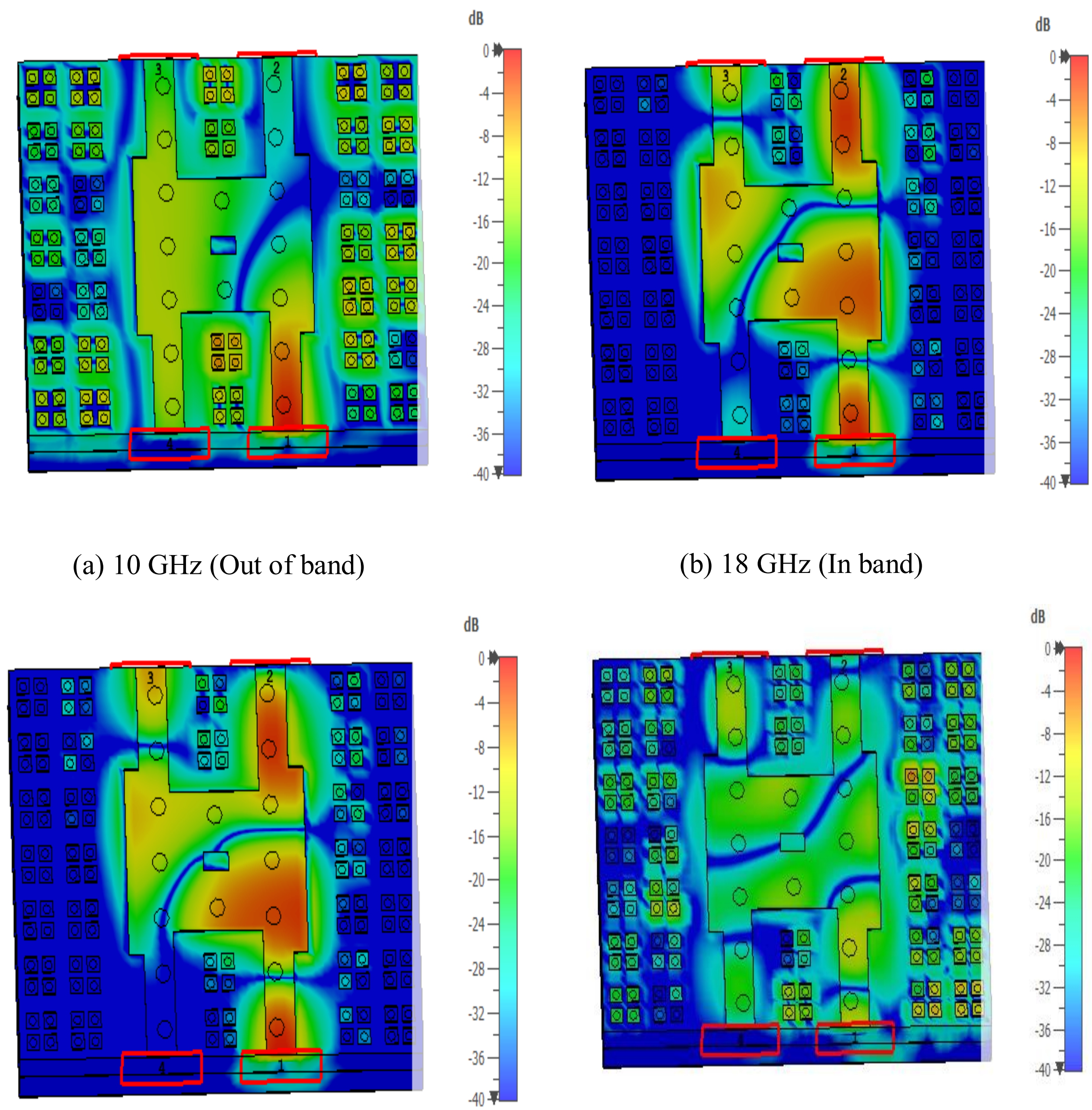

(a) 10 GHz (Out of band)

(b) 18 GHz (In band)

(c) 22 GHz (In band)

(d) 30 GHz (Out of band)

Figure 4.27: E-field distribution of the proposed lower band coupler at different frequencies. (a) 10 GHz, (b) 18 GHz, (c) 22 GHz, and (d) 30 GHz.

4.7.3 Proposed Coupler for Upper Band

The coupler size for the upper band $2.14\lambda_g/4x1.35\ \lambda_g/4$ at the center frequency of 37 GHz is our design target. The proposed coupler covers the two-and-a-half rows of cells around the middle junction; a slot is inserted in the middle of the coupler that has a size length & width of 1.0x0.6 mm. The coupler is accommodated based on PRGW technology that is well suited for Ka bands application, for instance, low loss due to the wave propagation inside the air gap. However, the dual-band PRGW supports a quasi-TEM mode with low dispersion. The proposed coupler is designed for an upper-frequency band that generates the passband from 33 to 41 GHz and is displayed in a light red bold shade for better visualization. To analyze the coupler, the dimensions are optimized to acquire the desired output: the coupling section length and width are 4.1 mm and 3.1mm, respectively. Figure 4.28 sketches the proposed coupler works for higher frequency band, (a) full configuration, (b) cross-section view, and (c) top view. The three rows surrounding the coupler are enough to suppress the unwanted electric field propagation. Figure 4.29 displays the proposed coupler's simulated S-parameters that act for upper-frequency wide band 33 to 41 GHz. As can be noticed from the scattering parameters, the phase difference between the coupled and through ports is $90^o \pm 10^o$. The isolation is more than -10 dB between the input and the isolation port over the fractional bandwidth of 21.6% at center frequency 37 GHz. However, the amplitude imbalance for both the through and coupled ports is about -8 ± 3 dB over 12.4% of the operating frequency band. The width of the coupler arms is 1.2 mm. The characteristic line impedance of the coupler is about 31.5 Ω, and a microstrip transition or adapter can be utilized in order to get 50 Ω. The coupler provides a good isolation level and compact size. The proposed coupler is promising for Ka-band applications. This coupler can be suitable for 5G communication as well.

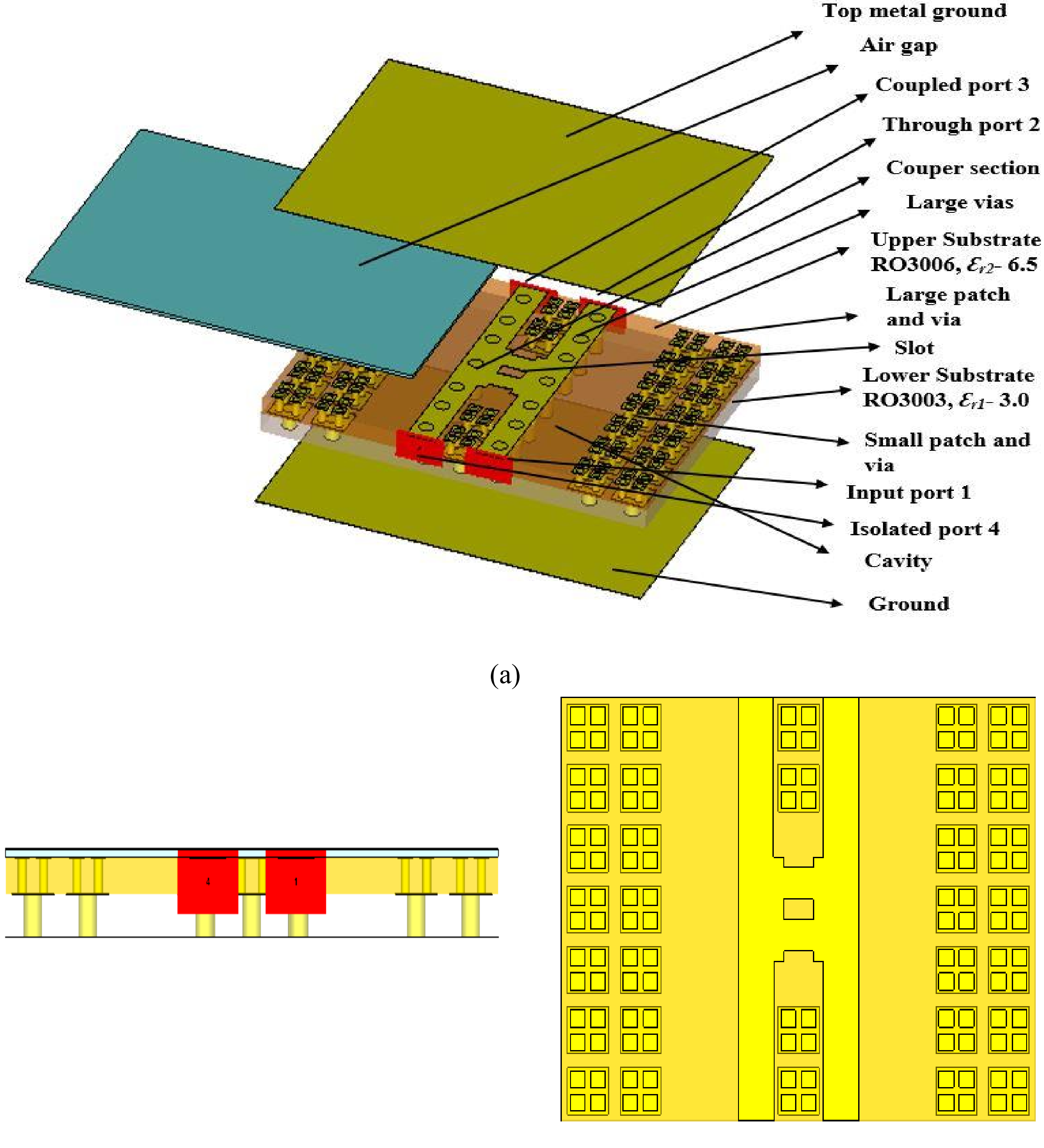

(a)

(b)

(c)

Figure 4.28: Proposed coupler for higher frequency band, (a) Full configuration, (b) Cross-section view, and (c) Top view.

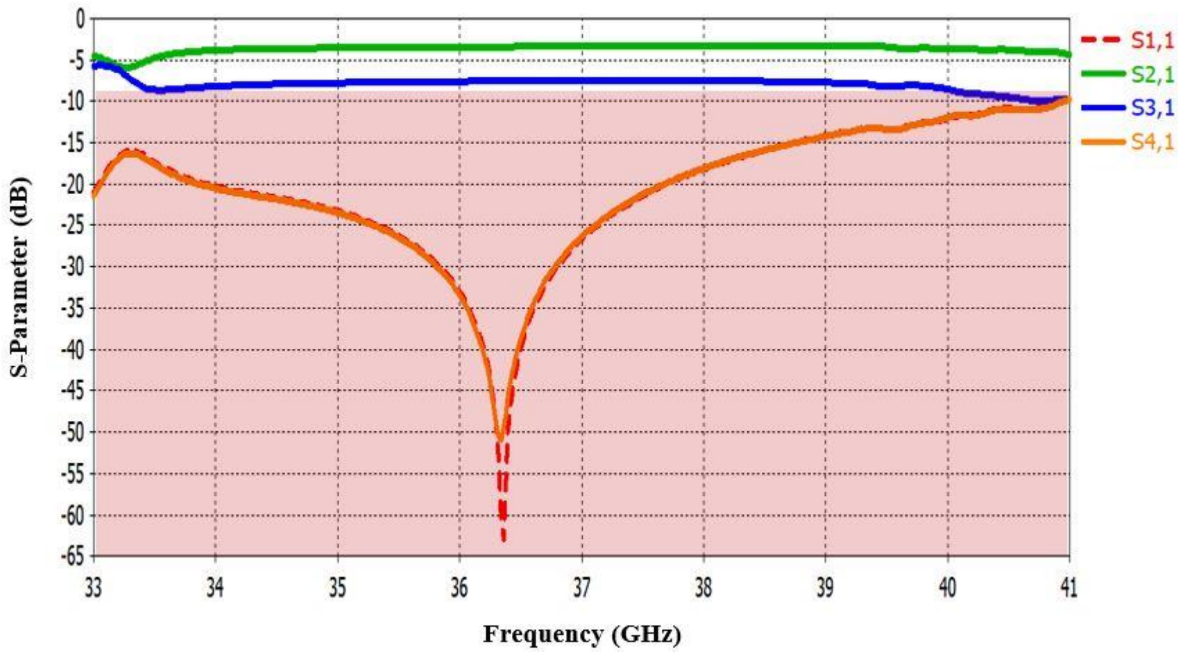

Figure 4.29: Simulated S-parameters of the proposed coupler for upper-frequency band 33-41 GHz.

4.7.4 Field Distribution of Upper Band Coupler

The electric field distribution provides information on how much fields travel throughout thestructure, their field direction as well as polarization. Figure 4.30 shows the electric field distribution of the proposed coupler that supports the upper band at frequency various frequency points 30, 35, 39, and 45 GHz. As can be noticed, the coupler works remarkably within the frequency band at 35 and 39 GHz where port 4 is isolated. No electric fields are circulating through this port, or very few are propagated within this isolated port. The EBG unit cell also works outstanding in suppressing the electric field throughout the structure, and the electric field travels within the coupler only

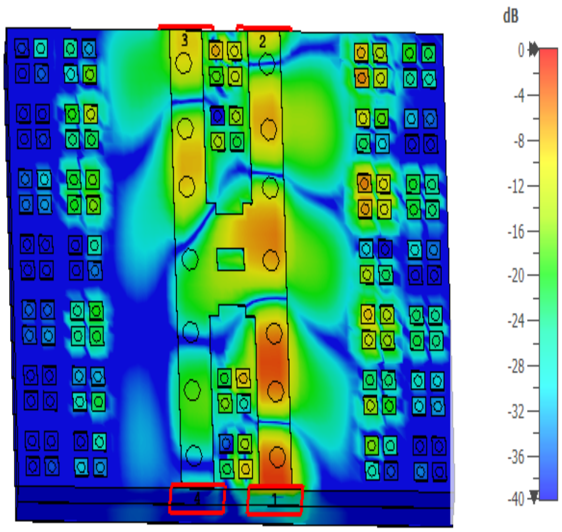

(a) 30 GHz (Out of band)

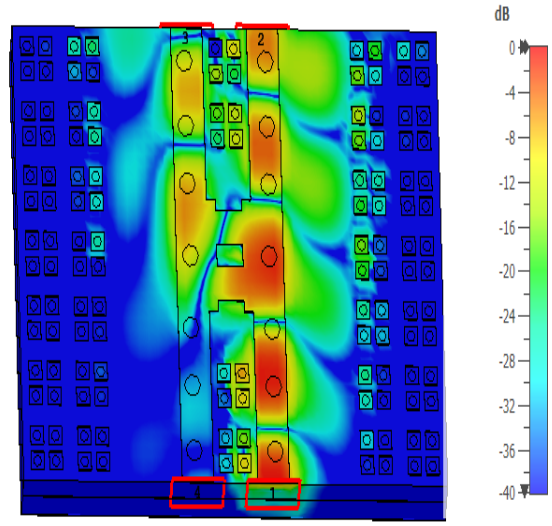

(b) 35 GHz (In band)

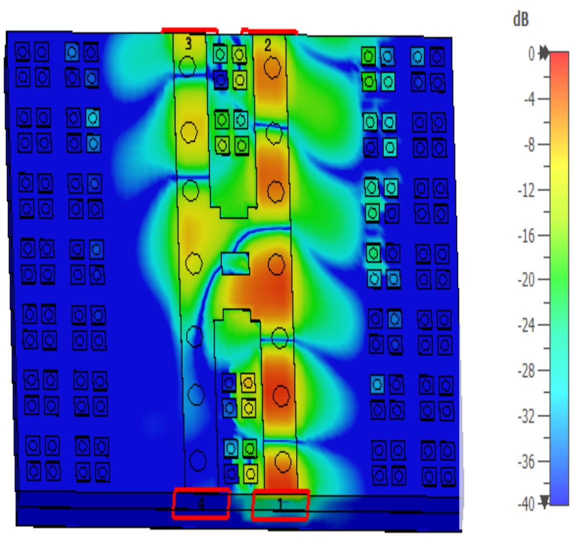

(c) 39 GHz (In band)

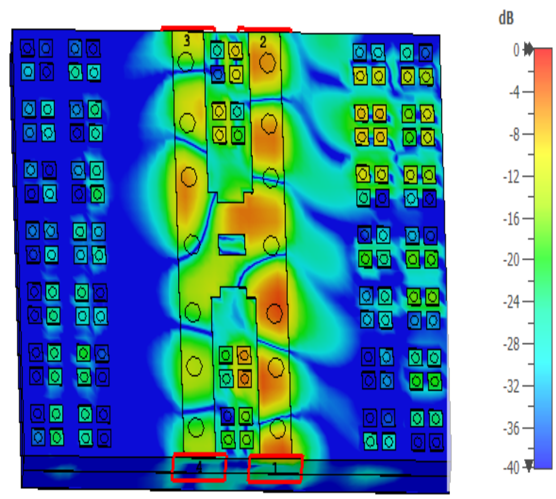

(d) 45 GHz (Out of band)

Figure 4.30: E-field distribution of the proposed upper band coupler at different frequencies, (a) 30 GHz, (b) 35 GHz, (c) 39 GHz, and (d) 45 GHz.

In contrast, at frequencies 30 and 45 GHz, they are out of the coupler band, so the electric field spreads all over the structure. Isolated port 4 does not work, and the field travels within this port and neighboring cells. Moreover, the coupler works excellent with 33-41 GHz frequency range with good matching and isolating levels below -10dB.

Chapter 5

Conclusion and Future Work

5.1 Conclusion

Ridge gap waveguides have already established themselves as renowned guiding structures in millimeter-wave applications. RGWs are suitable for higher frequency applications because they lack electrical contact between different layers, are low cost, are low profile, and are easy to install. In our research work, we have focused on the printed version of ridge gap waveguide technology. The concept of the EBG surface has been implemented here, and this surface allows wave propagation to the desired direction and forbids it to any other direction. In order to create an EBG surface, designing a unit cell, which is the main basic block of the surface, is required. A literature review of gap waveguide technology has been described in the thesis paper. A novel double layer 4 mushroom unit cell is introduced here with parametric studies of parameters, providing wide dual bands for 13-24 and 34-44 GHz. A dual-band 9 mushroom patches unit cell has shown that it also supports dual-band. Another proposal of the unit cell 4 mushroom patches looking downward at the unit cell has also been presented here. Still, unfortunately, this unit cell doesn't support dual-band unless the air gap becomes zero 0.01 mm, which works as a dielectric-filled SIW unit cell. The four-mushroom unit cell allocates two stop bands, and after inserting a ridge within the periodic EBG, two propagation modes that support two stop bands have been created. The unit cell controls the band gap in the structure. In the thesis work, a dual-band printed ridge gap waveguide is presented with an outstanding matching level, and the reflection coefficient is about below 15 dB for both bands. PRGW, with four different types of approaches by changing the ridge position and conditions, has shown the scattering parameters and excellent matching levels that can be utilized for K-, Ka-, or V-band applications. This is one of the benefits of using dual-band EBG unit cells.

A packaged RGW with bend discontinuities has also been demonstrated with the dual-band EBG cell that supports dual-bands with minimized discontinuity effects and suppression of cavity resonance created around the bend. This two 90^{o} degree bend line is vital in realizing future feeding networks or designing cheap microwave passive components such as power dividers, couplers, antennas, or antenna arrays, in which numerous discontinuities naturally exist. The ridge line with two 90^{o} degree bend lines assigns dual-band, 13-22 GHz and 32-42 GHz, with excellent matching, and the reflection coefficient level is below 10 dB and insertion loss is 1.5 dB. This suits dual-band higher frequency applications such as K-band or Ka-band. A dual-band power divider with a three-section transformer has been introduced with a dual-band EBG cell that supports two bands, one for 16-24 GHz and another for 32.5-42.5 GHz. The reflection coefficient is below 10 dB for both bands, and the insertion loss is below 5 dB due to multiple bends of the line. Two directional packaged hybrid couplers have been presented with dual-band EBG cells. Although our goal was to get a dual-band coupler, we didn't get a dual-band using a dual-band cell. However, two different couplers have been presented, providing two wide bands separately with good isolation levels and a $90^{o} \pm 10^{o}$ phase shift between the output coupling ports. One coupler is designed for the lower band that covers 14 - 26 GHz with 10 dB isolation between the input and isolation port, and the fractional bandwidth is 60% at the center frequency of 20 GHz. This coupler is suitable for Ku- and K-band applications. Another coupler for the upper band is 33 - 41 GHz with 10 dB isolation between the input and isolation port, and the fractional bandwidth is 21.6 % at the center frequency of 37 GHz. This coupler is preferable for K- and Ka-band applications.

This thesis work can be implemented for dual-band filter design, which can precisely generate dual-passband or dual-bandstop filter. Dual-band millimeter-wave applications are another novelty of this work.

5.2 Future Works

The initial step in future development will be fabricating these devices to offer measurements and verifications. Dual-band 1x4 and 1x8 power dividers could be the extension of future work. Other microwave components should be studied and designed through the dual-band unit cell, for instance, beamforming networks, cross-over coupler, dual-band antenna, and antenna array based on this guiding structure for future wireless communication. A dual-band diplexer can be a desirable candidate with the proposed dual-band PRGW. However, a gap waveguide is a packaged device; this technology might be accomplished in integrated circuits such as MMIC to reduce the mutual coupling between the circuit elements. In addition, considering the benefit of cost-effective fabrication and the suppression of undesired modes, these dual-band proposed components provide high performance in millimeter wave and high-frequency applications.

Future work could be related to realizing the dual-band EBG using different technologies, such as all-metal EBG, to reduce the insertion loss associated with the printed technology. As wide-separated dual-band printed circuits would suffer from severe radiation loss, particularly at the upper band, the proposed dual-band EBG can be used for packaging such circuits. The structure can also be considered a dual-band bandpass filter using the gap waveguide bands. However, if a dual-band filter is desired for particular bands smaller than the actual bands of the gap waveguide, it should be properly designed.

References

[1] E. Dahlman, S. Parkvall, and J. Sk¨old, 4G LTE/LTE-Advanced for Mobile Broadband. Academic Press, 2011.

[2] M. Elsaadany, A. Ali and W. Hamouda, "Cellular LTE-A Technologies for the Future internet-of-Things: Physical Layer Features and Challenges," in *IEEE Communications Surveys & Tutorials*, vol. 19, no. 4, pp. 2544-2572, Fourth Quarter 2017.

[3] P. Zhouyue and F. Khan, "An introduction to millimeter-wave mobile broadband Systems*," IEEE Communications Magazine,* vol. 49, no. 6, pp. 101–107, Jun. 2011.

[4] M. G. Kachhavay and Ajay P. Thakare, "5G Technology- Evolution and Revolution" *International Journal of Computer Science and Mobile Computing,* vol. 3, no. 3, pp. 1080-1087, Mar. 2014.

[5] T. S. Rappaport *et al.*, "Millimeter Wave Mobile Communications for 5G Cellular: It Will Work," in *IEEE Access*, vol. 1, pp. 335-349, May 2013.

[6] D. Pozar, Microwave Engineering, 3rd ed. New York: Jone Wiley Sons, 2004.

[7] J. Wenger, "Short range radar - being on the market," *in European Radar Conference*, EuRAD, pp. 255–258, Oct. 2007.

[8] K. C. Huang, and D.J. Edwards, Millimeter Wave Antennas for Gigabit Wireless Communications, New York: John Wiley & Sons, 2008.

[9] M. Marcus and B. Pattan, "Millimeter Wave Propagation; Spectrum Management Implications," *IEEE Microwave Magazine*, no. 6, pp. 54-62, Jun 2005.

[10] R. Simons, Coplanar Waveguide Circuits, Components, and Systems. Wiley, 2001.

[11] Y. Li, H. Wei, H. Guang, J. Chen, W. Ke, and T.-J. Cui, "Simulation and experiment on SIW slot array antennas*,"* in *IEEE Microwave Wireless Components Letters,* vol. 14, no. 9, pp. 446–448, Aug. 2004.

[12] J. Hirokawa and M. Ando, "Single-layer feed waveguide consisting of posts for Plane TEM wave excitation in parallel plates," in *IEEE Transactions on Antennas and Propagation,* vol. 46, no. 5, pp. 625–630, May 1998.

[13] P.S. Kildal, E. Alfonso, A. Valero-Nogueira and E. Rajo-Iglesias, "Local Metamaterial-Based Waveguides in Gaps Between Parallel Metal Plates," in *IEEE Antennas and Wireless Propagation Letters*, vol. 8, pp. 84-87, Jan. 2009.

[14] E. Rajo-Iglesias and P.S. Kildal, "Groove gap waveguide: A rectangular waveguide between contactless metal plates enabled by parallel-plate cut-off," in *4th European Conference on Antennas and Propagation (EuCAP)*, Barcelona, Spain, pp.1-4, Apr. 2010.

[15] M. Sharifi Sorkherizi, A. Dadgarpour, and A. A. Kishk, "Planar High-efficiency Antenna Array Using New Printed Ridge Gap Waveguide Technology," in *IEEE Transactions on Antennas and Propagation*, vol. 65, no. 7, pp. 3772-3776, Jul 2017.

[16] S. I. Shams and A. A. Kishk, "Double cone ultra wide band unit cell in ridge gap waveguides," in *IEEE Antennas and Propagation Society International Symposium (APSURSI)*, Memphis, TN, USA, pp. 1768-1769. Jul. 2014.

[17] P.S. Kildal, "Definition of artificially soft and hard surfaces for electromagnetic waves," *Electronics Letters.*, vol. 24, no. 3, pp. 168–170, Feb. 1988.

[18] P. S. Kildal, "Artificially soft and hard surfaces in electromagnetics," in *IEEE Transactions on Antennas and Propagation*, vol. 38, no. 10, pp.1537–1544, Oct. 1990.

[19] P.S. Kildal and A. Kishk, "EM modeling of surfaces with stop or go characteristics artificial magnetic conductors and soft and hard surfaces," in *ACES Journal Paper*, vol. 18, no. 1, pp. 32-40, Mar. 2003.

[20] Y. Zhang, J. von Hagen, and W. Wiesbeck, "Patch array as artificial magnetic conductors for antenna gain improvement," in *Microwave and Optical Technology Letters,* vol. 35, no. 3, pp. 172–175, Jan. 2002.

[21] D. Sievenpiper, J. Schaffner, and J. Navarro, "Axial ratio improvement in aperture antennas using high-impedance ground plane," *Electronics Letters*, vol. 38, no. 23, pp. 1411–1412, Sept. 2002.

[22] D. J. Salomonsson, J. Hirokawa, P. S. Kildal, and A. Tengs, "Corrugated soft sector horn with different beam properties in the two principal planes," in *IEEE Microwaves, Antennas and Propagation,* vol. 144, no. 1, pp. 13–19, Feb. 1997.

[23] E. Lier and P. S. Kildal, "Soft and hard horn antennas," in *IEEE Transactions on Antennas and Propagation*, vol. 36, no. 8, pp. 1152–1157, Aug. 1988.

[24] A. A. Kishk and P. S. Kildal, "Modelling of soft and hard surfaces using ideal perfect electric conducting/perfect magnetic conducting strip grids," in *IET Microwaves, Antennas & Propagation*, vol. 3, no. 2, pp. 296–302, 2009.

[25] D. Sievenpiper, Z. Lijun, R. F. J. Broas, N. G. Alexopolous, and E. Yablonovitch, "High-impedance electromagnetic surfaces with a forbidden frequency band," in *IEEE Transactions on Microwave Theory and Techniques*, vol. 47, no. 11, pp. 2059–2074, Nov. 1999.

[26] M. G. Silveirinha, C. A. Fernandes, and J. R. Costa, "Electromagnetic characterization of textured surfaces formed by metallic pins," in *IEEE Transactions on Antennas and Propagation,* vol. 56, no. 2, pp. 405–415, Feb. 2008.

[27] S. I. Shams and A. A. Kishk, "Determining the Stopband of a Periodic Bed of nails from the Dispersion Relation Measurements Prediction," in *IEEE Transactions on Components, Packaging and Manufacturing Technology*, vol. 7, no. 4, pp. 621-629, Apr. 2017.

[28] E. Rajo-Iglesias and P. S. Kildal, "Numerical studies of bandwidth of parallel-plate cut-off realized by a bed of nails, corrugations and mushroom-type electromagnetic bandgap for use in gap waveguides," in *IET Microwaves, Antennas & Propagation*, vol. 5, no. 3, pp. 282–289, Mar. 2011.

[29] P. S. Kildal, "Three metamaterial-based gap waveguides between parallel metal plates for mm/submm waves," in *3rd European Conference on Antennas and Propagation*, pp. 28-32, Mar. 2009.

[30] P. S. Kildal, A. U. Zaman, E. Rajo-Iglesias, E. Alfonso and A. Valero-Nogueira "Design and experimental verification of ridge gap waveguide in bed of nails for Parallel-plate mode suppression," in *IET Microwaves, Antennas and Propagation* vol. 5, no. 3, pp. 262-270, Feb. 2011.

[31] A. U. Zaman, V. Vassilev, P.S. Kildal, and A. Kishk, "Increasing parallel plate stop-band in gap waveguides using inverted pyramid-shaped nails for slot array application above 60ghz," in *5th European Conference on Antennas and Propagation* (*EUCAP*), Rome, Italy pp. 2254–2257, Apr. 2011.

[32] E. Alfonso, M. Baquero, A. Valero-Nogueira, J. I. Herranz, and P. S. Kildal, "Power divider in ridge gap waveguide technology," in *4th European Conference on Antennas and Propagation*, (EuCAP), Barcelona, Spain, pp. 1-4, Apr. 2010.

[33] S. I. Shams and A. A. Kishk, "Printed Texture With Triangle Flat Pins for Bandwidth Enhancement of the Ridge Gap Waveguide," in *IEEE Transactions on Microwave Theory and Techniques*, vol. 65, no. 6, pp. 2093-2100, Jun. 2017

[34] E. Pucci, E. Rajo-Iglesias, J. Vázquez-Roy, and P. Kildal, "Planar Dual-Mode Horn Array With Corporate-Feed Network in Inverted Microstrip Gap waveguide" in *IEEE Transactions on Antennas and Propagation*, vol. 62, no. 7, pp. 3534- 3542, Jul. 2014.

[35] A. U. Zaman, A. Kishk, and P. S. Kildal, "Narrow-band microwave filter using high Q groove gap waveguide resonators without sidewalls," in IEEE *Transactions on Components, Packaging and Manufacturing Technology*, vol. 2, no. 11, pp. 1882–1888, May. 2011.

[36] M. Bosiljevac, A. Polemi, S. Maci, and Z. Sipus, "Analytic approach to the analysis of ridge and groove gap waveguides - comparison of two methods," *in 5th European Conference on Antennas and Propagation*, (EuCAP), Rome, Italy, pp. 1886–1889, Apr. 2011.

[37] Y. Rahmat-Samii and H. Mosallaei, "Electromagnetic band-gap structures: classification, characterization, and applications," in *11th International Conference on Antennas and Propagation,* Manchester, UK, vol. 2, pp. 560-564, Apr. 2001

[38] E. Pucci, E. Rajo-Iglesias, and P. S. Kildal, "New Microstrip Gap Waveguide on Mushroom Type EBG for Packaging of Microwave Components," in *Microwave and Wireless Components Letters,* vol. 22, no. 3, pp. 129-131, Mar. 2012

[39] N. B. Lima, H. C. Miranda, J. R. Pereira, and H. M. Salgado, "Low-pass Filter Design using Two Overlapped Periodic EBG Structures with Low Spurious Responses," in *International Conference on Electromagnetics in Advanced Applications*, Turin, Italy, pp. 842-845, Sept. 2007.

[40] W. Zhang, L. Han, X. Sun and J. Mao, "Harmonic-suppression band-pass filter with microstrip EBG," in *Asia-Pacific Microwave Conference*, Suzhou, China, pp. 3, Dec. 2005.

[41 G. Harine, S. Abirami, B. Harini, S. Esther Florence, and I. Subramaniam, "Design and Analysis of Novel EBG/AMC Unit Cell," in *5th International Conference on Advanced Computing & Communication Systems (ICACCS)*, Coimbatore, India, pp. 684-688, Mar. 2019.

[42] M. S. Sorkherizi and A. A. Kishk, "Fully printed gap waveguide with facilitated design properties," in *IEEE Microwave Wireless Components Letters*, vol. 26, no. 9, pp. 657-659, Sep. 2016.

[43] A. Zaman and P. Kildal, "Gap waveguides," in Handbook of Antenna Technologies, Z. N. Chen, D. Liu, H. Nakano, X. Qing, and T. Zwick, Eds. Singapore: Springer, 2016.

[44] Constantine A. Balanis, Antenna Theory: Analysis and Design, 3rd Edition, NJ, USA: Wiley, 2005.

[45] H. Raza, J. Yang, P.S. Kildal, and E. Alfonso, "Microstrip-ridge gap waveguide study of losses, bends, and transition to WR-15," *IEEE Transactions Microwave Theory Technology,* vol. 62, no. 9, pp. 1943-1952, Sep. 2014.

[46] M. Sharifi Sorkherizi and A. A. Kishk, "Transition from microstrip to printed ridge gap waveguide for millimeter-wave application," in *IEEE International Symposium on Antenna and Propagation & USNC/URSI National Radio Science Meeting*, Vancouver, BC, Canada, pp. 1588-1589, Jul. 2015.

[47] A. A. Brazález, E. Rajo-Iglesias, J. L. Vázquez-Roy, A. Vosoogh, and P.S. Kildal "Design and validation of microstrip gap waveguides and their transitions to rectangular waveguide, for millimeter-wave applications," in *IEEE Transactions Microwave Theory Technology,* vol. 63, no. 12, pp. 4035-4050, Dec. 2015.

[48] I. Afifi, M. M. M. Ali, and A. Sebak, "Analysis and Design of a Wideband Coaxial Transition to Metal and Printed Ridge Gap Waveguide," in *IEEE Access*, vol. 6, pp. 70698-70706, Dec. 2018.

[49] S. I. Shams and A. A. Kishk, "Ridge gap waveguide to microstrip line transition with perforated substrate," in *USNC-URSI Radio Science Meeting,* Memphis, TN, USA, pp. 215-215, Jul. 2014.

[50] S. I. Shams and A. A. Kishk, "Wideband Coaxial to Ridge Gap Waveguide transition," in *IEEE Transactions Microwave Theory Technology*, vol. 64, no. 12, pp. 4117- 4125, Dec. 2016.

[51] E. Rajo-Iglesias, A. U. Zaman, and P. S. Kildal, "Parallel plate cavity mode suppression in microstrip circuit packages using a lid of nails," in *IEEE Microwave and Wireless Components Letters*, vol. 20, no. 1, pp.31–33, Jan. 2010.

[52] A. A. Brazalez, A. U. Zaman, and P. S. Kildal, "Improved microstrip filters using PMC packaging by lid of nails," in *IEEE Transactions on Components, Packaging and Manufacturing Technology*, vol. 2, no. 7, pp. 1075–1084, Jul. 2012.

[53] Elena Pucci, "Gap Waveguide Technology for Millimeter Wave Applications and Integration with Antennas" PhD Dissertation, Chalmers University of Technology, 2013

[54] K. W. Eccleston, "Compact planar 3-way power divider using left handed transmission lines," in *Asia-Pacific Microwave Conference Proceedings*, Suzhou, China, pp. 4, Dec. 2005

[55] A. B. Santiko, Edwar and A. Munir, "Development of Filtering Power Divider for WLAN Application Using SIW Bandpass Filter," in *IEEE Asia Pacific Conference on Wireless and Mobile (APWiMob)*, Bandung, Indonesia, pp. 233-237, Apr. 2021.

[56] Y. Liu, E. Wang, H. Zhang, and G. Zhang, "A New Two-Way Multilayer SIW Filtering Power Divider (FPD) with Good Isolation," in *International Applied Computational Electromagnetics Society Symposium (ACES)*, Nanjing, China, pp. 1-2, Aug. 2019.

[57] K. Song, F. Xia, Y. Zhou, S. Guo, and Y. Fan, "Microstrip/Slotline-Coupling Substrate Integrated Waveguide Power Divider with High Output Isolation," in *IEEE Microwave and Wireless Components Letters*, vol. 29, no. 2, pp. 95-97, Feb. 2019.

[58] J. Wu, Y.J. Cheng, and Y. Fan, "A Wideband high-gain high-efficiency hybrid integrated plate array antenna for V-band inter-satellite links," in *IEEE Transactions Antennas Propagation*, vol. 63, no. 4 pp. 1225-1233, Apr. 2015.

[59] Y. Li and K.M. Luk, "60-GHz substrate integrated waveguide fed cavity-backed aperture-coupled microstrip patch antenna arrays," in *IEEE Transactions Antennas Propagation,* vol. 63, no. 3, pp. 1075-1085, Mar. 2015.

[60] S. Gupta, A. R. Sebak, and V. K. Devabhaktuni, "Design of ridge gap waveguide power divider for reduced-sidelobe 60 GHz applications," *IEEE MTT-S International Microwave and RF Conference (IMaRC)*, Ahmedabad, India, 2017, pp. 302-305, Dec. 2017.

[61] S. I. Shams and A. A. Kishk, "Wideband power divider based on Ridge gap waveguide," in *17th International Symposium on Antenna Technology and Applied Electromagnetics (ANTEM)*, Montreal, QC, Canada, pp. 1-2, Jul. 2016.

[62] M. F. Emara, A. Allam, S. I. Shams, D. E. Fawzy and M. Elsaadany, "Dual Gap Wideband In-Phase Power Divider Based on Ridge Gap Waveguide Technology," *in 7th International Conference on Electrical and Electronics Engineering (ICEEE)*, Antalya, Turkey , pp. 86-89, Apr. 2020

[63] X. Jiang *et al*., "Millimeter-Wave Double Ridge Gap Waveguide Six-Port Network Based on Multi-Via Mushroom," in *IEEE Transactions on Plasma Science*, vol. 49, no. 12, pp. 3778-3785, Dec. 2021.

[64] D. Liu., Wang, L., Chen, Y, "User association in 5 g networks: a survey and an outlook", in *IEEE Communications Surveys & Tutorials*, vol. 18, no. 2, pp. 1018–1044, Jan. 2016.

[65] G. Araniti, M. Condoluci, P. Scopelliti, A. Molinaro and A. Iera, "Multicasting over Emerging 5G Networks: Challenges and Perspectives," in *IEEE Network*, vol. 31, no. 2, pp. 80-89, Apr. 2017.

[66] R. K. Gupta, S. E. Anderson and W. J. Getsinger, "Impedance-Transforming 3-dB 90° Hybrids," in *IEEE Transactions on Microwave Theory and Techniques*, vol. 35, no. 12, pp. 1303-1307, Dec. 1987.

[67] W. M. Fathelbab, "The Synthesis of a Class of Branch-Line Directional Couplers," in *IEEE Transactions on Microwave Theory and Techniques*, vol. 56, no. 8, pp. 1985-1994, Aug. 2008.

[68] X. Shen, Y. Liu, S. Zhou, and Y. Wu, ``Coupled-line directional coupler with tunable power division ratio and operating frequency," in *IET Microwaves, Antennas & Propagation*, vol. 11, no. 1, pp. 59-68, Jan. 2017.

[69] T. Djerafi, K. Wu and S. O. Tatu, "3 dB 90∘ Hybrid Quasi-Optical Coupler With Air Field Slab in SIW Technology," in *IEEE Microwave and Wireless Components Letters*, vol. 24, no. 4, pp. 221-223, Apr. 2014.

[70] R. Gomez-Garcia, J. I. Alonso, and D. Amor-Martin, "Using the branch line directional coupler in the design of microwave bandpass filters," *IEEE Transactions on Microwave Theory and Techniques*, vol. 53, no. 10, pp. 3221-3229, Oct. 2005.

[71] T. Djerafi and K. Wu, "Super-Compact Substrate Integrated Waveguide Cruciform Directional Coupler," in *IEEE Microwave and Wireless Components Letters*, vol. 17, no. 11, pp. 757-759, Nov. 2007.

[71] A. Doghri, T. Djerafi, A. Ghiotto, and K. Wu, "Broadband substrate-integrated-waveguide six-port applied to the development of polarimetric imaging radiometer," in *41st European Microwave Conference*, Manchester, UK, pp. 393-396, Oct. 2011.

[73] B. Liu, W. Hong, Y. -Q. Wang, Q. -H. Lai and K. Wu, "Half Mode Substrate Integrated Waveguide (HMSIW) 3-dB Coupler," in *IEEE Microwave and Wireless Components Letters*, vol. 17, no. 1, pp. 22-24, Jan. 2007

[74] A. Doghri, T. Djerafi, A. Ghiotto, and K. Wu, "Substrate Integrated Waveguide Directional Couplers for Compact Three-Dimensional Integrated Circuits," in *IEEE Transactions on Microwave Theory and Techniques*, vol. 63, no. 1, pp. 209-221, Jan. 2015.

[75] Z. Liu and G. Xiao, "Design of SIW-Based Multi-Aperture Couplers Using Ray Tracing Method," in *IEEE Transactions on Components, Packaging and Manufacturing Technology*, vol. 7, no. 1, pp. 106-113, Jan. 2017.

[76] W. M. Abdel-Wahab and S. Safavi-Naeini, "Low loss H-shape SIW hybrid coupler for millimeter-wave phased arrays antenna systems," in *IEEE International Symposium on Antennas and Propagation*, Chicago, IL, USA, pp. 1-2, Jul. 2012.

[77] E. Alfonso, M. Baquero, P. -S. Kildal, A. Valero-Nogueira, E. Rajo-Iglesias, and J. I. Herranz, "Design of microwave circuits in ridge-gap waveguide technology," in *IEEE MTT-S International Microwave Symposium*, Anaheim, CA, USA, pp. 1544-1547. May. 2010.

[78] M. S. Sorkherizi and A. A. Kishk, "Lowloss planar bandpass filters for millimeter-wave application," in *IEEE MTT-S International Microwave Symposium*, Phoenix, AZ, USA, pp. 1-4, May. 2015.

[79] M. M. M. Ali and A. Sebak," 2-D Scanning Magnetoelectric Dipole Antenna Array Fed by RGW Butler Matrix," *IEEE Transactions on Antennas and Propagation*, vol. 66, no. 11, pp. 6313-6321, Nov. 2018.

[80] S. I. Shams and A. A. Kishk, "Design of 3-dB Hybrid Coupler Based on RGW Technology," in *IEEE Transactions on Microwave Theory and Techniques*, vol. 65, no. 10, pp. 3849-3855, Oct. 2017.

[81] D. Zarifi, A. R. Shater., "Design of a 3-dB directional coupler based on groove gap waveguide technology", in *Microwave and optical technology letters*, vol. 59, pp. 1597–1600, Aug. 2017.

[82] M. M. M. Ali, M. S. El-Gendy, M. Al-Hasan, I. B. Mabrouk, A. Sebak and T. A. Denidni, "A Systematic Design of a Compact Wideband Hybrid Directional Coupler Based on Printed RGW Technology," in *IEEE Access*, vol. 9, pp. 56765-56772, Apr. 2021.

[83] M. M. Mahmoud Ali, S. I. Shams, and A. Sebak., "Ultra-wideband printed ridge gap waveguide hybrid directional coupler for millimetre wave applications," in *IET Microwaves, Antennas & Propagation*, vol.13, no. 8, pp. 1181-1187, Jul. 2019.

[84] D. Shen, K. Wang and X. Zhang, "A Substrate Integrated Gap Waveguide Based Wideband 3-dB Coupler for 5G Applications," in *IEEE Access*, vol. 6, pp. 66798-66806, Nov. 2018.